

Doctoral Thesis

Novel Strategies to Modulate Adaptive Immune Responses for  
Preventing Atherosclerosis and Abdominal Aortic Aneurysm  
Development

Kobe Pharmaceutical University

Laboratory of Medical Pharmaceutics

Aga Krisnanda

2025

## **Abbreviation**

AAA : abdominal aortic aneurysm  
ApoE : apolipoprotein E  
CAD : coronary artery disease  
CCL17 : C-C chemokine ligand 17  
CCL22 : C-C chemokine ligand 22  
CD : cluster of differentiation  
CTLA-4 : cytotoxic T lymphocyte associated protein 4  
DAPI : 4',6-diamidino-2-phenylindol  
DC : dendritic cell  
ELISA : enzyme-linked immunosorbent assay  
FACS : fluorescence-activated cell sorting  
FBS : fetal bovine serum  
Foxp3 : forkhead box P3  
HRP : horseradish peroxidase  
ICS : intracellular cytokine staining  
IFN : interferon  
Ig : immunoglobulin  
IL : interleukin  
LED : light-emitting diode  
LDL : low-density lipoprotein  
LN : lymph node  
MACS : magnetic-activated cell sorting  
MFI : mean fluorescence intensity  
MMP : matrix metalloproteinase  
mRNA : messenger ribonucleic acid  
NK : natural killer  
oxLDL : oxidized LDL  
PBS : phosphate-buffered saline  
PCR : polymerase chain reaction

RNA : ribonucleic acid

RPMI : Roswell Park Memorial Institute medium

s.d. : standard deviation

Tbet : T-box expressed in T cells

Teff : effector memory T cell

TGF : transforming growth factor

Th1 : type 1 T helper

Th17 : type 17 T helper

Th2 : type 2 T helper

TNF : tumor necrosis factor

Treg : regulatory T cell

UVB : ultraviolet B

## Table of contents

Abbreviation .....	i
Table of contents .....	iii
Introduction.....	1
Main thesis body .....	6
Chapter 1. Unveiling the role of CCR4 in atherosclerotic disease: insights from gene deletion models and implications for novel therapeutic strategies .....	6
1.1. Introduction.....	6
1.2. Results.....	9
1.2.1. Confirmation of CCR4 expression in Tregs/non-Tregs and detections of its ligands CCL17/CCL22 in the atherosclerotic plaque and aneurysmal tissue .....	9
1.2.2. CCR4 deficiency conversely accelerated early atherosclerosis while attenuating angiotensin II-induced AAA in <i>Apoe</i> <sup>-/-</sup> mice.....	14
1.2.3. Reduction of inflammatory responses in aneurysmal tissues and preservation of the arterial wall integrity of angiotensin II-treated mice in the absence of CCR4 .....	24
1.2.4. Deletion of CCR4 reduced Treg suppressive activity and increased Treg and effector T cell frequencies in peripheral lymphoid tissues, independent of angiotensin II treatment .....	30
1.2.5. Promotion of Th1 cell immune responses in peripheral lymphoid tissues and reduction of plasma IgE levels in angiotensin II-infused mice in the absence of CCR4.....	37
1.2.6. Deficiency of CCR4 enhanced Th1 cell responses in para-aortic LNs and the thoracoabdominal aorta of angiotensin II-infused mice .....	43
1.3. Discussion.....	51
1.4. Conclusion .....	56
Chapter 2. Evaluating the efficacy of clinically feasible 312 nm UVB irradiation as phototherapy for atherosclerosis .....	56
2.1. Introduction.....	58
2.2. Results.....	60
2.2.1. Irradiation with 312 nm UVB prevented atherosclerosis development and promoted a less inflammatory plaque phenotype .....	60
2.2.2. Teff/Treg balance in peripheral lymphoid tissues shifted toward Treg responses following 312 nm UVB irradiation.....	65
2.2.3. Irradiation with 312 nm UVB decreased the Th1 cell/Th2 cell ratio without affecting other immune cell responses in peripheral lymphoid tissues .....	68
2.2.4. Elevation of proresolving lipid mediator levels in the skin after 312 nm UVB irradiation.....	70

2.3. Discussion .....	73
2.4. Conclusion .....	73
Summary .....	78
Acknowledgments.....	80
Experimental section.....	82
Chapter 1. Materials .....	82
1.1. General equipment .....	82
1.2. Consumables .....	83
1.3. Buffers, chemicals, media, and solutions.....	84
1.4. Reagents and kits .....	84
1.5. Primers for real-time PCR .....	85
1.6. Antibodies for immunostaining.....	85
1.7. Antibodies for flow cytometry .....	86
1.8. Angiotensin II and miniosmotic pump.....	87
Chapter 2. Methods .....	88
2.1. Mouse acquisition and housing conditions .....	88
2.2. Angiotensin II-induced AAA model .....	88
2.3. UVB irradiation .....	88
2.4. Blood pressure measurement .....	89
2.5. Assessment of biochemical parameters .....	90
2.6. Morphological analysis of AAA .....	90
2.7. Assessment of atherosclerotic lesions.....	90
2.8. Histological and immunohistochemical analysis of atherosclerosis and aneurysmal lesions .....	91
2.9. In situ zymography of aneurysmal lesions.....	92
2.10. Preparation of primary cell suspension.....	94
2.11. Flow cytometry .....	94
2.12. Antibody staining of intracellular cytokine.....	94
2.13. Cytokine assay .....	95
2.14. Treg suppression assay.....	95
2.15. Quantitative reverse transcription PCR analysis.....	95
2.16. Statistical analysis .....	96
References.....	98

## Introduction

Global health priorities have shifted significantly in recent decades. With advancements in infectious disease control, epidemiological evidence shows an alarming rise in mortality rates attributed to chronic diseases. Among these, atherosclerotic diseases have consistently ranked as leading causes of death for decades.<sup>1</sup> The combined increasing trend of sedentary lifestyles and unhealthy diets contributes significantly to atherosclerotic plaque formation. Atherosclerosis often remains underdiagnosed and untreated in its early stages, leading patients to present with advanced disease and complications, such as coronary artery disease (CAD), ischemic stroke, or aortic aneurysm rupture. Such cases impose high treatment costs and result in poor outcomes, including elevated mortality rates and permanent disability. Thus, early detection and intervention for atherosclerosis and related diseases are critical.

New studies have revealed the central role of inflammation in atherosclerosis development, as immune cells drive nearly all stages of the disease. Understanding the pathways of proatherogenic immune responses can help identify novel therapeutic targets.<sup>2, 3</sup> The innate immune response of monocytes initiates the early stages of atherosclerosis. Circulating monocytes infiltrate blood vessels by binding to endothelial adhesion molecules, which are upregulated in aged or injured vessels. After entering the subendothelial space, monocytes differentiate into macrophages or dendritic cells (DCs). Endothelial cells transfer cholesterol, particularly low-density lipoprotein (LDL), into the subendothelial space, primarily at sites of flow disturbance or endothelial dysfunction. Macrophages oxidize LDL, forming oxidized LDL (oxLDL), which accumulates in macrophage-derived foam cells, marking the onset of early atherogenesis (**Figure 1**).<sup>2, 4</sup>

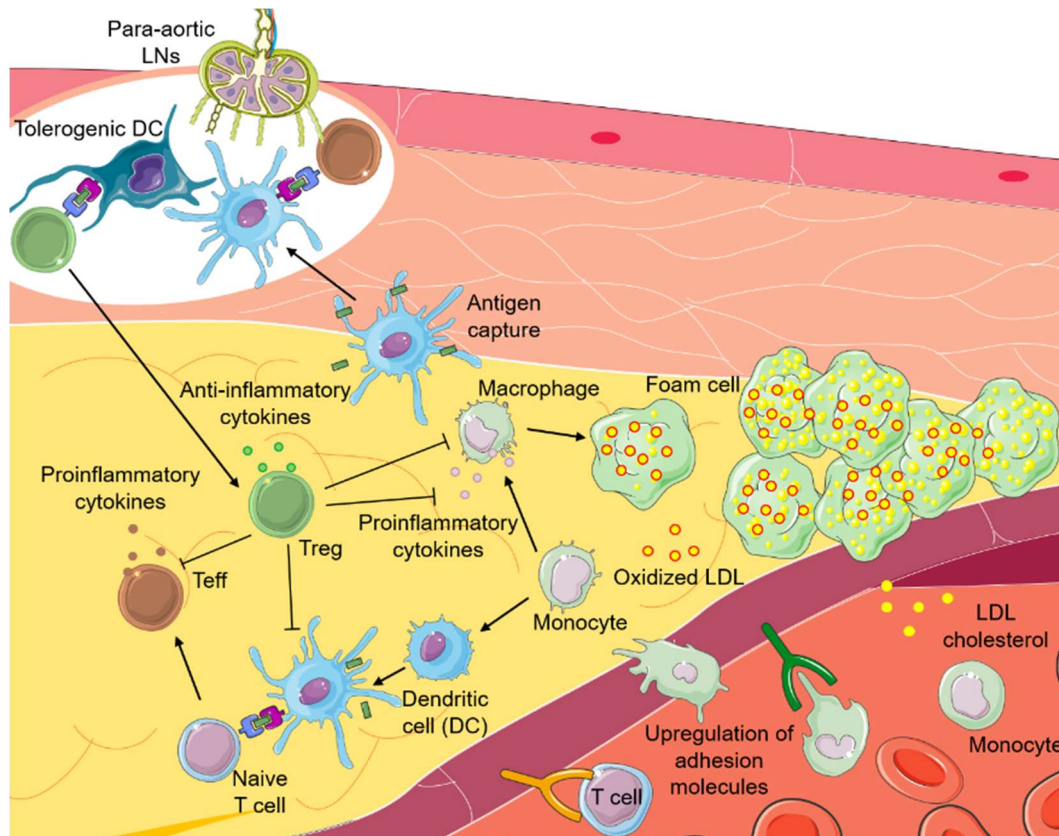


**Figure 1. Immunoinflammatory responses in atherogenesis.**

An illustrated image depicting immune cell recruitment into the subendothelial space, engaging both innate and adaptive immune responses. This process results in the accumulation of lipid-laden macrophages (foam cells), marking the early stage of atherogenesis. This figure was partly generated using Servier Medical Art, by Servier (<http://smart.servier.com>).

As atherosclerosis progresses, DCs, including those derived from circulating monocytes, activate T cells through antigen presentation. Naïve cluster of differentiation (CD)<sup>4+</sup> T cells differentiate into subsets, including type 1 helper T (Th1), type 2 helper T (Th2), type 17 helper T (Th17), and regulatory T cells (Tregs). Th1, Th2, and Th17 cells are often collectively called effector memory T cells (Teffs).<sup>5</sup> Among these, Th1 cells are unanimously recognized as proatherogenic, driven by cytokines such as interferon (IFN)- $\gamma$  and tumor necrosis factor (TNF)- $\alpha$ .<sup>6, 7</sup> Th2 cells are thought to be antiatherogenic due to their ability to counteract Th1 cell-driven inflammation. However, a strong association between Th2 cell-mediated allergic diseases and an increased risk of cardiovascular events<sup>8</sup> suggests proinflammatory roles for Th2 cells in some contexts. This duality remains controversial.

Abdominal aortic aneurysm (AAA), a major form of atherosclerotic disease, consequently linked to inflammatory responses. Its initiation often mirrors the early stages of

atherosclerosis, beginning with intimal injury and Th1 cell-predominant immune responses. Aortic plaque formation seems mandatory to cause aortic dilation, particularly in the angiotensin II-induced AAA model in LDL receptor-deficient mice, in which a high-fat, high-cholesterol diet is required to sustain plaque progression. Switching to a chow diet in these mice halted AAA dilation.<sup>9</sup> However, the effect of Th1 cell/Th2 cell balance in AAA likely differs from that in atherosclerosis (**Figure 2**). Surgically removed human AAA tissue showed a predominance of Th2-related cytokines.<sup>10</sup> In addition, the induction of Th2-cell-mediated inflammation promoted aneurysm in the allografted aorta in mice.<sup>11</sup> Accordingly, a shift to Th2 cell predominance after the establishment of early atherosclerosis induces AAA development, whereas persistent Th1 cell predominance proceeds to a stenotic lesion.<sup>11</sup>

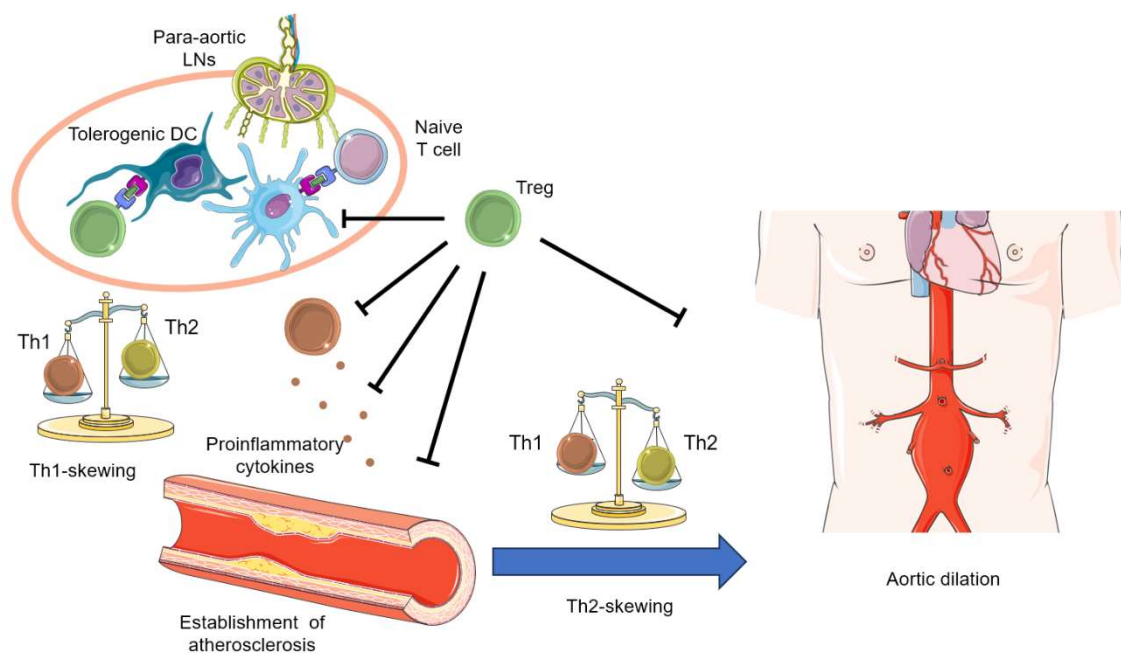


**Figure 2. Treg/Th1 and Th1/Th2 cell balance in aortic dilation pathogenesis.**

Adaptive immune responses by Th1 cells are crucial in early atherogenesis. The Th1/Th2 balance seems to decide the fate of aortic pathology after the establishment of atherosclerosis. A persistent Th1-skewed responses induce a stenotic growth while a switch toward Th2-skewed responses endorses aortic dilation. Meanwhile, Treg inhibits all inflammatory process by Treg providing protection against the disease. This figure was partly generated using Servier Medical Art, by Servier (<http://smart.servier.com>).

Th17 cells primarily produce interleukin (IL)-17, particularly the major isoform IL-17A. Inciting vascular inflammation thus are considered proatherogenic and known to cause aneurysm aggravation.<sup>12-14</sup> Studies have linked the IL-23/Th17 axis to AAA development, as



IL-23 promotes Th17 differentiation.<sup>15</sup> The relationship between obesity and increased IL-23 levels highlights the broader role of cardiometabolic factors in Th17 cell-driven inflammation.<sup>16</sup>

In contrast, Tregs exhibit consistent anti-inflammatory and antiatherogenic properties in both atherosclerosis and AAA development. Tregs suppress immune activation through cell-to-cell contact via cytotoxic T lymphocyte-associated antigen-4 (CTLA-4) and produce anti-inflammatory cytokines such as IL-10 and transforming growth factor (TGF)- $\beta$ . The balance between helper T cell subsets, such as Th1/Th2, Th1/Treg, and Th17/Treg ratios, determines the inflammatory trajectory in atherosclerosis and AAA.

Given the crucial role of helper T cells, the laboratory I belong to has focused on identifying novel targets for the treatment of atherosclerosis and related diseases through the regulation of immune responses. As an immunotherapy target, the modulation of the helper T cell subset balance is the topic of interest. Experimental approaches targeting T cell balance have included antibodies,<sup>17-19</sup> cytokines,<sup>19</sup> an active form of vitamin D<sub>3</sub>,<sup>20</sup> vaccination,<sup>21</sup> overexpression of CTLA-4,<sup>22, 23</sup> and ultraviolet B (UVB) phototherapy.<sup>24-26</sup>

Among the above treatments, UVB phototherapy has long been used in clinical settings to manage inflammatory skin conditions without significant detrimental side effects. Despite its promise, UVB therapy poses risks, including skin irritation, immune suppression, and skin cancer. To mitigate these effects, a recent study explored the efficacy of single-wavelength UVB irradiation using light-emitting diode (LED) devices at 282, 301, and 312 nm.<sup>4</sup> Results revealed that 282 nm UVB significantly reduced atherosclerosis by promoting Treg responses, including increased expression of C-C chemokine receptor 4 (CCR4), while 301 nm UVB had no protective effect. In contrast, 312 nm UVB, resembling clinically used narrowband UVB (NB-UVB), showed a tendency toward atheroprotective effects, suggesting its potential in clinical applications.<sup>4</sup>

A different approach involving a chemokine receptor likely responsible for facilitating T cell migration into inflammatory sites is also promising. CCR4 is expressed primarily in Tregs and Th2 cells. Unlike Th1 cells, which never express CCR4,<sup>27, 28</sup> its high specificity in helper T cell subsets makes it a promising target for modulating T cell responses. CCR4 is already a therapeutic target in cutaneous T cell lymphomas, treated with the monoclonal antibody mogamulizumab. However, its role in vascular inflammation and atherosclerotic diseases remains unclear.

Based on these findings, this thesis aimed to explore novel therapeutic strategies utilizing CCR4 and 312 nm UVB irradiation with particular focus on modulation of helper T cell responses in atherosclerotic diseases. Given that UVB irradiation increased Treg expression of CCR4, this thesis also sought to evaluate the possibility applying synergistic effect of both interventions. Thus, the objectives of this thesis are as follows:

1. Unveiling the role of CCR4 in atherosclerotic disease: insights from gene deletion models and implications for novel therapeutic strategies.
2. Evaluating the efficacy of clinically feasible 312 nm UVB irradiation as phototherapy for atherosclerosis.

## **Main thesis body**

### **Chapter 1. Unveiling the role of CCR4 in atherosclerotic disease: insights from gene deletion models and implications for novel therapeutic strategies**

#### **1.1. Introduction**

Atherosclerosis is characterized by the accumulation of cholesterol-rich plaques within the intimal layer of the arteries. While the condition itself is typically asymptomatic, the prolonged buildup of these plaques can lead to severe cardiovascular and cerebrovascular events, including myocardial infarction, ischemic stroke, and rupture of aortic aneurysm. These complications are often fatal or result in significant long-term disability. Despite advancements in intensive medical interventions, patients with atherosclerotic diseases continue to face substantial residual risk, which may, in part, be attributed to persistent vascular inflammation.<sup>29</sup> Recent clinical trials have shown that anti-inflammatory therapies offer novel strategies for preventing secondary cardiovascular events in individuals with a history of atherosclerosis. However, these treatments have not led to significant improvements in overall mortality rates.<sup>30,</sup>

31

Among the major cardiovascular events associated with atherosclerosis, the rupture of AAA is particularly concerning due to its high lethality and its substantial contribution to global morbidity and mortality.<sup>32</sup> Although there is an established correlation between AAA formation and atherosclerotic progression, conventional anti-atherosclerotic therapies, including the management of lifestyle-related risk factors, have shown limited efficacy in slowing AAA progression or preventing rupture. Currently, there are no effective pharmacological treatments for AAA. As a result, early-stage AAA is typically managed through a "watchful waiting" approach, involving regular monitoring of aneurysm growth, with surgical intervention reserved for cases where rupture risk exceeds that of the procedure itself. Thus, a more

comprehensive understanding of the mechanisms underlying AAA formation, as well as the development of non-invasive therapeutic strategies for early-stage intervention, is urgently needed.

Accumulating evidence suggests that pathological aortic inflammation, driven by dysregulated innate and adaptive immune responses, plays a critical role in the development of AAA.<sup>33</sup> Similarly, chronic T cell-mediated immune dysregulation is a key factor in the pathogenesis of atherosclerosis.<sup>34</sup> Single-cell RNA sequencing (scRNA-seq) of abdominal aortas from mouse models of AAA, induced by either angiotensin II or elastase, has revealed that immune cells, including macrophages, T cells, and B cells, are the predominant infiltrating cell types in aneurysmal lesions.<sup>35, 36</sup> In line with these findings, clinical data from human carotid artery plaques, analyzed through single-cell proteomics and transcriptomics, show that activated and differentiated T cells are major constituents of the immune infiltrates.<sup>37</sup> These observations highlight the involvement of adaptive T cell-mediated immune responses in both atherosclerotic plaque formation and AAA development.

Specific autoantigens may drive adaptive immune responses contributing to the pathogenesis of atherosclerosis and AAA, although the precise antigens remain to be determined.<sup>33</sup> Upon antigen presentation by antigen-presenting cells, such as DCs, naïve CD4<sup>+</sup> T cells differentiate into various effector cells, including Th1, Th2, and Th17 cells. Uniquely among differentiated CD4<sup>+</sup> T cell subsets, Tregs expressing CD25 (IL-2 receptor  $\alpha$ -chain) molecule and the transcription factor forkhead box P3 (Foxp3) are pivotal in maintaining immunological self-tolerance and homeostasis.<sup>38</sup> Tregs have been shown to play a protective role in the development of experimental AAA<sup>39</sup> and atherosclerosis.<sup>40, 41</sup>

Although chronic aortic inflammation mediated by helper T cells is recognized as a significant contributor to both atherosclerosis<sup>34</sup> and AAA,<sup>33</sup> the immunological mechanisms underlying these diseases remain incompletely understood. Th1 cells reportedly promote

atherosclerosis by secreting proinflammatory IFN- $\gamma$ .<sup>34</sup> In contrast, genetic deletion of IFN- $\gamma$  in apolipoprotein E-deficient (*ApoE*<sup>-/-</sup>) mice has been shown to protect against AAA formation,<sup>42</sup> suggesting a differential role of IFN- $\gamma$  signaling in atherosclerosis and AAA pathogenesis. A shift in the Th1/Th2 balance toward Th1 cell predominance is associated with accelerated atherosclerosis,<sup>34</sup> while a Th2 cell-skewed immune responses may exacerbate AAA development.<sup>33</sup> This discrepancy indicates that distinct helper T cell subsets may differentially influence plaque formation and aortic dilation in hypercholesterolemic mice.

The coinhibitory molecule CTLA-4 has been shown to protect against experimental atherosclerosis<sup>23</sup> and AAA<sup>22</sup> by broadly suppressing T cell-mediated immune responses, including those mediated by Th1 and Th2 cells. This suggests that global suppression of helper T cell responses could limit atherosclerosis and AAA. However, the specific effects of modulating individual helper T cell subsets on these diseases have yet to be fully elucidated.

The chemokine system plays a crucial role in the recruitment of monocytes and T cells to sites of aortic inflammation during AAA development.<sup>33, 43</sup> Chemokines such as CCL17 (thymus- and activation-regulated chemokine) and CCL22 (macrophage-derived chemokine) interact with their specific receptor, CCR4, to direct immune cell trafficking to inflammatory sites.<sup>44</sup> CCR4 is expressed by various T cell subsets, including Th2, Th17, and Tregs.<sup>28</sup> In models of inflammatory autoimmune diseases, the CCL17/CCL22-CCR4 axis has been shown to recruit Tregs to inflamed tissues, where they exert protective effects.<sup>45, 46</sup> However, the role of this axis in the development of atherosclerosis and AAA remains unexplored. Given the distinct roles of Th1 and Th2 cells in atherosclerosis and AAA, the deletion of CCR4 may exacerbate atherosclerosis by disrupting Treg homeostasis and promoting Th1-mediated inflammation. In contrast, the effect of CCR4 deletion on AAA may depend on which modulation—Treg dysregulation or Th1 cell augmentation—has a greater impact on aortic dilation.

This study aims to address these gaps by investigating the role of CCR4 in the development of atherosclerosis and angiotensin II-induced AAA using CCR4-deficient (*Ccr4*<sup>-/-</sup>) mice on a hypercholesterolemic *Apoe*<sup>-/-</sup> background. The focus will be on elucidating the immunoinflammatory mechanisms mediated by T cells.

## 1.2. Results

### 1.2.1. Confirmation of CCR4 expression in Tregs/non-Tregs and detections of its ligands CCL17/CCL22 in the atherosclerotic plaque and aneurysmal tissue

CCR4 is expressed by T cells with a particular predominance of CD4<sup>+</sup>Foxp3<sup>+</sup> Tregs. This study evaluated this expression by isolating immune cells from the peripheral lymph nodes (LNs), spleen, and para-aortic LNs of wild-type, *Apoe*<sup>-/-</sup>, and *Ccr4*<sup>-/-</sup>*Apoe*<sup>-/-</sup> mice. The cells were stained accordingly and gated on Foxp3 to differentiate Tregs and non-Tregs, and the CCR4 expression was plotted through flow cytometric analysis. Among the two helper T cell subsets, high expression of CCR4 can be detected in 15%–25% CD4<sup>+</sup>Foxp3<sup>+</sup> Tregs from wild-type or *Apoe*<sup>-/-</sup> mice. Conversely, CCR4 expression on CD4<sup>+</sup>Foxp3<sup>-</sup> non-Tregs of these mice was conspicuously lower. Accordingly, CCR4 was predominantly expressed by Tregs, and the expression levels were likely not affected by hypercholesterolemia (**Figure 3A–C**). A similar experiment was performed using cells isolated from the whole aorta sample, and consistent findings were obtained (**Figure 3D**).

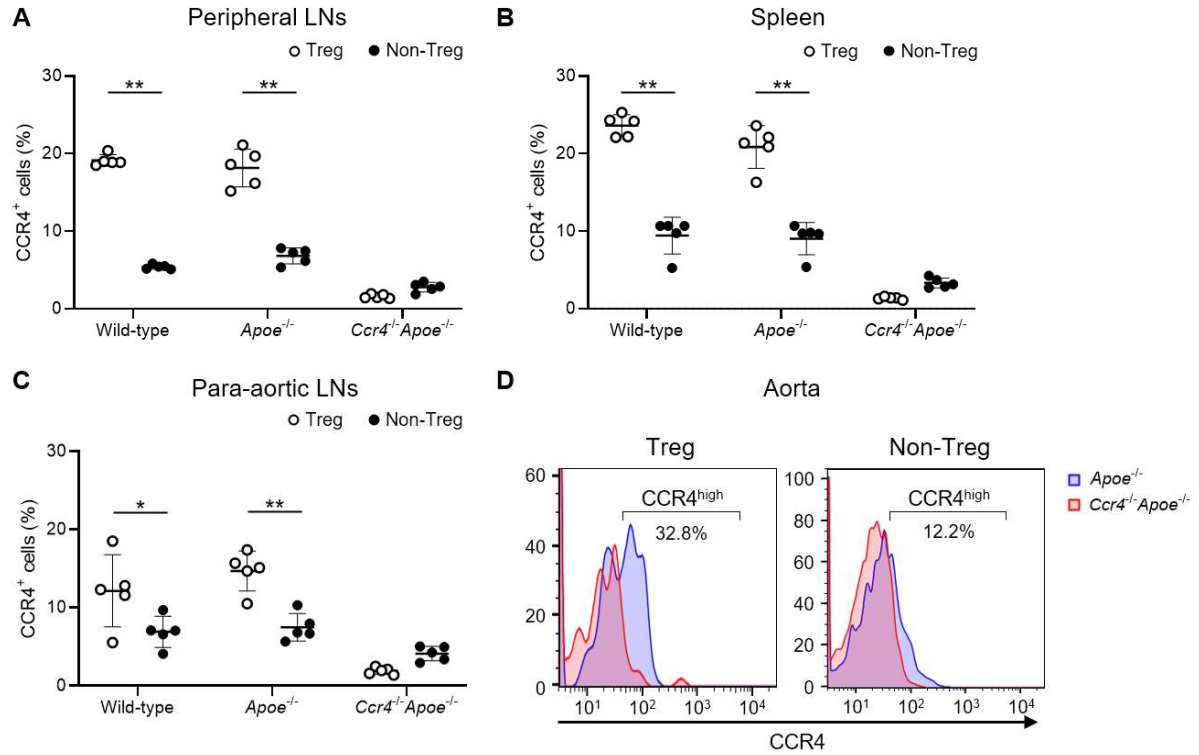


**Figure 3. CCR4 is predominantly expressed on CD4<sup>+</sup>Foxp3<sup>+</sup> Tregs.** (A-C), The graphs represent the proportions of CCR4<sup>+</sup> cells in CD4<sup>+</sup>Foxp3<sup>+</sup> Tregs and CD4<sup>+</sup>Foxp3<sup>-</sup> non-Tregs in the peripheral LNs (A), spleen (B), and para-aortic LNs (C) of 18-week-old wild-type, *Apoe*<sup>-/-</sup>, or *Ccr4*<sup>-/-</sup>*Apoe*<sup>-/-</sup> mice assessed by flow cytometry. n=5 per group. Data points represent individual animals. Horizontal bars represent means. Error bars indicate s.d. \**P* < 0.05, \*\**P* < 0.01; 2-way ANOVA followed by Tukey's multiple comparisons test. (D), Representative flow cytometric analysis of CCR4 expression in aortic CD4<sup>+</sup>Foxp3<sup>+</sup> Tregs and CD4<sup>+</sup>Foxp3<sup>-</sup> non-Tregs from 18-week-old *Apoe*<sup>-/-</sup> or *Ccr4*<sup>-/-</sup>*Apoe*<sup>-/-</sup> mice. Pooled aortic lymphoid cells from 7-8 mice in each group were used. Data are representative of two independent experiments.

In addition to performing experiments using a mouse model of AAA, particularly via angiotensin II infusion into hypercholesterolemic mice, the effect of angiotensin II administration on the expression of CCR4 was observed. Flow cytometric analysis of CD4<sup>+</sup> helper T cells revealed that 10%–20% of CD4<sup>+</sup>Foxp3<sup>+</sup> Tregs in the peripheral LNs and spleens of saline-infused *Apoe*<sup>-/-</sup> mice expressed CCR4, whereas much lower expression was detected on CD4<sup>+</sup>Foxp3<sup>-</sup> non-Tregs in these mice (**Figure 4**). In addition, angiotensin II infusion led to the modest upregulation of CCR4 expression in peripheral LN Tregs (**Figure 4A**).

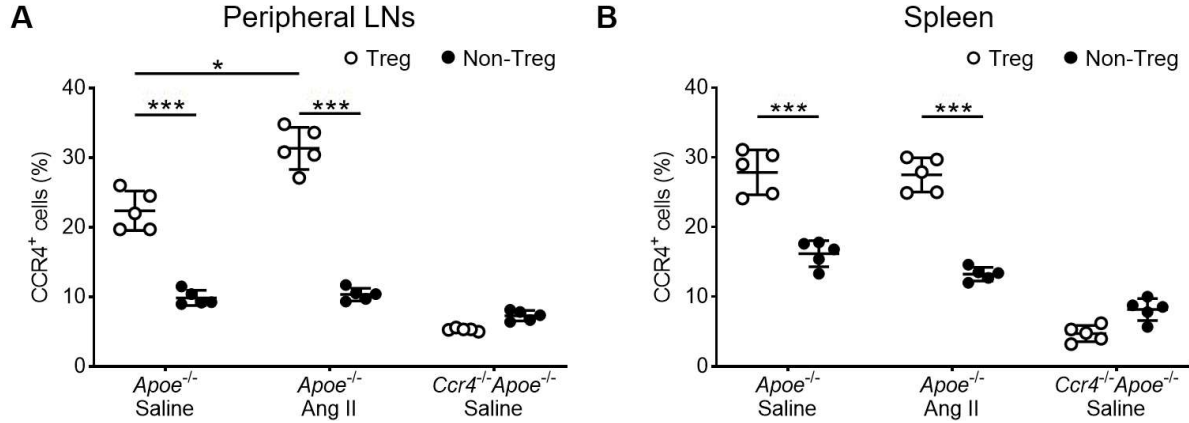


**Figure 4. CCR4 is predominantly expressed on CD4<sup>+</sup>Foxp3<sup>+</sup> Tregs under angiotensin II treatment.**

Seven days after the pump implantation, the mice were euthanized and lymphoid cells from LNs and spleen were prepared. *Apoe*<sup>-/-</sup> mice infused with angiotensin II or saline served as controls. (A) and (B), The graphs represent the proportions of CCR4<sup>+</sup> cells in CD4<sup>+</sup>Foxp3<sup>+</sup> Tregs and CD4<sup>+</sup>Foxp3<sup>-</sup> non-Tregs in the peripheral LNs (A) and spleen (B) of *Apoe*<sup>-/-</sup> or *Ccr4*<sup>-/-</sup>*Apoe*<sup>-/-</sup> mice infused with angiotensin II or saline assessed by flow cytometry. n=5 per group. Data points represent individual animals. Horizontal bars represent means. Error bars indicate s.d. \**P*<0.05, \*\*\**P*<0.001; 2-way ANOVA followed by Tukey's multiple comparisons test.

High expression levels of CCL17 and CCL22, the two chemokines known as specific ligands for CCR4, are constitutively secreted by DCs in lymphoid tissues.<sup>47, 48</sup> Therefore, I examined their presence in the peripheral LNs of saline- or angiotensin II-infused *Apoe*<sup>-/-</sup> and *Ccr4*<sup>-/-</sup>*Apoe*<sup>-/-</sup> mice by immunofluorescence staining. Abundant expression of these chemokines was observed in the peripheral LNs of *Apoe*<sup>-/-</sup> and *Ccr4*<sup>-/-</sup>*Apoe*<sup>-/-</sup> mice regardless of angiotensin II treatment (**Figure 5**). Although I did not stain any cell markers, both ligands were presumably secreted by DCs, as the nearly exclusive secretion of CCL17<sup>47</sup> and CCL22<sup>49</sup> by DCs in LNs was previously reported by other groups.

To further evaluate the role of these chemokines in atherosclerosis, I observed the presence of CCL17 and CCL22 in the aortic sinus of wild-type, *Apoe*<sup>-/-</sup>, and *Ccr4*<sup>-/-</sup>*Apoe*<sup>-/-</sup> mice similarly through immunofluorescence staining. CCL17 expression was detected in the atherosclerotic lesions of *Apoe*<sup>-/-</sup> and *Ccr4*<sup>-/-</sup>*Apoe*<sup>-/-</sup> mice, and some lesional MOMA-2 macrophages expressed this chemokine. However, CCL17 expression was not detected in the aortic sinus of wild-type mice without atherosclerotic plaques (**Figure 6**).



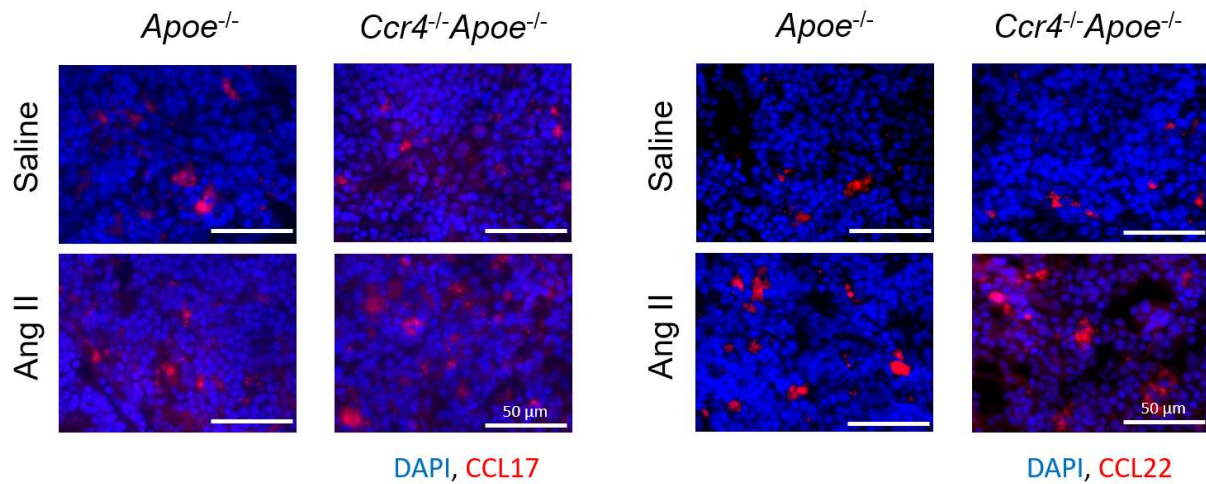


**Figure 5. CCR4 ligands are constitutively expressed in lymphoid tissues.**

Immunostaining (red) for CCL17 (left) or for CCL22 (right) in the peripheral LN of 16-week-old *Apoe*<sup>-/-</sup> or *Ccr4*<sup>-/-</sup>*Apoe*<sup>-/-</sup> mice. Nuclei were stained with DAPI (blue). Data are representative of five mice analyzed in each group. White bars represent 50  $\mu$ m.

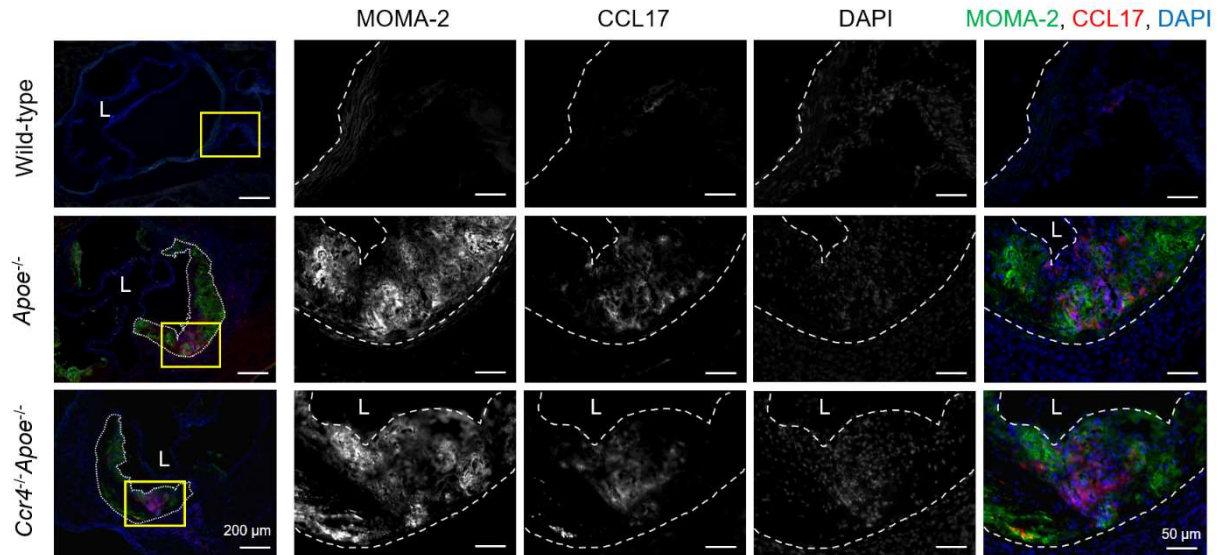


**Figure 6. Detection of CCL17 in atherosclerotic plaques.**

Immunostaining for CCL17 (red) and MOMA-2 (green) in the aortic sinus of 18-week-old wild-type, *Apoe*<sup>-/-</sup>, or *Ccr4*<sup>-/-</sup>*Apoe*<sup>-/-</sup> mice. Boxed area is expanded to show high-power fields. Nuclei were stained with DAPI (blue). Dashed lines demarcate atherosclerotic lesions or indicate the inner lining of arteries; L, lumen. Data are representative of five mice analyzed in each group. White bars represent 50 or 200  $\mu$ m as described.

Meanwhile, the other CCR4 ligand, CCL22, was modestly expressed in atherosclerotic lesions and mostly did not colocalize with lesional MOMA-2 macrophages in *Apoe*<sup>-/-</sup> or *Ccr4*<sup>-/-</sup>*Apoe*<sup>-/-</sup> mice, whereas its expression was not detected in the aortic sinus of wild-type mice (**Figure 7**).

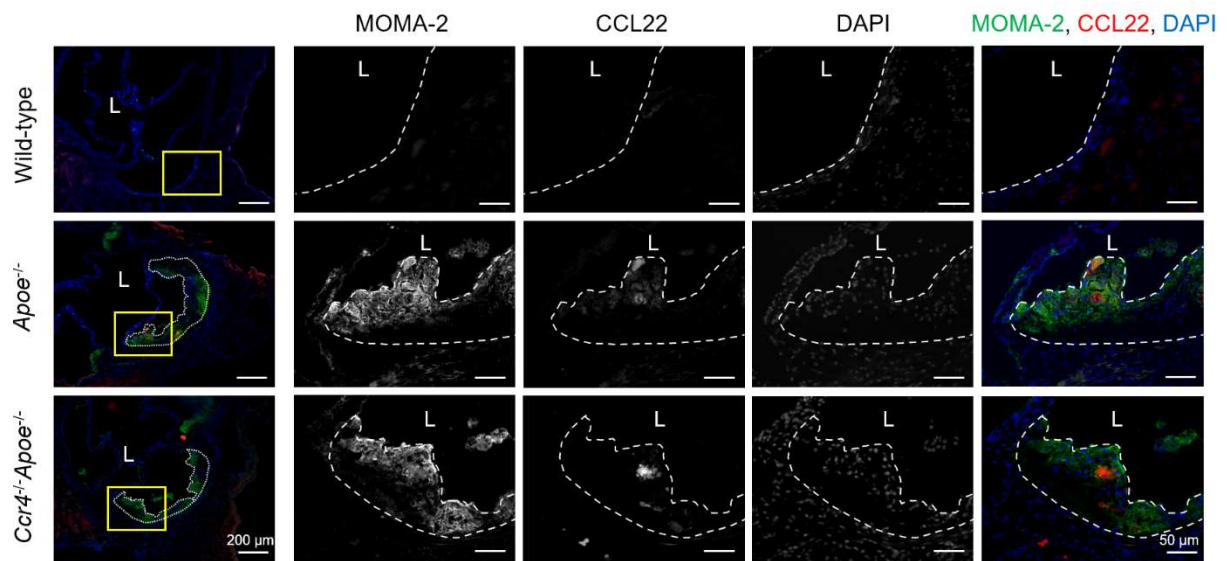


**Figure 7. Detection of CCL22 in atherosclerotic plaques.** Immunostaining for CCL22 (red) and MOMA-2 (green) in the aortic sinus of 18-week-old wild-type, *Apoe*<sup>-/-</sup>, or *Ccr4*<sup>-/-</sup>*Apoe*<sup>-/-</sup> mice. Boxed area is expanded to show high-power fields. Nuclei were stained with DAPI (blue). Dashed lines demarcate atherosclerotic lesions or indicate the inner lining of arteries; L, lumen. Data are representative of five mice analyzed in each group. White bars represent 50 or 200 μm as described.

To confirm the importance of the CCL17/CCL22–CCR4 axes within the angiotensin II-induced aneurysm model, Immunofluorescence staining was performed to detect the presence of CCL17 (**Figure 8**) and CCL22 (**Figure 9**) in the suprarenal aorta of saline- or angiotensin II-infused *Apoe*<sup>-/-</sup> and *Ccr4*<sup>-/-</sup>*Apoe*<sup>-/-</sup> mice.

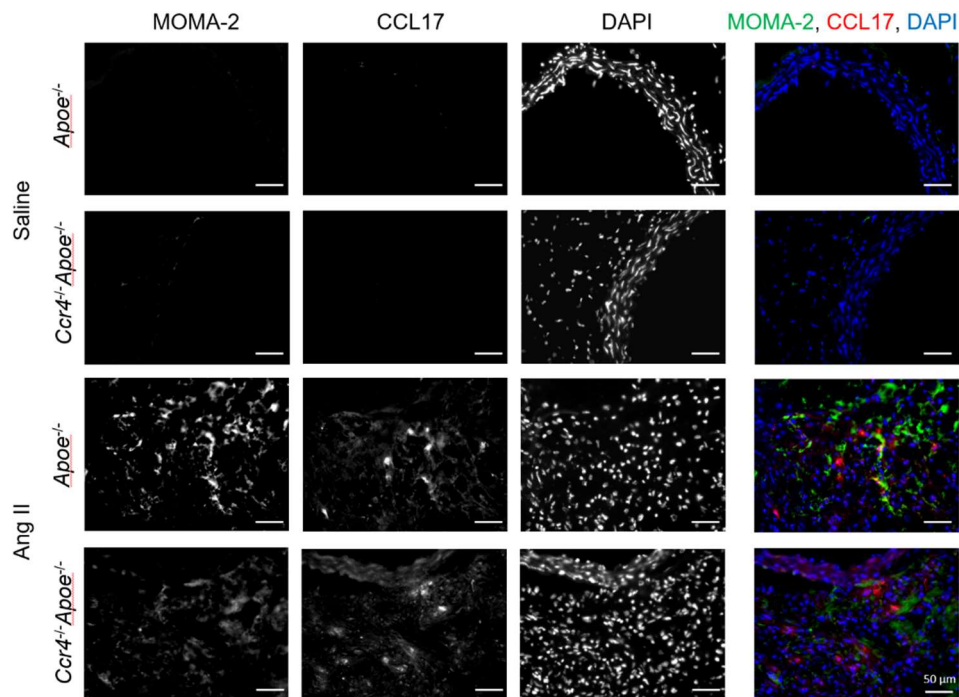


**Figure 8. Detection of CCL17 in the suprarenal aorta of angiotensin II-treated mice.** Immunostaining of CCR4 ligand CCL17 (red) and macrophage MOMA-2 (green) in the suprarenal aorta of 16-week-old *Apoe*<sup>-/-</sup> or *Ccr4*<sup>-/-</sup>*Apoe*<sup>-/-</sup> mice. Nuclei were stained with DAPI (blue). Data are representative of five mice analyzed in each group. White bars represent 50 μm.

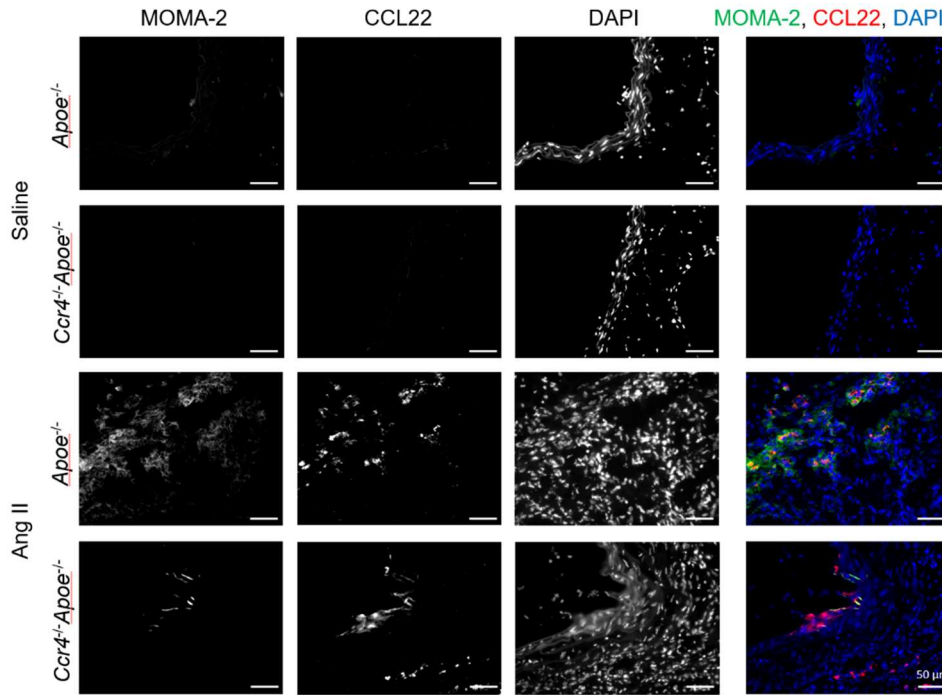


**Figure 9. Detection of CCL22 in the suprarenal aorta of angiotensin II-treated mice.** Immunostaining of CCR4 ligand CCL22 (red) and macrophage MOMA-2 (green) in the suprarenal aorta of 16-week-old *Apoe*<sup>-/-</sup> or *Ccr4*<sup>-/-</sup>*Apoe*<sup>-/-</sup> mice. Nuclei were stained with DAPI (blue). Data are representative of five mice analyzed in each group. White bars represent 50  $\mu$ m.

Similarly, CCL17 and CCL22 were observed in the suprarenal aorta of angiotensin II-treated mice. Meanwhile, CCL17 and CCL22 expression was not detected in the suprarenal aorta of saline-infused *Apoe*<sup>-/-</sup> and *Ccr4*<sup>-/-</sup>*Apoe*<sup>-/-</sup> mice.

These findings indicate that CCR4-expressing Tregs migrate to peripheral LNs and atherosclerotic lesions partly via the activation of the CCL17/CCL22–CCR4 axes under hypercholesterolemia. In the case of the angiotensin II-induced AAA model, the above evidence also reveals that CCR4-expressing Tregs migrate to the suprarenal aorta, where AAA is predilected, under angiotensin II treatment.

### **1.2.2. CCR4 deficiency conversely accelerated early atherosclerosis while attenuating angiotensin II-induced AAA in *Apoe*<sup>-/-</sup> mice**

Several studies have documented evidence of the aggravation of immune-mediated diseases in the absence of CCR4. In this study, 18-week-old *Apoe*<sup>-/-</sup> and *Ccr4*<sup>-/-</sup>*Apoe*<sup>-/-</sup> mice

were fed a standard chow diet to determine the effect of CCR4 deletion on the supposedly immune-mediated development of early atherosclerosis. Consequently, *Ccr4*<sup>-/-</sup>*Apoe*<sup>-/-</sup> mice developed normally without any spontaneous inflammatory disease. Observations of the atherosclerotic lesions in the aortic sinus of these mice distinctively showed a notable size increment compared with the control *Apoe*<sup>-/-</sup> mice. The lesion size was quantified as mean  $\pm$  s.d. and the aortic sinus mean plaque area of  $1.46 \pm 0.50 \times 10^5 \mu\text{m}^2$  was obtained for control *Apoe*<sup>-/-</sup> mice versus  $2.04 \pm 0.82 \times 10^5 \mu\text{m}^2$  for *Ccr4*<sup>-/-</sup>*Apoe*<sup>-/-</sup> mice ( $P < 0.05$ ; **Figure 10**).

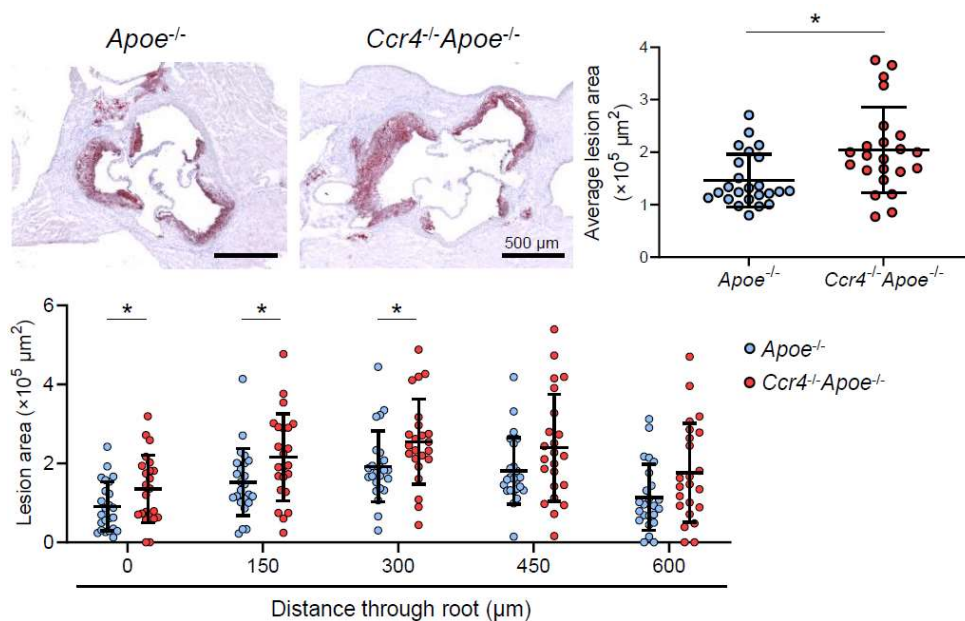


**Figure 10. CCR4 deficiency accelerates atherosclerotic plaque development in the aortic sinus.**

Representative photomicrographs of Oil Red O staining and quantitative analysis of atherosclerotic lesion area at five different levels and the average area in the aortic sinus of 18-week-old *Apoe*<sup>-/-</sup> mice (n=24) or *Ccr4*<sup>-/-</sup>*Apoe*<sup>-/-</sup> mice (n=23). Data points represent individual animals. Horizontal bars represent means. Error bars indicate s.d. \* $P < 0.05$ ; Mann-Whitney *U*-test.

Extending the observation to atherosclerosis in the entire thoracoabdominal aorta, I colorized the lipid area to define atherosclerosis lesions on the en face preparation of 18-week-old *Apoe*<sup>-/-</sup> and *Ccr4*<sup>-/-</sup>*Apoe*<sup>-/-</sup> mice fed a standard chow diet via oil red O staining. Unlike the findings for the aortic sinus, no notable differences were observed in the en face analysis of the plaque burden of the thoracoabdominal aorta between the two mouse strains. Representative photomicrographs and data plots are shown in **Figure 11**.



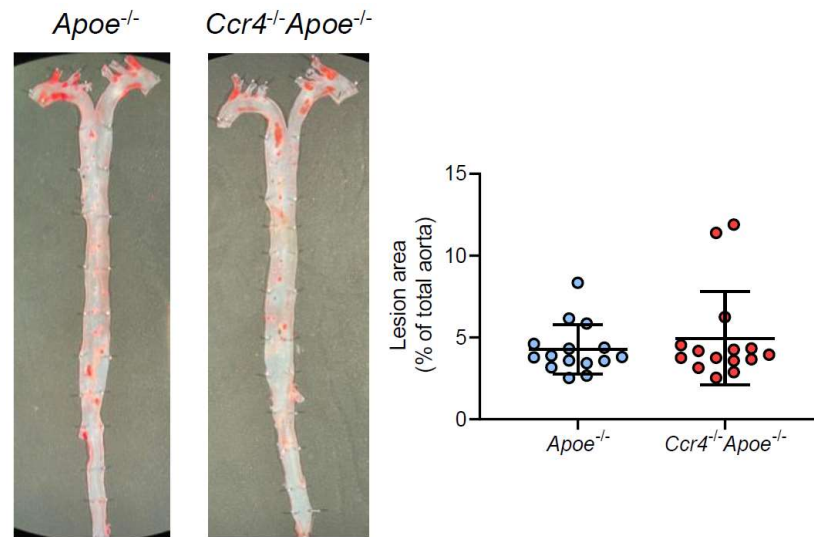


**Figure 11. En face analysis of atherosclerotic lesions in the thoracoabdominal aorta.** Representative photomicrographs of Oil Red O staining and quantitative analysis of atherosclerotic lesion area in the aorta of 18-week-old *Apoe*<sup>-/-</sup> (n=15) or *Ccr4*<sup>-/-</sup>*Apoe*<sup>-/-</sup> mice (n=15). Data points represent individual animals. Horizontal bars represent means. Error bars indicate s.d.

Despite the distinct plaque burden in the aortic sinus, no significant differences were observed in body weight or plasma lipid profile between the two strains at the time of sacrifice (Table 1).

**Table 1. Body weight and plasma lipid profile in 18-week-old mice.**

	<i>Apoe</i> <sup>-/-</sup>	<i>Ccr4</i> <sup>-/-</sup> <i>Apoe</i> <sup>-/-</sup>
Body weight (g)	31.76 ± 1.94 (n=27)	31.69 ± 2.24 (n=27)
Total cholesterol (mg/dL)	526.5 ± 146.3 (n=10)	520.4 ± 150.6 (n=10)
HDL-cholesterol (mg/dL)	24.90 ± 6.49 (n=10)	19.80 ± 5.87 (n=10)
Triglycerides (mg/dL)	89.70 ± 21.07 (n=10)	86.40 ± 39.58 (n=10)

HDL, high-density lipoprotein.

The degree of inflammation was inferred by analyzing the immune cells within the lesion. Immunostaining was performed using anti-MOMA-2 antibodies in atherosclerosis lesions of the aortic sinus, which marked the presence of proinflammatory macrophages. Both strains of mice showed positive MOMA-2 staining within their atherosclerotic lesions. However, compared with the atherosclerotic lesions of *Apoe*<sup>-/-</sup> mice, those of

*Ccr4<sup>-/-</sup>Apoe<sup>-/-</sup>* mice showed a 20% larger proportion of macrophage area. Representative photomicrographs and data plots are shown in **Figure 12**.

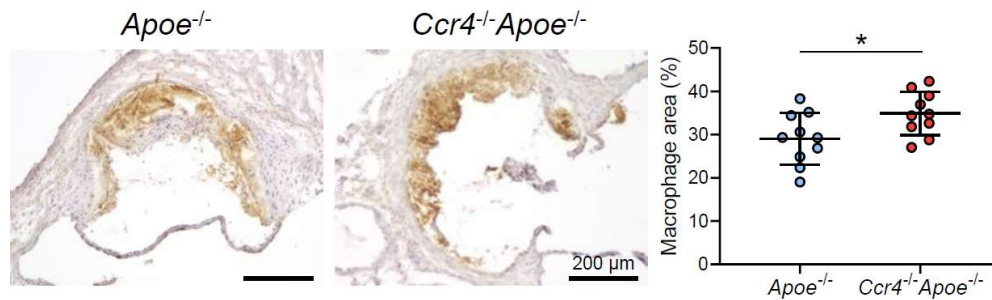


**Figure 12.** Representative sections and quantitative analysis of MOMA-2<sup>+</sup> macrophages area in the aortic sinus of 18-week-old *Apoe<sup>-/-</sup>* or *Ccr4<sup>-/-</sup>Apoe<sup>-/-</sup>* mice. Data points represent individual animals. n=10 per group. Horizontal bars represent means. Error bars indicate s.d. \**P*<0.05; 2-tailed Student's *t*-test.

Clinical and experimental studies have demonstrated the importance of the helper T cell immune response in the development of atherosclerosis. Immunostaining of CD4 molecules was performed to assess whether CCR4 deficiency affects helper T cell infiltration into the atherosclerotic plaque. Immunohistochemical analysis of positively stained cells revealed a remarkable 42% increase in CD4<sup>+</sup> T cell infiltration. Representative photomicrographs and data plots are shown in **Figure 13**. Additionally, this study further identified the Treg subset within these helper T cells by specifically staining Foxp3<sup>+</sup> Tregs in atherosclerotic lesions using an anti-Foxp3 antibody. Only a few Foxp3<sup>+</sup> Tregs were detected within the plaques of *Apoe<sup>-/-</sup>* or *Ccr4<sup>-/-</sup>Apoe<sup>-/-</sup>* mice, making it incompatible for comparison between the two strains.

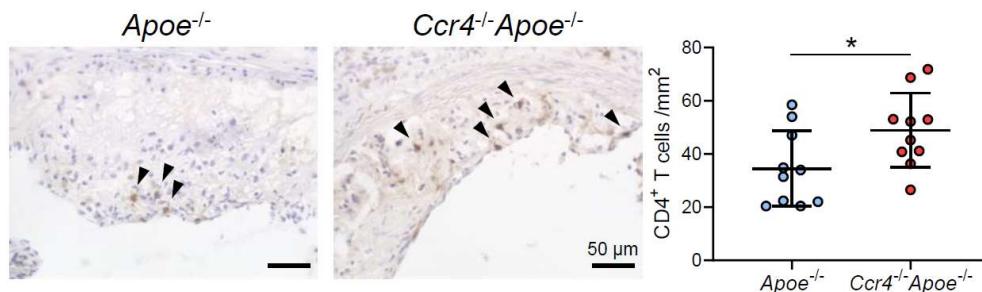


**Figure 13.** Representative sections and quantitative analysis of CD4<sup>+</sup> T cells in the aortic sinus of 18-week-old *Apoe<sup>-/-</sup>* or *Ccr4<sup>-/-</sup>Apoe<sup>-/-</sup>* mice. Arrowheads indicate the CD4<sup>+</sup> T cells. n=10 per group. Data points represent individual animals. Horizontal bars represent means. Error bars indicate s.d. \**P*<0.05; 2-tailed Student's *t*-test.

Collagen contributes to determining the stability of the atherosclerotic plaque. Higher collagen content within a plaque indicates the robustness of the structure against rupture. To evaluate the effect of CCR4 deletion on plaque stability, collagen fibers within the plaques were distinguished using Masson's trichrome collagen staining. The proportion of collagen (blue) in the aortic sinus plaques of *Ccr4*<sup>-/-</sup>*Apoe*<sup>-/-</sup> mice was significantly lower than that in the aortic sinus plaques of *Apoe*<sup>-/-</sup> mice. Representative photomicrographs and data plots are shown in **Figure 14**.

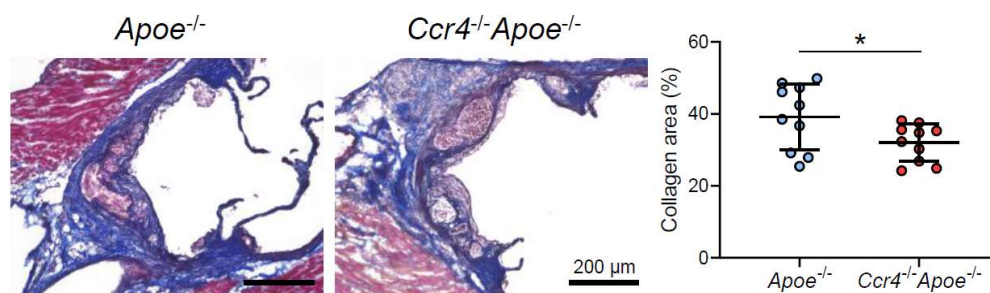


**Figure 14.** Representative sections and quantitative analysis of collagen in the aortic sinus of 18-week-old *Apoe*<sup>-/-</sup> or *Ccr4*<sup>-/-</sup>*Apoe*<sup>-/-</sup> mice. n=10 per group. Data points represent individual animals. Horizontal bars represent means. Error bars indicate s.d. \**P*<0.05; 2-tailed Student's *t*-test.

To further evaluate aortic immunoinflammatory responses, I analyzed the mRNA expression of pro- and anti-inflammatory cytokines and transcription factors specific to Tregs or helper T cell subsets in the atherosclerotic aorta by quantitative reverse transcription PCR. The mRNA expression of proinflammatory cytokines (*Il1b* and *Il6*), Th1-related *Tbx21*, and Th17-related *Rorc* was markedly upregulated in the aorta of *Ccr4*<sup>-/-</sup>*Apoe*<sup>-/-</sup> mice, indicating augmented proatherogenic immune responses in the atherosclerotic aorta. The respective data plots are shown in **Figure 15**. Meanwhile, the mRNA expression of the Treg-specific transcription factor *Foxp3* was undetectable.

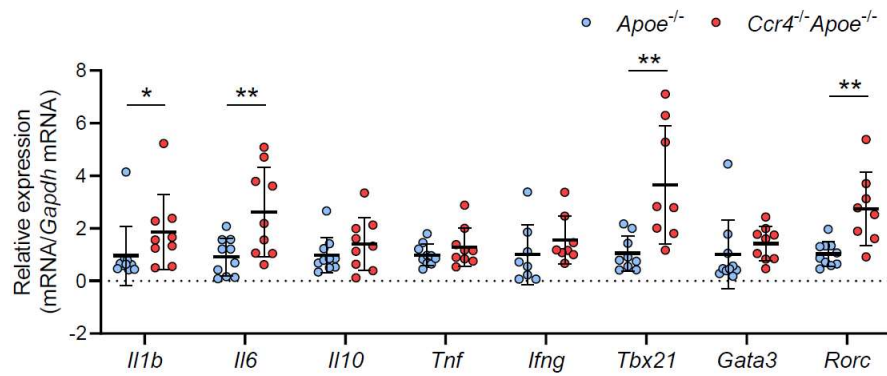


**Figure 15. Messenger RNA expression of pro- or anti-inflammatory cytokines and helper T cell-associated transcription factors in the aorta of 18-week-old *Apoe*<sup>-/-</sup> or *Ccr4*<sup>-/-</sup>*Apoe*<sup>-/-</sup> mice.**

The expression levels of the target genes were normalized so that the mean values in *Apoe*<sup>-/-</sup> mice were set to 1. n=8 to 10 per group. Data points represent individual animals. Horizontal bars represent means. Error bars indicate s.d. \**P*<0.05, \*\**P*<0.01; Mann-Whitney *U*-test: *Il1b*; 2-tailed Student's *t*-test: *Il6*, *Tbx21*, and *Rorc*.

These collective findings on atherosclerotic lesion size and component characteristics reveal the essential roles of CCR4 in preventing the progression of early atherosclerotic lesions and mediating a less inflammatory plaque phenotype. Moreover, quantitative real-time PCR data revealed a generally more inflamed aorta in CCR4-deficient mice under a hypercholesterolemic state.

AAA is one of the most prominent vascular diseases related to atherosclerosis because of its likely fatal outcome. This study further elucidated the effect of CCR4 deficiency on the development of an aneurysm in the experimental mouse model of angiotensin II-induced AAA. Similarly, *Ccr4*<sup>-/-</sup> mice were used on an atherosclerosis-prone *Apoe*<sup>-/-</sup> background. AAA was induced by implanting a miniosmotic pump that continuously infused angiotensin II into *Ccr4*<sup>-/-</sup>*Apoe*<sup>-/-</sup> and control *Apoe*<sup>-/-</sup> mice, which were fed a high-fat and high-cholesterol diet. Mice were euthanized for the analysis of AAA formation 4 weeks after the initiation of angiotensin II treatment. Some *Apoe*<sup>-/-</sup> and *Ccr4*<sup>-/-</sup>*Apoe*<sup>-/-</sup> mice were infused with saline instead of angiotensin II to serve as sham groups and euthanized at the same time point. The experimental flowchart is shown in **Figure 16**.



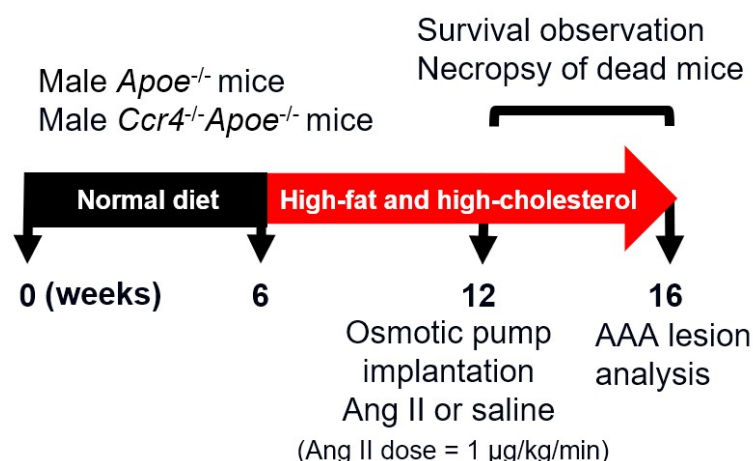


**Figure 16. Experimental flowchart for AAA experiments.**  
Ang II indicates angiotensin II.

At the time of sacrifice at 16 weeks of age, CCR4-deficient mice showed significantly higher body weight and visibly more abundant abdominal fat tissue. This difference was apparent at 12 weeks of age when the mice were weighed to adjust the angiotensin II dose. These findings indicate that, the 6-week high-fat and high-cholesterol diet led to greater adipose tissue accumulation in CCR4-deficient mice compared with controls, which is consistent with a previous report linking the CCL22/CCR4 axis to adipocyte thermogenesis and obesity prevention.<sup>50</sup> However, the plasma lipid profiles of *Apoe*<sup>-/-</sup> and *Ccr4*<sup>-/-</sup>*Apoe*<sup>-/-</sup> mice remained at similar levels. As expected, four weeks of angiotensin II treatment effectively induced a hypertensive state marked by an elevation in systolic blood pressure (SBP) in *Apoe*<sup>-/-</sup> and *Ccr4*<sup>-/-</sup>*Apoe*<sup>-/-</sup> mice. Nevertheless, no significant differences in SBP were observed between the two strains before and after treatment (**Table 2**).

The survival analysis curve recorded a chronological survival rate, counting the number of days after angiotensin II or saline pump implantation. Angiotensin II-infused mice exhibited a reduced survival rate over time, with most deaths occurring in the first week of treatment. Although angiotensin II-infused *Ccr4*<sup>-/-</sup>*Apoe*<sup>-/-</sup> exhibited a slightly higher survival rate, it was not statistically significant. Expectedly, the saline-infused sham groups showed a 100% survival rate until the end of the experiment (**Figure 17**)

**Table 2. Body weight, systolic blood pressure, and plasma lipid profile of *Apoe*<sup>-/-</sup> or *Ccr4*<sup>-/-</sup>*Apoe*<sup>-/-</sup> mice sacrificed at 16 weeks of age**

Parameters	<i>Apoe</i> <sup>-/-</sup>	<i>Ccr4</i> <sup>-/-</sup> <i>Apoe</i> <sup>-/-</sup>
Body weight, g	26.3 ± 2.3 (n=33)	28.9 ± 2.5 (n=37)***
SBP (before), mmHg	92.4 ± 6.1 (n=15)	92 ± 5.9 (n=15)
SBP (after), mmHg	153.2 ± 14.4 (n=15) †††	153.2 ± 9.1 (n=15) †††
Total-cholesterol, mg/dL	885 ± 226.4 (n=10)	935.6 ± 109.4 (n=10)
HDL, mg/dL	20.4 ± 8.5 (n=10)	18.5 ± 6.2 (n=10)
Triglycerides, mg/dL	102.5 ± 41 (n=10)	104.5 ± 30.2 (n=10)

Data are expressed as the mean ± s.d. \*\*\*; vs. *Apoe*<sup>-/-</sup> *P*<0.001; two-tailed Student's *t*-test; †††; vs. SBP (before) *P*<0.001; paired *t*-test. HDL indicates high density lipoprotein; SBP, systolic blood pressure; SBP (before), SBP before angiotensin II infusion; SBP (after), SBP after angiotensin II infusion for 4 weeks.

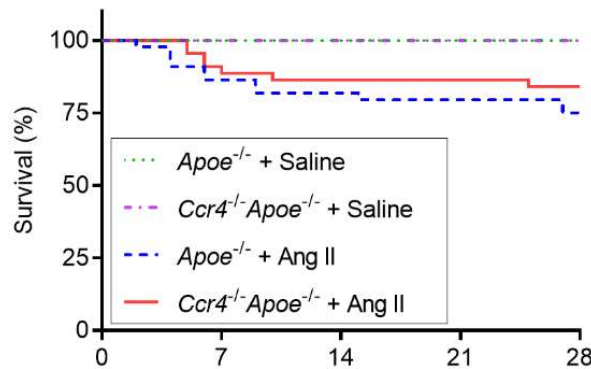


**Figure 17. Survival curve of mice 4 weeks after pump implantation.**

Twelve-week-old *Apoe*<sup>-/-</sup> or *Ccr4*<sup>-/-</sup>*Apoe*<sup>-/-</sup> mice fed a high-fat and high-cholesterol diet were infused with angiotensin II or saline for 28 days and were euthanized at 16 weeks of age for evaluation of AAA formation. *Apoe*<sup>-/-</sup> mice infused with angiotensin II or saline served as controls. Kaplan-Meier curve shows survival rate in angiotensin II-infused *Apoe*<sup>-/-</sup> (n=44) and *Ccr4*<sup>-/-</sup>*Apoe*<sup>-/-</sup> mice (n=44), or saline-infused *Apoe*<sup>-/-</sup> (n=8) and *Ccr4*<sup>-/-</sup>*Apoe*<sup>-/-</sup> (n=8) mice. Ang II indicates angiotensin II.

Forty-four mice of each mouse strain were infused with angiotensin II. In terms of mortality, 11 deaths were recorded in angiotensin II-infused *Apoe*<sup>-/-</sup> mice, representing a 25% mortality rate. Meanwhile, seven deaths were recorded in angiotensin II-infused *Ccr4*<sup>-/-</sup>*Apoe*<sup>-/-</sup> mice, amounting to a 15.9% mortality rate. Nevertheless, the differences between *Apoe*<sup>-/-</sup> and *Ccr4*<sup>-/-</sup>*Apoe*<sup>-/-</sup> mice were not statistically significant (**Figure 18**, left). All deaths were attributed to aortic rupture (either thoracic or abdominal), which was discovered through necropsy (**Figure 18**, right).

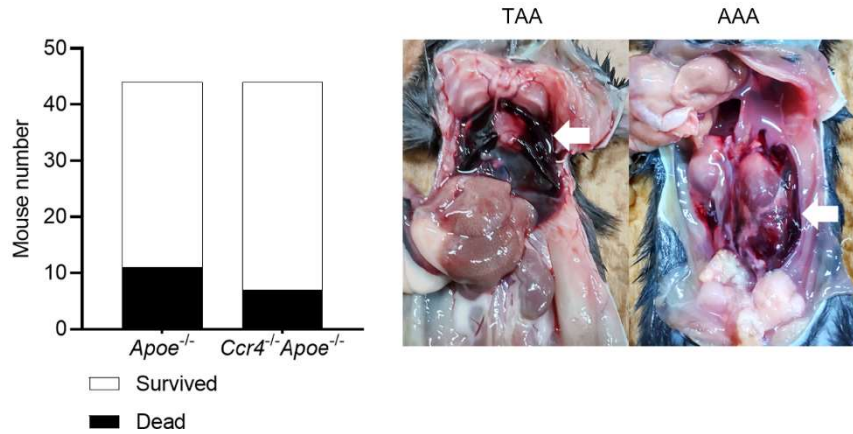


**Figure 18. Mortality analysis of angiotensin II-infused mice.**

Twelve-week-old *Apoe*<sup>-/-</sup> or *Ccr4*<sup>-/-</sup>*Apoe*<sup>-/-</sup> mice fed a high-fat and high-cholesterol diet were infused with angiotensin II or saline for 28 days and were euthanized at 16 weeks of age for evaluation of AAA formation. *Apoe*<sup>-/-</sup> mice infused with angiotensin II or saline served as controls. Left, mortality due to AAA rupture in angiotensin II-infused *Apoe*<sup>-/-</sup> (n=44), *Ccr4*<sup>-/-</sup>*Apoe*<sup>-/-</sup> (n=44) mice. Right, representative images from necropsy. White arrows indicate blood pool due to aortic rupture. TAA: thoracic aortic aneurysm; AAA: abdominal aortic aneurysm.

Angiotensin II infusion effectively induced the dilation of the suprarenal aorta in hypercholesterolemic mice. In general, gross visual observation of aorta samples indicated a less dilated suprarenal aorta phenotype in angiotensin II-infused *Ccr4*<sup>-/-</sup>*Apoe*<sup>-/-</sup> mice. Meanwhile, saline-infused mice from both strains exhibited smooth, nondilated aortas (**Figure 19**).

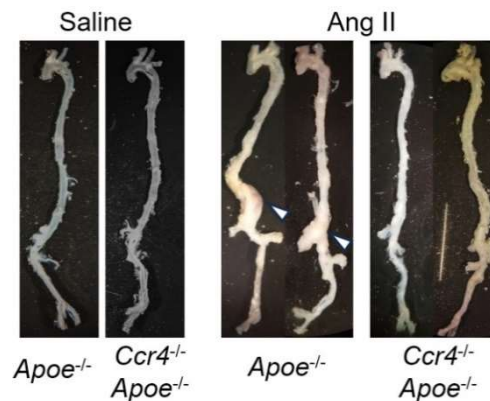


**Figure 19. Gross anatomy of thoracoabdominal aortas.**

Twelve-week-old *Apoe*<sup>-/-</sup> or *Ccr4*<sup>-/-</sup>*Apoe*<sup>-/-</sup> mice fed a high-fat and high-cholesterol diet were infused with angiotensin II or saline for 28 days and were euthanized at 16 weeks of age for evaluation of AAA formation. *Apoe*<sup>-/-</sup> mice infused with angiotensin II or saline served as controls. Representative photographs displaying macroscopic features of aneurysms induced by angiotensin II. None of the animals infused with saline developed aneurysm. Arrowheads indicate AAA. Ang II indicates angiotensin II.

Almost all (93.2%) angiotensin II-infused *Apoe*<sup>-/-</sup> mice developed AAA. This strikingly high incidence was abated by CCR4 deficiency, which reduced the incidence by almost half (52.3%), as observed in angiotensin II-infused *Ccr4*<sup>-/-</sup>*Apoe*<sup>-/-</sup> mice. Moreover, when the severity

of AAA was analyzed using the accepted grading scale, the AAA phenotype of angiotensin II-infused *Ccr4<sup>-/-</sup>Apoe<sup>-/-</sup>* mice scored much lower severity compared to angiotensin II-infused *Apoe<sup>-/-</sup>* mice (**Figure 20**).

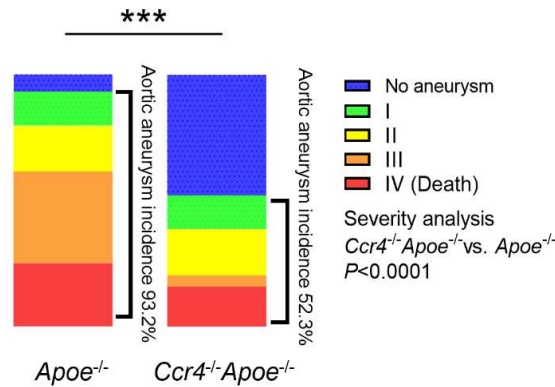


**Figure 20. Incidence and severity analysis of angiotensin II-induced AAA.**

Twelve-week-old *Apoe<sup>-/-</sup>* or *Ccr4<sup>-/-</sup>Apoe<sup>-/-</sup>* mice fed a high-fat and high-cholesterol diet were infused with angiotensin II for 28 days and were euthanized at 16 weeks of age for evaluation of AAA formation. Incidence and severity of aneurysm in angiotensin II-infused *Apoe<sup>-/-</sup>* (n=44) and *Ccr4<sup>-/-</sup>Apoe<sup>-/-</sup>* (n=44) mice. \*\*\* $P < 0.001$ ; chi-squared test: incidence analysis; Mann-Whitney *U*-test: severity analysis.

Furthermore, a quantitative analysis of the AAA phenotype was performed by measuring the maximum diameter of the dilated suprarenal aorta. Consistently, lower maximum diameters of the suprarenal aortas were discovered in angiotensin II-infused *Ccr4<sup>-/-</sup>Apoe<sup>-/-</sup>* mice compared with angiotensin II-infused *Apoe<sup>-/-</sup>* mice (**Figure 21**).

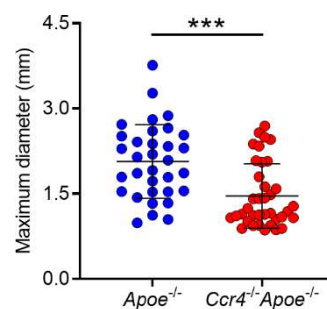


**Figure 21. Quantitative analysis of maximum suprarenal aorta diameter.**

Twelve-week-old *Apoe<sup>-/-</sup>* or *Ccr4<sup>-/-</sup>Apoe<sup>-/-</sup>* mice fed a high-fat and high-cholesterol diet were infused with angiotensin II for 28 days and were euthanized at 16 weeks of age for evaluation of AAA formation. Maximum diameter of abdominal aorta in angiotensin II-infused *Apoe<sup>-/-</sup>* (n=33) and *Ccr4<sup>-/-</sup>Apoe<sup>-/-</sup>* (n=37) mice. Data points represent individual animals. Horizontal bars represent means. Error bars indicate s.d. \*\*\* $P < 0.001$ ; Mann-Whitney *U*-test.

These results demonstrate two different directions of CCR4 deficiency on atherosclerotic diseases. They revealed a detrimental effect on early atherosclerosis

accumulation while displaying beneficial effects of CCR4 deficiency on AAA development, although no difference in rupture incidence was observed.

### 1.2.3. Reduction of inflammatory responses in aneurysmal tissues and preservation of the arterial wall integrity of angiotensin II-treated mice in the absence of CCR4

The angiotensin II-induced AAA model of hypercholesterolemic mice repeatedly showed that aortic inflammation initiates the development of AAA.<sup>32</sup> Although several types of immune cells are recruited during aneurysm progression, the main constituents of the infiltrating cells in aneurysmal tissues are macrophages and CD4<sup>+</sup> T cells. To assess phenotypic changes in angiotensin II-induced aortic wall inflammation in CCR4-deficient aorta, I performed immunohistochemical studies on aneurysm tissue cross-sections to detect immune cell infiltration. Through MOMA-2 immunostaining, compared with the aneurysmal lesions of angiotensin II-infused *Apoe*<sup>-/-</sup> mice, those of angiotensin II-infused *Ccr4*<sup>-/-</sup>*Apoe*<sup>-/-</sup> mice showed significantly lower accumulation of macrophages (**Figure 22**).

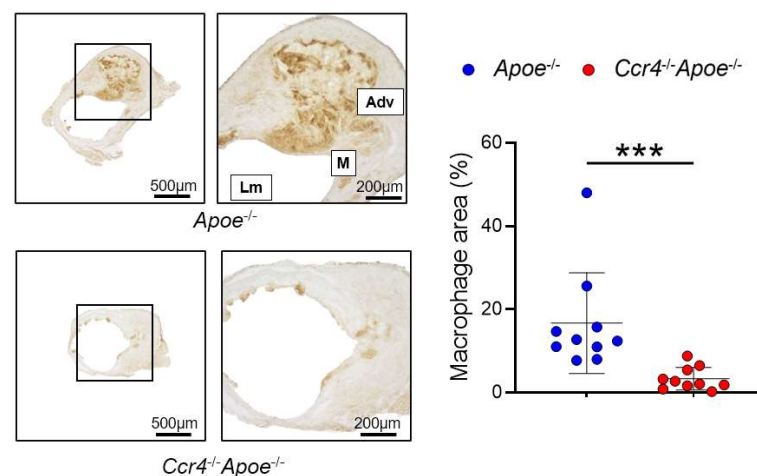


**Figure 22. Representative sections and quantitative analysis of MOMA-2<sup>+</sup> macrophages in the AAA lesions of angiotensin II-infused *Apoe*<sup>-/-</sup> or *Ccr4*<sup>-/-</sup>*Apoe*<sup>-/-</sup> mice.**

Suprarenal aorta crosssections of *Apoe*<sup>-/-</sup> or *Ccr4*<sup>-/-</sup>*Apoe*<sup>-/-</sup> mice fed a high-fat and high-cholesterol diet, infused with angiotensin II for 28 days, and euthanized at 16 weeks of age. Boxed areas are expanded to show representative high-power fields in serial sections. Lm indicates lumen; M, media; Adv, adventitia. Black bars represent 200 or 500 µm as described. Data points represent individual animals, n=10 per group. Horizontal bars represent means. Error bars indicate s.d. \*\*\**P*<0.001; Mann-Whitney *U*-test.

The effects of CCR4 deletion on the adaptive immune response cellular mediator, CD4<sup>+</sup> helper T cells, were evaluated by immunostaining CD4 molecules in aneurysmal tissue cross-sections. Similarly, this study identified a marked reduction in CD4<sup>+</sup> T cell infiltration into the suprarenal aorta of angiotensin II-infused *Ccr4*<sup>-/-</sup>*Apoe*<sup>-/-</sup> mice compared with angiotensin II-infused *Apoe*<sup>-/-</sup> mice. Representative photomicrographs and quantitative plots are shown in **Figure 23**.

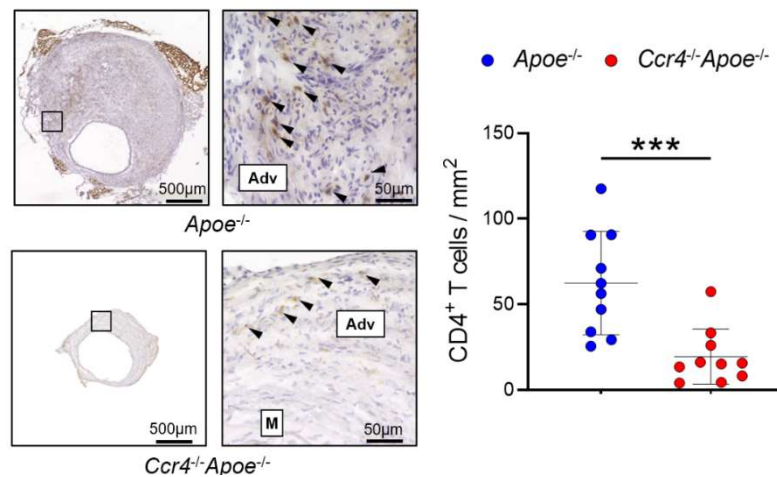


**Figure 23. Representative sections and quantitative analysis of CD4<sup>+</sup> T cells in the AAA lesions of angiotensin II-infused *Apoe*<sup>-/-</sup> or *Ccr4*<sup>-/-</sup>*Apoe*<sup>-/-</sup> mice.**

Suprarenal aorta crosssections of *Apoe*<sup>-/-</sup> or *Ccr4*<sup>-/-</sup>*Apoe*<sup>-/-</sup> mice fed a high-fat and high-cholesterol diet, infused with angiotensin II for 28 days, and euthanized at 16 weeks of age. Boxed areas are expanded to show representative high-power fields in serial sections. Lm indicates lumen; M, media; Adv, adventitia. Arrowheads indicate CD4<sup>+</sup> T cells. Black bars represent 50 or 500 μm as described. Data points represent individual animals, n=10 per group. Horizontal bars represent means. Error bars indicate s.d. \*\*\**P*<0.001; Mann-Whitney *U*-test.

The aortic immunoinflammatory reaction promotes various matrix metalloproteinases (MMPs) and upregulates their activity in the aortic wall to enact matrix destruction or remodeling during AAA formation. The inflammatory burden was assessed in depth by evaluating the presence and activity of these MMPs. Immunohistochemical studies of MMP-2 of the aortic wall of aneurysmal tissues were conducted, revealing a remarkable decrease in MMP-2 expression in the aortic wall of angiotensin II-infused *Ccr4*<sup>-/-</sup>*Apoe*<sup>-/-</sup> mice compared with angiotensin II-infused *Apoe*<sup>-/-</sup> mice (**Figure 24**).

A similar observation was made in the immunohistochemical studies of another major matrix proteinase, MMP-9. Immunostaining of MMP-9 displayed a favorable reduction of



MMP-9 expression in angiotensin II-infused *Ccr4*<sup>-/-</sup>*Apoe*<sup>-/-</sup> mice compared with angiotensin II-infused *Apoe*<sup>-/-</sup> mice (Figure 25).

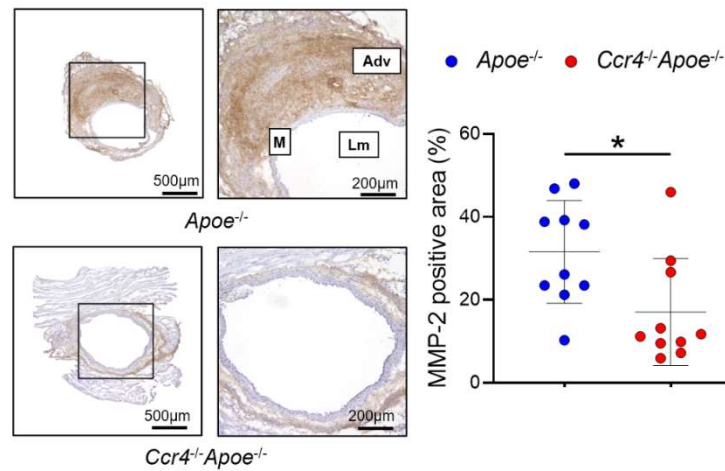


**Figure 24. Representative sections and quantitative analysis of MMP-2 expression in the AAA lesions of angiotensin II-infused *Apoe*<sup>-/-</sup> or *Ccr4*<sup>-/-</sup>*Apoe*<sup>-/-</sup> mice.**

Suprarenal aorta crosssections of *Apoe*<sup>-/-</sup> or *Ccr4*<sup>-/-</sup>*Apoe*<sup>-/-</sup> mice fed a high-fat and high-cholesterol diet, infused with angiotensin II for 28 days, and euthanized at 16 weeks of age. Boxed areas are expanded to show representative high-power fields in serial sections. Lm indicates lumen; M, media; Adv, adventitia. Black bars represent 200 or 500 μm as described. Data points represent individual animals, n=10 per group. Horizontal bars represent means. Error bars indicate s.d. \**P*<0.05; Mann-Whitney *U*-test.

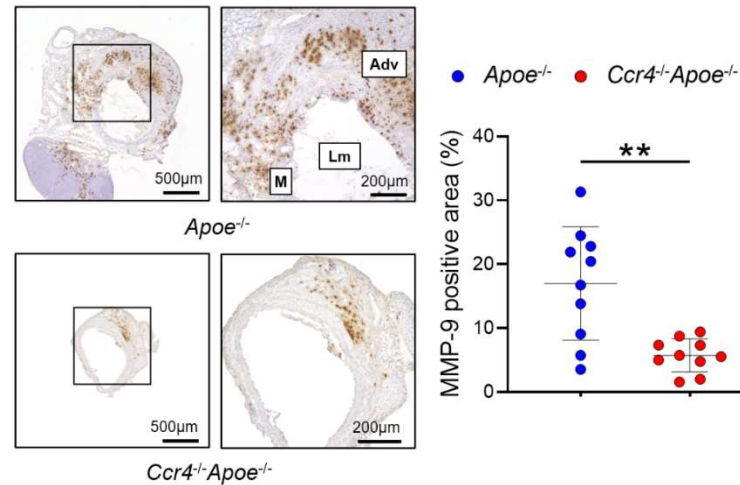


**Figure 25. Representative sections and quantitative analysis of MMP-9 expression in the AAA lesions of angiotensin II-infused *Apoe*<sup>-/-</sup> or *Ccr4*<sup>-/-</sup>*Apoe*<sup>-/-</sup> mice.**

Suprarenal aorta crosssections of *Apoe*<sup>-/-</sup> or *Ccr4*<sup>-/-</sup>*Apoe*<sup>-/-</sup> mice fed a high-fat and high-cholesterol diet, infused with angiotensin II for 28 days, and euthanized at 16 weeks of age. Boxed areas are expanded to show representative high-power fields in serial sections. Lm indicates lumen; M, media; Adv, adventitia. Black bars represent 200 or 500 μm as described. Data points represent individual animals, n=10 per group. Horizontal bars represent means. Error bars indicate s.d. \*\**P*<0.01; Welch's *t*-test.

Subsequently, this study evaluated whether the enzymatic activities of these MMPs were equally upregulated. Using *in situ* zymography, I confirmed a lower aortic MMP activity

in the aneurysmal region of the aorta of angiotensin II-infused *Ccr4<sup>-/-</sup>Apoe<sup>-/-</sup>* compared with that of angiotensin II-infused *Apoe<sup>-/-</sup>* mice (**Figure 26**).

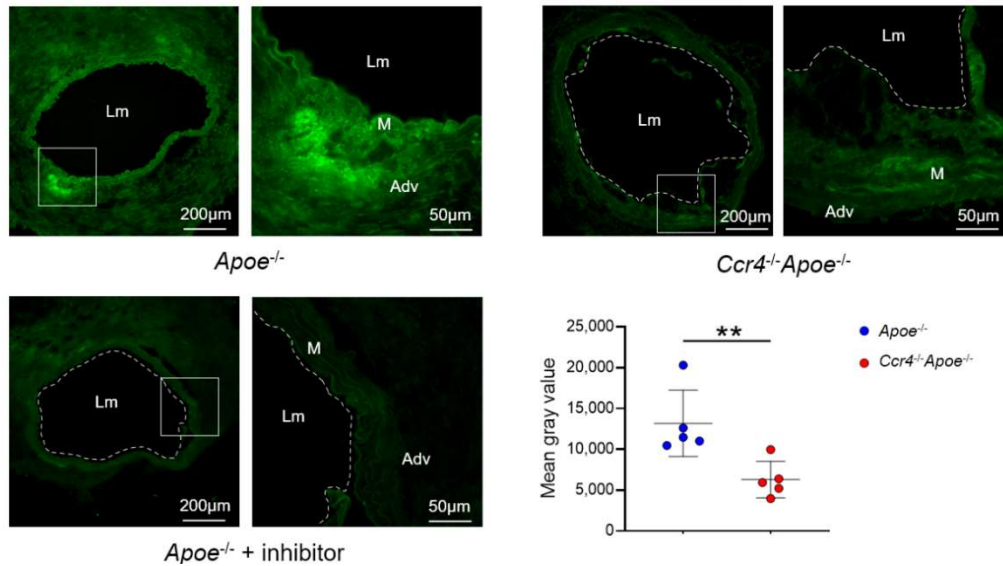


**Figure 26. CCR4 deficiency attenuates the upregulation of MMP activity in the aneurysmal lesions of angiotensin II-infused mice.** Representative sections and quantitative analysis of MMP activity in the AAA lesions of *Apoe<sup>-/-</sup>* or *Ccr4<sup>-/-</sup>Apoe<sup>-/-</sup>* mice fed a high-fat and high-cholesterol diet, infused with angiotensin II for 28 days, and euthanized at 16 weeks of age. Black bars represent 50 or 200  $\mu$ m as described. Data points represent individual animals, n=5 per group, representative of two independent experiments. Horizontal bars represent means. Error bars indicate s.d. \*\* $P < 0.01$ ; Mann-Whitney *U*-test.

After confirming the reduction of MMP expression and activity in CCR4 deficient mice, this study analyzed whether the phenotype of aortic structure integrity in angiotensin II-infused mice was also beneficially affected by CCR4 deletion. The main matrix constituents of the aortic wall are elastin and collagen. The suprarenal aorta was stained with the Elastica van Gieson staining method to evaluate elastin. Histological analysis of the aneurysmal tissues revealed that angiotensin II-infused *Ccr4<sup>-/-</sup>Apoe<sup>-/-</sup>* mice had more preserved elastin content than angiotensin II-infused *Apoe<sup>-/-</sup>* mice (**Figure 27**).



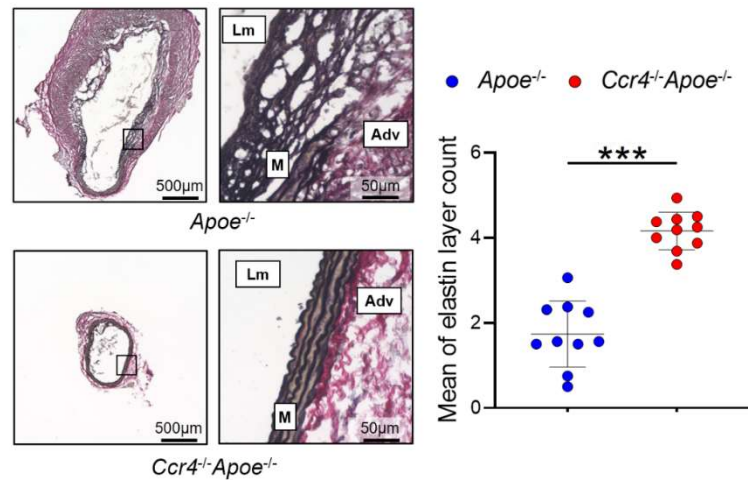


**Figure 27.** Representative sections and the average count of elastin layers in the aneurysmal lesions of angiotensin II-infused *Apoe*<sup>-/-</sup> or *Ccr4*<sup>-/-</sup>*Apoe*<sup>-/-</sup> mice.

Supraceliac aorta crosssections of *Apoe*<sup>-/-</sup> or *Ccr4*<sup>-/-</sup>*Apoe*<sup>-/-</sup> mice fed a high-fat and high-cholesterol diet, infused with angiotensin II for 28 days, and euthanized at 16 weeks of age. Boxed areas are expanded to show representative high-power fields in serial sections. Lm indicates lumen; M, media; Adv, adventitia. Black bars represent 200 or 500 μm as described. Data points represent individual animals, n=10 per group. Horizontal bars represent means. Error bars indicate s.d. \*\*\**P*<0.001; two-tailed Student's *t*-test.

Cross-sections of the supraceliac aorta were stained with Masson's trichrome to quantify collagen content. Although the proportion of collagen in the aneurysmal lesions of angiotensin II-infused *Ccr4*<sup>-/-</sup>*Apoe*<sup>-/-</sup> mice was significantly lower than that in the aneurysmal lesions of *Apoe*<sup>-/-</sup> mice (**Figure 28**), it was at a similar level to the proportion of collagen within the nonaneurysmal aorta of saline-infused sham groups. Accordingly, pathological collagen deposition accumulated in response to angiotensin II administration in *Apoe*<sup>-/-</sup> mice. This abnormal collagen production was attenuated in the supraceliac aortic wall of angiotensin II-infused *Ccr4*<sup>-/-</sup>*Apoe*<sup>-/-</sup> mice.

Abnormal collagen deposition is often observed in the fibrotic aorta. Therefore, profibrotic mediators were likely involved. Profibrotic cytokine TGF-β1 was stained using an immunohistochemical approach. As expected, the expression levels of TGF-β1 were markedly lower in the aneurysmal lesions of angiotensin II-infused *Ccr4*<sup>-/-</sup>*Apoe*<sup>-/-</sup> mice than in those of angiotensin II-infused *Apoe*<sup>-/-</sup> mice (**Figure 29**).

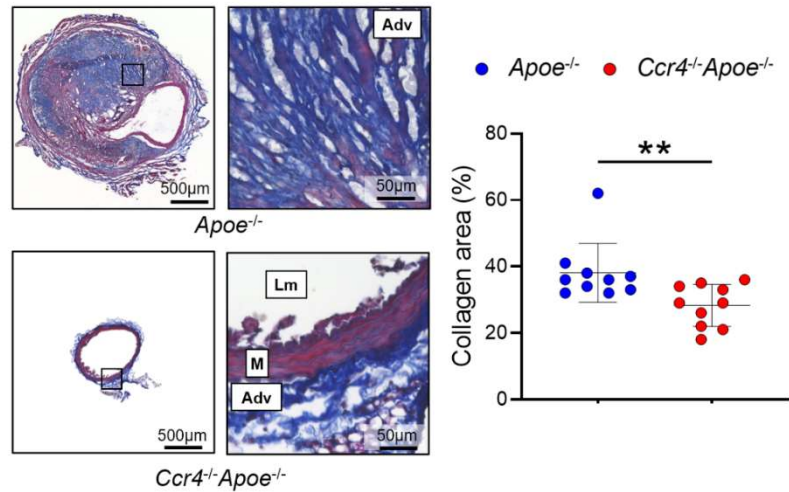


**Figure 28. Representative sections and quantitative analysis of collagen in the AAA lesions of angiotensin II-infused *Apoe*<sup>-/-</sup> or *Ccr4*<sup>-/-</sup>*Apoe*<sup>-/-</sup> mice.**

Suprarenal aorta crosssections of *Apoe*<sup>-/-</sup> or *Ccr4*<sup>-/-</sup>*Apoe*<sup>-/-</sup> mice fed a high-fat and high-cholesterol diet, infused with angiotensin II for 28 days, and euthanized at 16 weeks of age. Boxed areas are expanded to show representative high-power fields in serial sections. Lm indicates lumen; M, media; Adv, adventitia. Black bars represent 50 or 500  $\mu$ m as described. Data points represent individual animals, n=10 per group. Horizontal bars represent means. Error bars indicate s.d. \*\**P*<0.01; Mann-Whitney *U*-test.

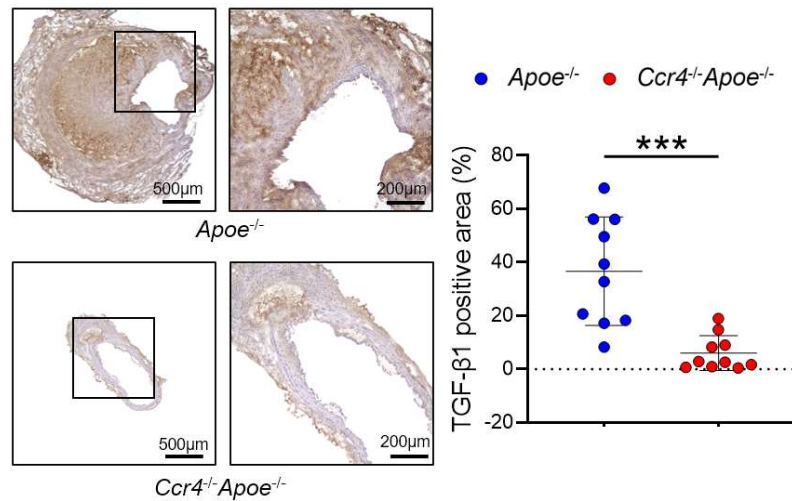


**Figure 29. Representative sections and quantitative analysis of TGF-β1 expression in the AAA lesions of angiotensin II-infused *Apoe*<sup>-/-</sup> or *Ccr4*<sup>-/-</sup>*Apoe*<sup>-/-</sup> mice.**

Suprarenal aorta crosssections of *Apoe*<sup>-/-</sup> or *Ccr4*<sup>-/-</sup>*Apoe*<sup>-/-</sup> mice fed a high-fat and high-cholesterol diet, infused with angiotensin II for 28 days, and euthanized at 16 weeks of age. Boxed areas are expanded to show representative high-power fields in serial sections. Lm indicates lumen; M, media; Adv, adventitia. Black bars represent 200 or 500  $\mu$ m as described. Data points represent individual animals, n=10 per group. Horizontal bars represent means. Error bars indicate s.d. \*\*\**P*<0.001; Mann-Whitney *U*-test.

Supporting evidence of upregulated TGF-β1 in the aorta of angiotensin II-infused *Apoe*<sup>-/-</sup> mice at the protein level, quantitative real-time PCR analysis of *Tgfb* mRNA revealed consistent findings. Angiotensin II infusion increased mRNA expression of *Tgfb* in the aorta of *Apoe*<sup>-/-</sup> mice. In contrast, these expression levels were markedly lower in II-infused *Ccr4*<sup>-/-</sup>*Apoe*<sup>-/-</sup> mice than in II-infused *Apoe*<sup>-/-</sup> mice (**Figure 30**).

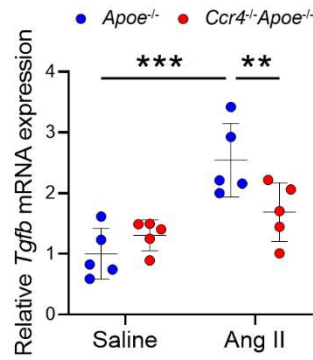


**Figure 30. The angiotensin II-dependent upregulation of aortic *Tgfb* mRNA expression was markedly attenuated in *Ccr4*<sup>-/-</sup>*Apoe*<sup>-/-</sup> mice.** The mRNA expression of *Tgfb* in the thoracoabdominal aortas of *Apoe*<sup>-/-</sup> or *Ccr4*<sup>-/-</sup>*Apoe*<sup>-/-</sup> mice fed a high-fat and high-cholesterol diet, infused with angiotensin II or saline for seven days, and euthanized at 13 weeks of age. The expression levels of the target genes were standardized to *Gapdh* and normalized so that the mean values in *Apoe*<sup>-/-</sup> mice were set to 1. Data points represent individual animals, n=5 per group. \*\**P*<0.01, \*\*\**P*<0.001; 2-way ANOVA followed by Tukey's multiple comparisons test.

#### 1.2.4. Deletion of CCR4 reduced Treg suppressive activity and increased Treg and effector

##### T cell frequencies in peripheral lymphoid tissues, independent of angiotensin II treatment

This study provided conclusive evidence of AAA attenuation in the absence of CCR4 and aimed to investigate its underlying mechanisms. First, this study focused on the alterations of CD4<sup>+</sup>Foxp3<sup>+</sup> Treg and CD4<sup>+</sup>Foxp3<sup>-</sup> non-Treg populations within peripheral lymphoid tissues. The frequency and number of anti-inflammatory CD4<sup>+</sup>Foxp3<sup>+</sup> Tregs were significantly higher in the LNs and spleens of *Ccr4*<sup>-/-</sup>*Apoe*<sup>-/-</sup> mice than in those of *Apoe*<sup>-/-</sup> mice independent of angiotensin II infusion (**Figure 31**).

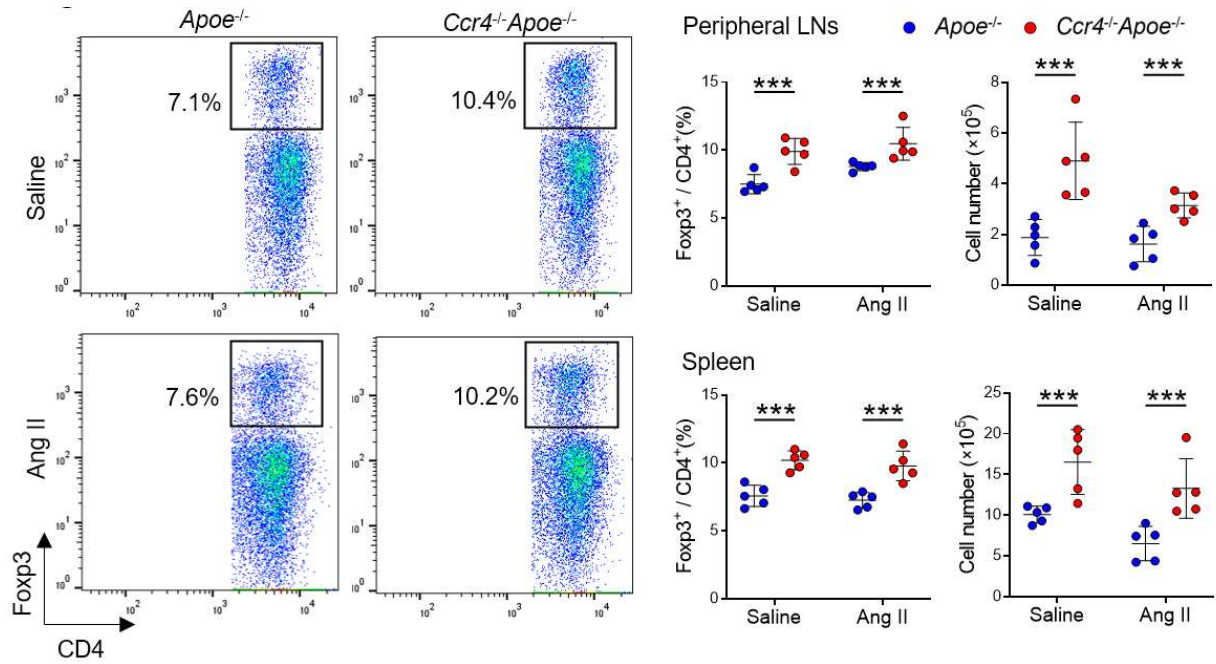


**Figure 31. Representative flow cytometric analysis of CD4<sup>+</sup> Foxp3<sup>+</sup> Tregs in the peripheral LNs and spleen of *Apoe*<sup>-/-</sup> or *Ccr4*<sup>-/-</sup>*Apoe*<sup>-/-</sup> mice.**

Seven days after the pump implantation, the mice were euthanized and lymphoid cells from LNs and spleen were prepared. *Apoe*<sup>-/-</sup> mice infused with angiotensin II or saline served as controls. The graphs represent the total numbers and proportions of CD4<sup>+</sup>Foxp3<sup>+</sup> Tregs in the peripheral LNs and spleen. n=5 per group. Data points represent individual animals. Horizontal bars represent means. Error bars indicate s.d. \*\*\**P*<0.001; 2-way ANOVA followed by Tukey's multiple comparisons test. Ang II indicates angiotensin II.

The frequency and number of CD4<sup>+</sup>CD44<sup>high</sup>CD62L<sup>low</sup> effector memory T cells were also higher in the LNs and spleens of *Ccr4*<sup>-/-</sup>*Apoe*<sup>-/-</sup> mice than in those of *Apoe*<sup>-/-</sup> mice independent of angiotensin II infusion (**Figure 32**). The expansion of CD4<sup>+</sup>Foxp3<sup>+</sup> Tregs and CD4<sup>+</sup>CD44<sup>high</sup>CD62L<sup>low</sup> effector memory T cells indicates that CCR4 deficiency induces global augmentation of T cell activation in peripheral lymphoid tissues. Additionally, angiotensin II infusion increased the frequency of proinflammatory CD4<sup>+</sup>CD44<sup>high</sup>CD62L<sup>low</sup> effector memory T cells in the spleens of *Apoe*<sup>-/-</sup> and *Ccr4*<sup>-/-</sup>*Apoe*<sup>-/-</sup> mice (**Figure 32**). In contrast, infusion did not significantly enhance the frequency of anti-inflammatory CD4<sup>+</sup>Foxp3<sup>+</sup> Tregs (**Figure 31**). Collectively, proinflammatory T cell immune responses were augmented by angiotensin II treatment.

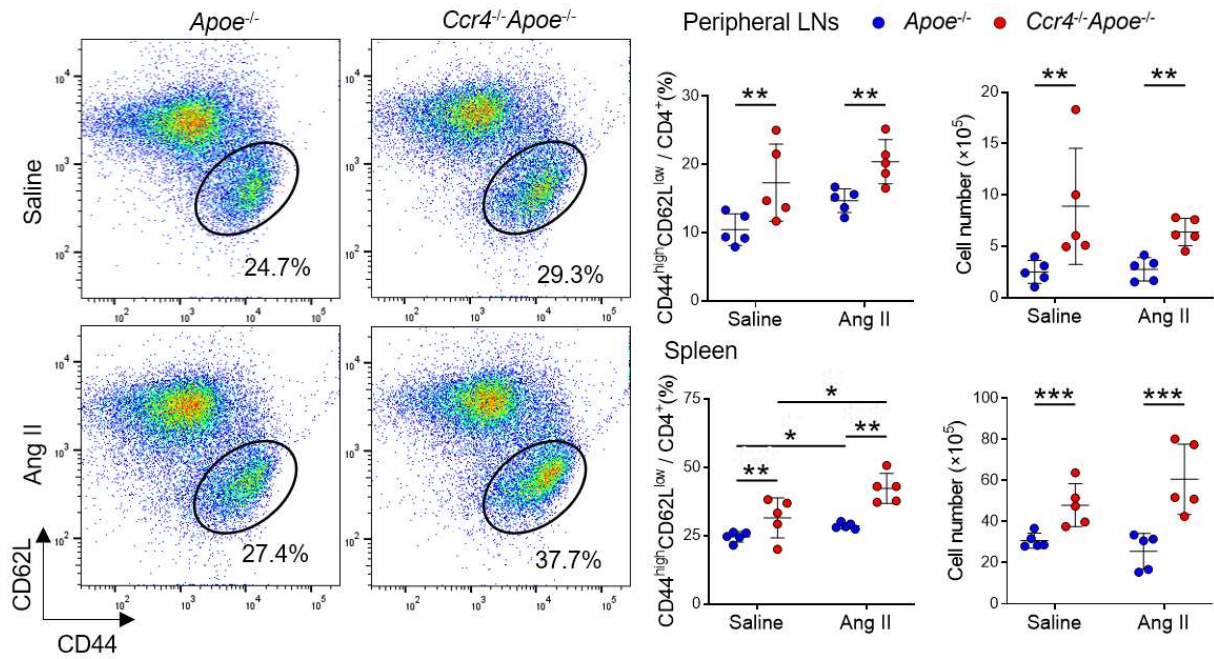


**Figure 32. Representative flow cytometric analysis of CD4<sup>+</sup>CD44<sup>high</sup>CD62L<sup>low</sup> effector memory T cells in the peripheral LNs and spleen of *Apoe*<sup>-/-</sup> or *Ccr4*<sup>-/-</sup>*Apoe*<sup>-/-</sup> mice.**

Seven days after the pump implantation, the mice were euthanized and lymphoid cells from LNs and spleen were prepared. *Apoe*<sup>-/-</sup> mice infused with angiotensin II or saline served as controls. The graphs represent the total numbers and proportions of CD4<sup>+</sup>CD44<sup>high</sup>CD62L<sup>low</sup> effector memory T cells in the peripheral LNs and spleen. n=5 per group. Data points represent individual animals. Horizontal bars represent means. Error bars indicate s.d. \*P<0.05, \*\*P<0.01, \*\*\*P<0.001; 2-way ANOVA followed by Tukey's multiple comparisons test. Ang II indicates angiotensin II.

The expansion of CD4<sup>+</sup>Foxp3<sup>+</sup> Tregs and CD4<sup>+</sup>CD44<sup>high</sup>CD62L<sup>low</sup> effector memory T cells may be derived from either enhanced development in the thymus or promoted proliferation in peripheral lymphoid tissues. To confirm the cause, I isolated thymocytes from 4-week-old *Apoe*<sup>-/-</sup> or *Ccr4*<sup>-/-</sup>*Apoe*<sup>-/-</sup> mice because it is generally easier to observe developmental differences in younger mice. T cell subsets in the isolated thymocytes were analyzed using flow cytometry. No differences were detected in thymic T cell development between the two strains, which is consistent with the findings of two previous reports experimenting with similar *Ccr4* knockout mice (**Figure 33**).<sup>51, 52</sup>



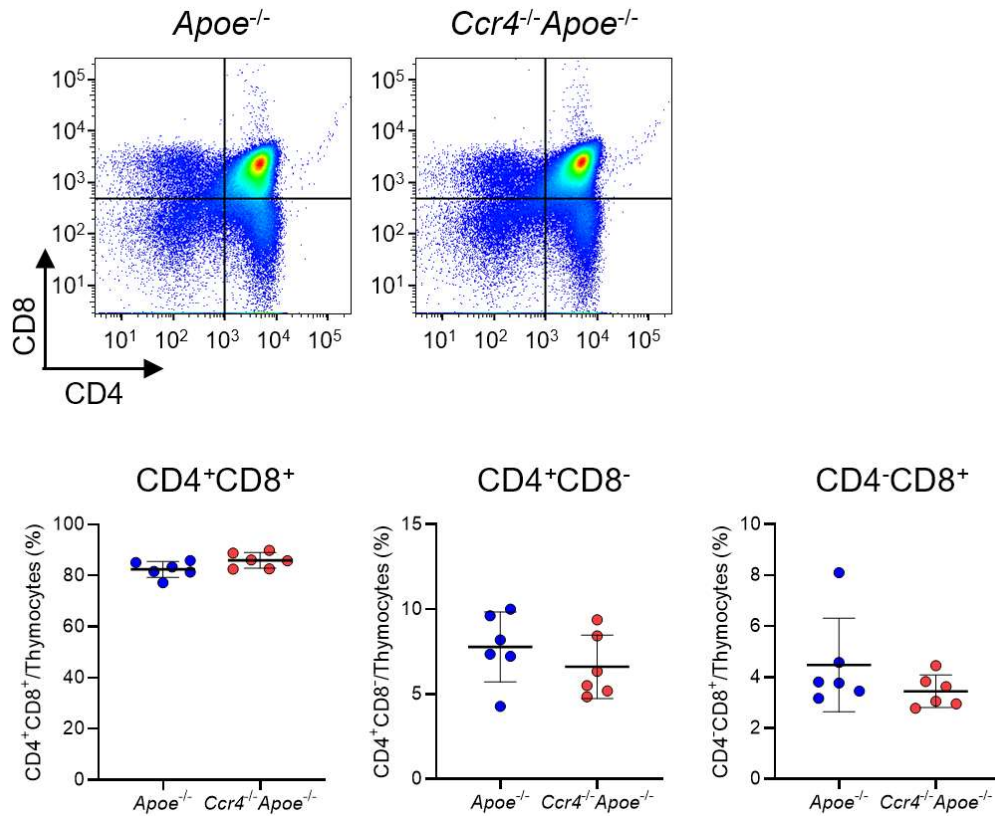


**Figure 33. CCR4 deficiency does not affect T cell development in the thymus.**

Lymphoid cells were prepared from the thymus of 4-week-old *Apoe*<sup>-/-</sup> or *Ccr4*<sup>-/-</sup>*Apoe*<sup>-/-</sup> mice. Representative flow cytometric analysis of CD4 and CD8 expression in thymocytes. The graphs represent the numbers and proportions of CD4/CD8 double positive (CD4<sup>+</sup>CD8<sup>+</sup>), CD4 single positive (CD4<sup>+</sup>), and CD8 single positive (CD8<sup>+</sup>) T cells among thymocytes. n=6 per group. Data points represent individual animals. Horizontal bars represent means. Error bars indicate s.d.

Subsequently, no differences were observed in the frequency of thymic CD4<sup>+</sup>Foxp3<sup>+</sup> Tregs between strains (**Figure 34**), which aligns with a previous report<sup>52</sup> but contradicts another.<sup>51</sup> Accordingly, the effect of *Ccr4* gene deletion on thymic Treg development remains open for interpretation. However, the findings of the current model indicate that the observed higher frequencies and numbers of CD4<sup>+</sup>Foxp3<sup>+</sup> Tregs and CD4<sup>+</sup>CD44<sup>high</sup>CD62L<sup>low</sup> effector memory T cells in the peripheral lymphoid tissues of *Ccr4*<sup>-/-</sup>*Apoe*<sup>-/-</sup> mice may not result from their promoted development in the thymus, but rather from enhanced proliferation in the periphery.

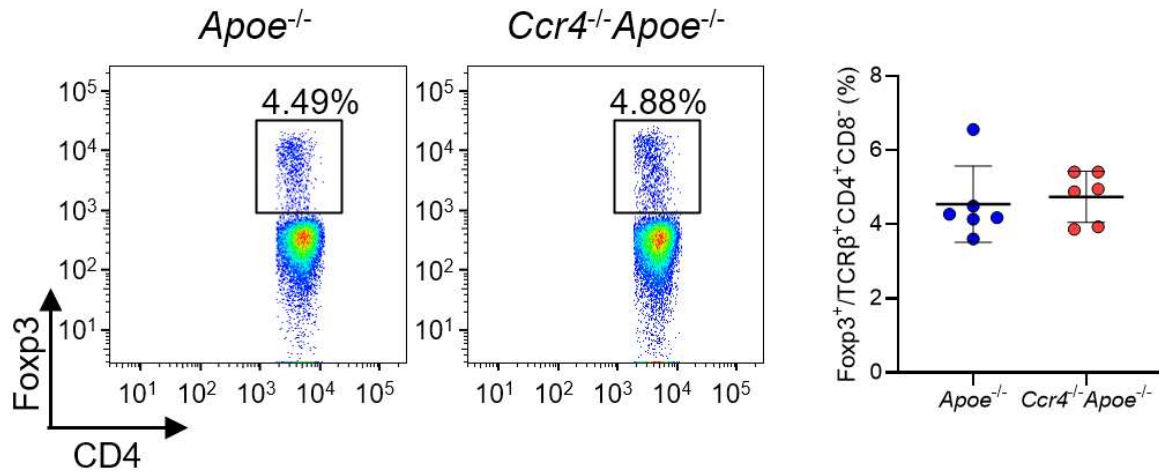


**Figure 34. Representative flow cytometric analysis of thymic Foxp3 expression among the TCR-β<sup>+</sup>CD4<sup>+</sup>CD8<sup>-</sup> population.** Lymphoid cells were prepared from the thymus of 4-week-old *Apoe*<sup>-/-</sup> or *Ccr4*<sup>-/-</sup>*Apoe*<sup>-/-</sup> mice. The graph represents the proportion of Foxp3<sup>+</sup> Tregs among the TCR-β<sup>+</sup>CD4<sup>+</sup>CD8<sup>-</sup> population. n=6 per group. Data points represent individual animals. Horizontal bars represent means. Error bars indicate s.d.

A closer examination of Tregs revealed that CCR4 deficiency did not alter the expression of the function-associated molecule CTLA-4 in CD4<sup>+</sup>Foxp3<sup>+</sup> Tregs in the peripheral LNs or spleens of *Apoe*<sup>-/-</sup> mice infused with either angiotensin II or saline. Conversely, angiotensin II infusion modestly decreased CTLA-4 expression in Tregs in the peripheral LNs of *Apoe*<sup>-/-</sup> and *Ccr4*<sup>-/-</sup>*Apoe*<sup>-/-</sup> mice (**Figure 35**), implying impaired Treg cell-to-cell suppressive function in angiotensin II-treated mice.

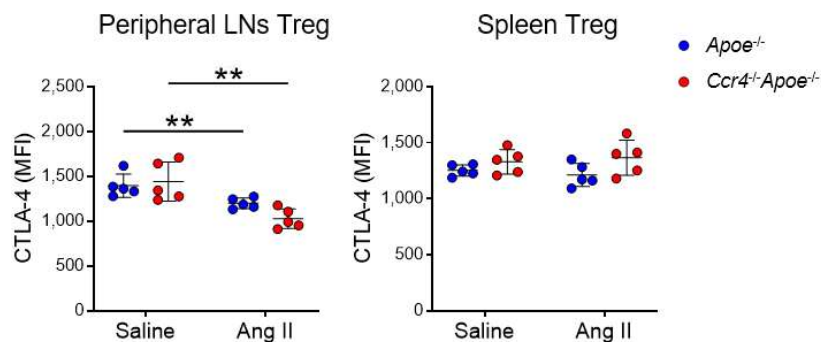


**Figure 35. Decreased CTLA-4 expression in Tregs following angiotensin II treatment.** Seven days after the pump implantation, the mice were euthanized and lymphoid cells from LNs and spleen were prepared. *Apoe*<sup>-/-</sup> mice infused with angiotensin II or saline served as controls. Expression levels of activation-associated molecule CTLA-4 were analyzed by gating on CD4<sup>+</sup>Foxp3<sup>+</sup> Tregs in the peripheral LNs and spleen of *Apoe*<sup>-/-</sup> or *Ccr4*<sup>-/-</sup>*Apoe*<sup>-/-</sup> mice. n=5 per group. Data points represent individual animals. Horizontal bars represent means. Error bars indicate s.d. \*\**P*<0.01; 2-way ANOVA followed by Tukey's multiple comparisons test. MFI indicates mean fluorescence intensity; Ang II, angiotensin II.

Previous studies have reported the pivotal contribution of CCR4 in mediating Treg function in migration and cell-to-cell communication (particularly with DCs) in autoimmune or allergic diseases.<sup>45, 46</sup> Therefore, these cells are likely dysfunctional despite the expansion and unaltered expression of activation- or function-associated molecules in CCR4-deficient Tregs. An *in vitro* suppression assay was conducted to confirm the suppression capability of these cells. The suppressive function of CCR4-deficient Treg isolated from hypercholesterolemic mice was significantly impaired (**Figure 36**). Accordingly, CCR4 deficiency impaired the Treg suppression capability regardless of its activation status.

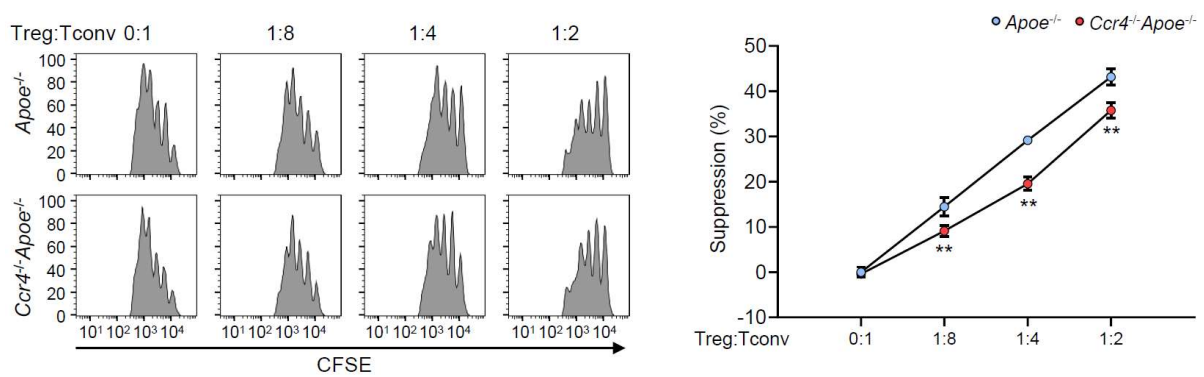


**Figure 36. Treg suppression assay.**

The suppressive function of Tregs was assessed by evaluating the proliferation of carboxyfluorescein diacetate succinimidyl ester (CFSE)-labeled conventional T cells (Tconv) cocultured with Tregs purified from LNs and spleen of *Apoe*<sup>-/-</sup> or *Ccr4*<sup>-/-</sup>*Apoe*<sup>-/-</sup> mice. Data are presented as the results of triplicate wells and are representative of two independent experiments. Data are expressed as the mean ± s.d. The results are presented as the mean ± s.d. of three independent experiments. \*\**P* < 0.01; 2-way ANOVA followed by Tukey's multiple comparisons test.

To fit the AAA model, I determined whether CCR4 deficiency impaired the suppressive function of Tregs in angiotensin II-treated mice through a similar *in vitro* suppression assay using Tregs from angiotensin II-infused *Apoe*<sup>-/-</sup> or *Ccr4*<sup>-/-</sup>*Apoe*<sup>-/-</sup> mice. Consistently, CCR4-deficient Tregs showed impaired suppressive activity (**Figure 37**), mirroring previous findings in non-angiotensin II-infused mice.



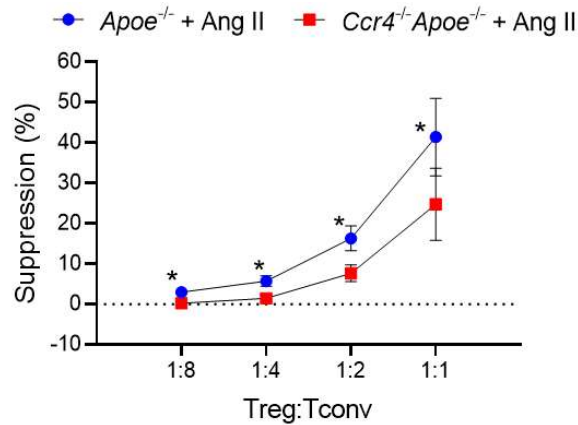


**Figure 37. Treg suppression assay in angiotensin II-treated mice.**

Seven days after the pump implantation, the mice were euthanized and lymphoid cells from LNs and spleen were prepared. Purified Tregs from angiotensin II-infused *Apoe*<sup>-/-</sup> or *Ccr4*<sup>-/-</sup>*Apoe*<sup>-/-</sup> mice were cocultured with carboxyfluorescein diacetate succinimidyl ester (CFSE)-labeled conventional T cells (Tconv) from *Apoe*<sup>-/-</sup> mice at the indicated ratios. The suppressive function of Tregs was assessed by evaluating the proliferation of CFSE-labeled Tconv. Data are presented as the results of triplicate wells and are representative of two independent experiments. Data are expressed as the mean±s.d. \**P*<0.05; 2-way ANOVA followed by Tukey's multiple comparisons test. Ang II indicates angiotensin II.

This study confirmed the modulation of T cell responses in the absence of CCR4, I checked and determined whether other immune cells were equally affected. Various immune cells isolated from the spleens of angiotensin II-infused *Apoe*<sup>-/-</sup> or *Ccr4*<sup>-/-</sup>*Apoe*<sup>-/-</sup> mice were analyzed using flow cytometry. Nevertheless, no essential differences in the proportions of immune cells or the expression of costimulatory molecules on DCs were detected between the two strains (**Figure 38**).

The above findings indicate that CCR4 deficiency effectively modulates T cell responses. CCR4 deficiency impairs Treg suppressive function despite expanding its frequency. However, combined with angiotensin II treatment, it enhances effector T cell response. Meanwhile, other immune cells seem unaffected. Given the attenuation of AAA in angiotensin II-infused *Ccr4*<sup>-/-</sup>*Apoe*<sup>-/-</sup> mice, these data indicate that the augmented effector T cell responses may have a greater influence on the beneficial effect than changes in Treg responses.

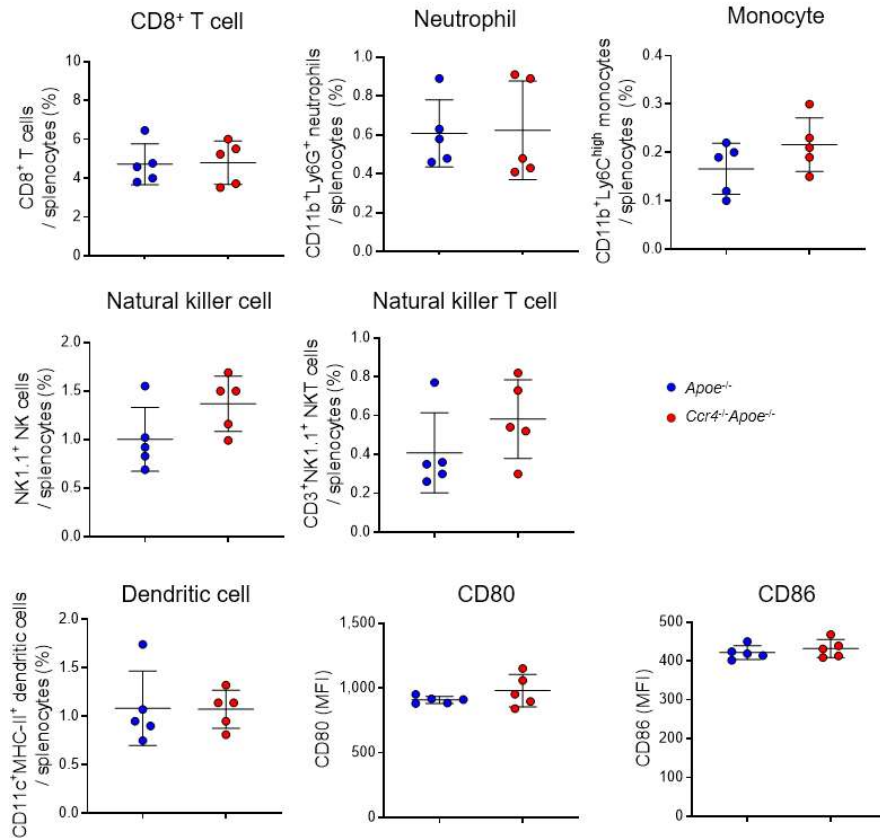


**Figure 38. CCR4 deficiency has a minor effect on the proportions of other immune cells in spleen.**

Seven days after the pump implantation, the mice were euthanized and lymphoid cells from spleen were prepared. Saline-infused *Apoe*<sup>-/-</sup> mice served as controls. Proportions of splenic CD8<sup>+</sup> T cells, CD11b<sup>+</sup>Ly6G<sup>+</sup> neutrophils, CD11b<sup>+</sup>Ly6C<sup>high</sup> monocyte, natural killer (NK) cells, NKT cells, and CD11c<sup>+</sup> major histocompatibility complex (MHC)-II<sup>+</sup> DCs, and the expression of CD80 and CD86 on CD11c<sup>+</sup>MHC-II<sup>+</sup> DCs in angiotensin II-infused *Apoe*<sup>-/-</sup> mice or *Ccr4*<sup>-/-</sup>*Apoe*<sup>-/-</sup> mice were determined by flow cytometry. n=5 per group. Data points represent individual animals. Horizontal bars represent means. Error bars indicate s.d. MFI indicates mean fluorescence intensity.

### 1.2.5. Promotion of Th1 cell immune responses in peripheral lymphoid tissues and reduction of plasma IgE levels in angiotensin II-infused mice in the absence of CCR4

Considering the findings on enhanced effector T cell responses in *Ccr4*<sup>-/-</sup>*Apoe*<sup>-/-</sup> mice, I evaluated whether CCR4 deficiency endorses specific CD4<sup>+</sup> T cell immune responses, including helper T cell polarization and production of various cytokines, by intracellular cytokine staining (ICS) in CD4<sup>+</sup> T cells isolated from peripheral LNs and spleens. After 5 h of stimulation of cytokine production, the stimulated immune cells were stained with antibodies specific to T cell subset cytokines: IFN- $\gamma$ , IL-4, IL-10, and IL-17.

A strikingly higher proportion of IFN- $\gamma$ -producing Th1 cells was detected in the peripheral LNs of *Ccr4*<sup>-/-</sup>*Apoe*<sup>-/-</sup> mice than in those of *Apoe*<sup>-/-</sup> mice regardless of angiotensin II infusion. Although no differences in IL-4-producing Th2 were observed between strains in saline- or angiotensin II-infused mice, an enhanced fraction of these cells was confirmed in the peripheral LNs of mice treated with angiotensin II infusion (**Figure 39**). When assessing the Th1/Th2 balance, CCR4 deficiency led to a substantial increase in the Th1 cell/Th2 cell ratio in peripheral LNs in saline- and angiotensin II-treated mice. Angiotensin II infusion effectively reduced the Th1 cell/Th2 cell ratio in the peripheral LNs of both strains (**Figure 39**). Neither IL-10-producing CD4<sup>+</sup> T cells nor IL-17-producing Th17 cells were affected by angiotensin II and CCR4 deficiency.

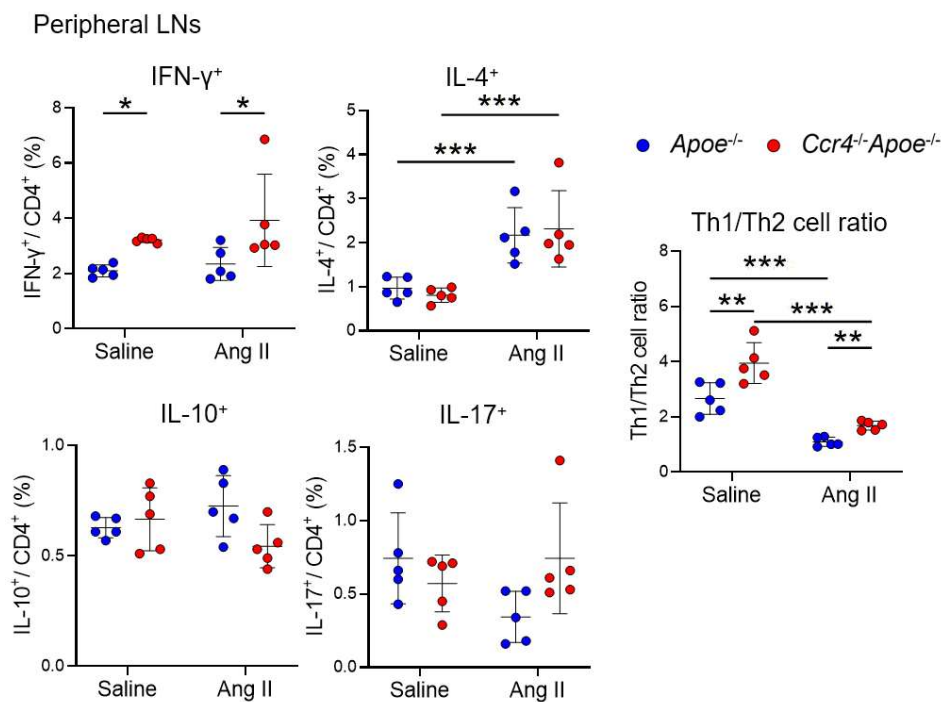


**Figure 39. Analysis of helper T cell subsets in peripheral LNs.**

Seven days after the pump implantation, the mice were euthanized and lymphoid cells from LNs were prepared. *Apoe*<sup>-/-</sup> mice infused with angiotensin II or saline served as controls. The graphs represent the frequencies of IFN- $\gamma$ <sup>+</sup>, IL-4<sup>+</sup>, IL-10<sup>+</sup>, and IL-17<sup>+</sup> CD4<sup>+</sup> T cells and the ratio of IFN- $\gamma$ <sup>+</sup> Th1 cells to IL-4<sup>+</sup> Th2 cells in the peripheral LNs of *Apoe*<sup>-/-</sup> or *Ccr4*<sup>-/-</sup>*Apoe*<sup>-/-</sup> mice infused with angiotensin II or saline. n=5 per group. Data points represent individual animals. Horizontal bars represent means. Error bars indicate s.d. \**P*<0.05, \*\**P*<0.01, \*\*\**P*<0.001; 2-way ANOVA followed by Tukey's multiple comparisons test. Ang-II indicates angiotensin II.

Reports on data obtained from the spleens reached a similar conclusion. Angiotensin II infusion markedly decreased the Th1 cell/Th2 cell ratio in the spleens of *Apoe*<sup>-/-</sup> and

*Ccr4<sup>-/-</sup>Apoe<sup>-/-</sup>* mice. However, this ratio was higher in *Ccr4<sup>-/-</sup>Apoe<sup>-/-</sup>* mice than in *Apoe<sup>-/-</sup>* mice, regardless of angiotensin II infusion (**Figure 40**). Angiotensin II infusion did not affect other T cell fractions, such as IL-10-producing CD4<sup>+</sup> T cells and IL-17-producing Th17 cells in the spleen. Meanwhile, CCR4 deficiency increased the fraction of IL-17-producing Th17 cells in the spleen (**Figure 40**).

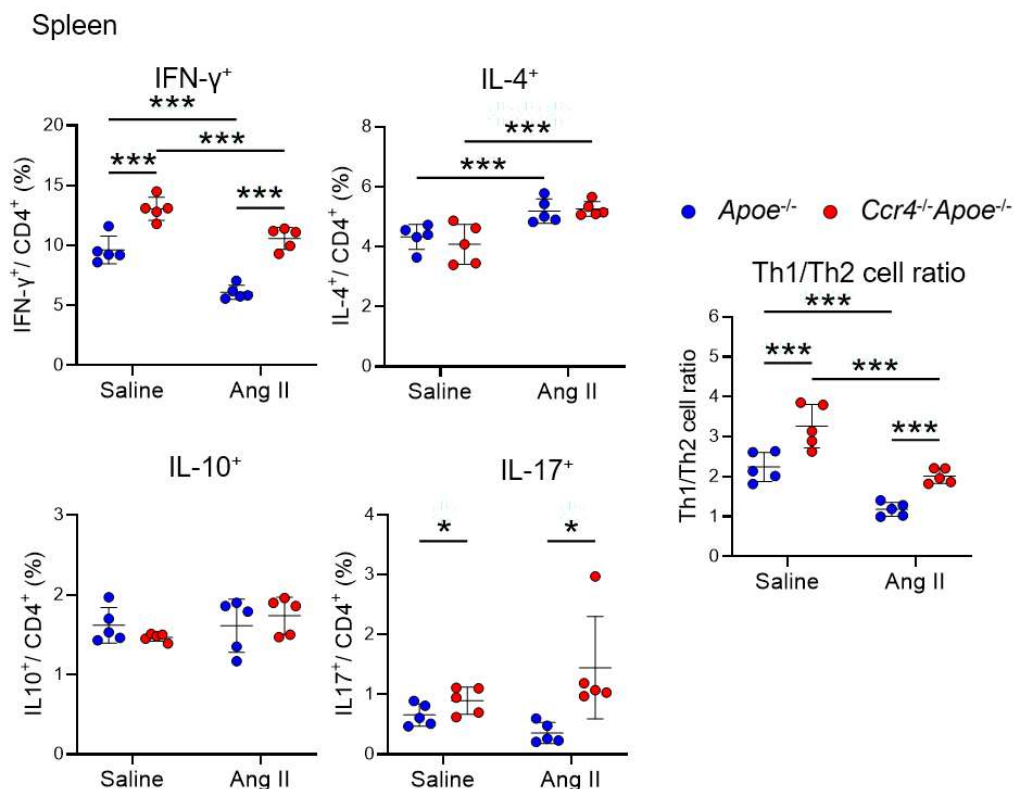


**Figure 40. Analysis of helper T cell subsets in spleen.**

Seven days after the pump implantation, the mice were euthanized and lymphoid cells from the spleen were prepared. *Apoe<sup>-/-</sup>* mice infused with angiotensin II or saline served as controls. The graphs represent the frequencies of IFN-γ<sup>+</sup>, IL-4<sup>+</sup>, IL-10<sup>+</sup>, and IL-17<sup>+</sup> CD4<sup>+</sup> T cells and the ratio of IFN-γ<sup>+</sup> Th1 cells to IL-4<sup>+</sup> Th2 cells in the spleen of *Apoe<sup>-/-</sup>* or *Ccr4<sup>-/-</sup>Apoe<sup>-/-</sup>* mice infused with angiotensin II or saline. n=5 per group. Data points represent individual animals. Horizontal bars represent means. Error bars indicate s.d. \*P<0.05, \*\*\*P<0.001; 2-way ANOVA followed by Tukey's multiple comparisons test. Ang-II indicates angiotensin II.

A consistent expansion of Th1 cells was observed in the peripheral lymphoid tissues of CCR4-deficient mice. In addition, the effect of CCR4 deficiency on cytokine production by splenic CD4<sup>+</sup> T cells under angiotensin II treatment was investigated. Splenic CD4 cells were isolated by magnetic separation from the spleens of angiotensin II-infused *Apoe<sup>-/-</sup>* or *Ccr4<sup>-/-</sup>Apoe<sup>-/-</sup>* mice. The cells were incubated for 48 h in an anti-CD3-coated 96-well plate with

a medium containing anti-CD28 antibodies. Cytokine levels within the culture supernatants were calculated using enzyme-linked immunosorbent assay (ELISA).

Among the quantified cytokines, the cytokine levels of Th1 cell-associated IFN- $\gamma$ , Treg-associated anti-inflammatory IL-10, and Th17 cell-associated cytokine IL-17 in the culture supernatants of angiotensin II-infused *Ccr4*<sup>-/-</sup>*Apoe*<sup>-/-</sup> mice were uniformly upregulated in comparison with those of angiotensin II-infused *Apoe*<sup>-/-</sup> mice. No differences were detected in the levels of the Th2 cell-associated cytokine IL-4 in the culture supernatants of the two strains (**Figure 41**). Consequently, CCR4 deficiency augmented cytokine-mediated CD4<sup>+</sup> helper T cell immune responses, excluding Th2 cell-derived IL-4 responses, in angiotensin II-infused mice.

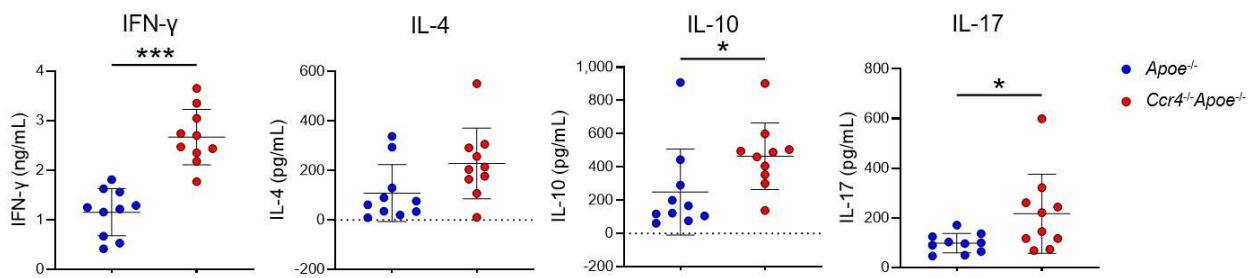


**Figure 41. In vitro cytokine production by helper T cells isolated from mice treated with angiotensin II.**

Seven days after the pump implantation, the mice were euthanized and lymphoid cells from LNs and spleen were prepared. *Apoe*<sup>-/-</sup> mice infused with angiotensin II or saline served as controls. Purified splenic CD4<sup>+</sup> T cells from angiotensin II-infused *Apoe*<sup>-/-</sup> or *Ccr4*<sup>-/-</sup>*Apoe*<sup>-/-</sup> mice were stimulated with plate-bound anti-CD3 and soluble anti-CD28 antibodies for 48 hours in vitro. Cytokine concentrations in the cell supernatants were measured by ELISA. n=10 per group. Data points represent individual animals. Horizontal bars represent means. Error bars indicate s.d. \**P*<0.05, \*\*\**P*<0.001; Mann-Whitney *U*-test: IL-10 and IL-17; two-tailed Student's *t*-test: IFN- $\gamma$ .

The changes observed in adaptive immune responses by T cells indicate that CCR4 deficiency may influence B cell responses under an inseparable interaction between T cells and B cells. First, this study identified the proportion of B cells in the spleen using flow cytometric analysis of splenocytes from angiotensin II-infused *Apoe*<sup>-/-</sup> or *Ccr4*<sup>-/-</sup>*Apoe*<sup>-/-</sup> mice. No differences were detected in the proportions of B1 or B2 cells between the two strains (**Figure 42**).

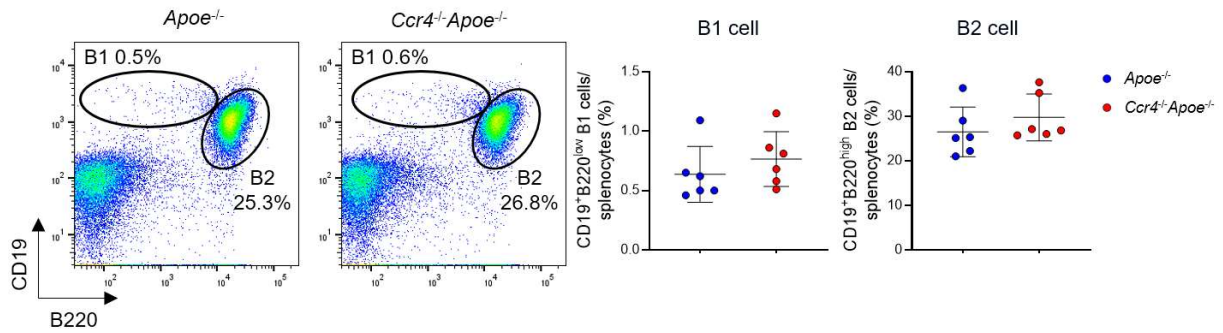


**Figure 42. Flow cytometric analysis of splenic B cells of angiotensin II-treated mice.**

Seven days after the pump implantation, the mice were euthanized and lymphoid cells from LNs and spleen were prepared. Representative flow cytometric analysis of splenic B cell populations in angiotensin II-infused *Apoe*<sup>-/-</sup> or *Ccr4*<sup>-/-</sup>*Apoe*<sup>-/-</sup> mice. The graphs represent the proportion of splenic CD19<sup>+</sup>B220<sup>low</sup> B1 or CD19<sup>+</sup>B220<sup>high</sup> B2 cells. n=5 per group. Data points represent individual animals. Horizontal bars represent means. Error bars indicate s.d.

Subsequently, I investigated the GL7<sup>+</sup>CD95<sup>+</sup>CD19<sup>+</sup>B220<sup>high</sup> germinal center B cells, the progenitor of high-affinity class-switched antibody-producing plasma cells. Notably, CCR4 deficiency reduced the proportion of these cell populations within splenic B cells (**Figure 43**).

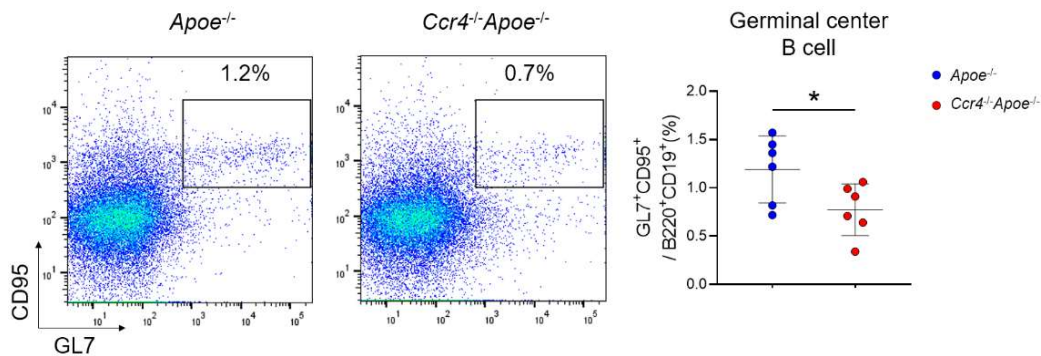


**Figure 43. CCR4 deficiency reduces the proportion of splenic germinal center B cells in angiotensin II-infused mice.**

Seven days after the pump implantation, the mice were euthanized and lymphoid cells from spleen were prepared. Representative flow cytometric analysis of germinal center B cells in the spleen of angiotensin II-infused *Apoe*<sup>-/-</sup> or *Ccr4*<sup>-/-</sup>*Apoe*<sup>-/-</sup> mice. The graphs represent the proportions of GL7<sup>+</sup>CD95<sup>+</sup>CD19<sup>+</sup>B220<sup>high</sup> germinal center B cells in spleen. n=6 per group. Data points represent individual animals. Horizontal bars represent means. Error bars indicate s.d. \**P*<0.05; two-tailed Student's *t*-test.

The antibody-producing subsets of CD138<sup>+</sup>B220<sup>high</sup> plasmablasts and CD138<sup>+</sup>B220<sup>low</sup> plasma cell population in the spleen were also identified. A significant reduction in the frequency of CD138<sup>+</sup>B220<sup>high</sup> plasmablasts within splenocytes in *Ccr4*<sup>-/-</sup>*Apoe*<sup>-/-</sup> mice was detected, whereas no significant changes in CD138<sup>+</sup>B220<sup>low</sup> plasma cells were observed (**Figure 44**).



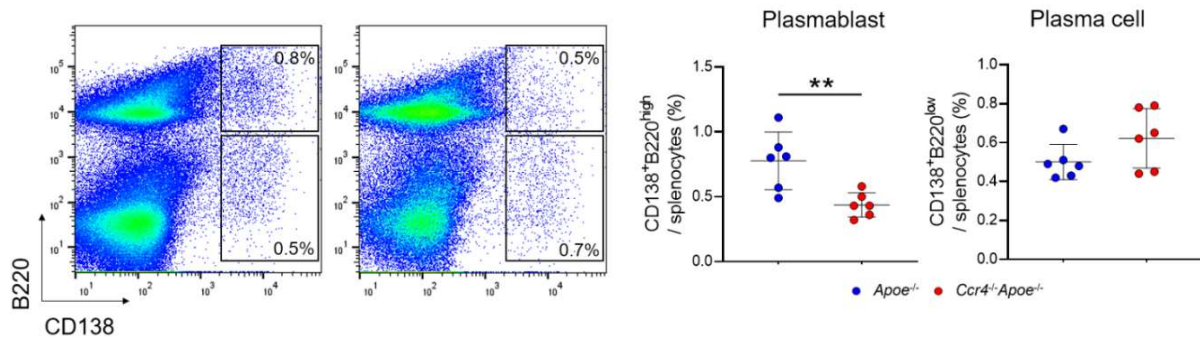


**Figure 44. CCR4 deficiency reduces the proportion of splenic plasmablasts in angiotensin II-infused mice.**

Seven days after the pump implantation, the mice were euthanized and lymphoid cells from spleen were prepared. Representative flow cytometric analysis of plasmablasts and plasma cells in the spleen of angiotensin II-infused *Apoe*<sup>-/-</sup> or *Ccr4*<sup>-/-</sup>*Apoe*<sup>-/-</sup> mice. The graphs represent the proportions of CD138<sup>+</sup>B220<sup>high</sup> plasmablasts or CD138<sup>+</sup>B220<sup>low</sup> plasma cells in spleen. n=6 per group. Data points represent individual animals. Horizontal bars represent means. Error bars indicate s.d. \*\**P*<0.01; two-tailed Student's *t*-test.

Changes were observed in the frequencies of antibody-producing B cell subsets. I aimed to detect any difference in the plasma levels of antibodies of angiotensin II-treated *Apoe*<sup>-/-</sup> or *Ccr4*<sup>-/-</sup>*Apoe*<sup>-/-</sup> mice. Various immunoglobulins in the plasma of angiotensin II-infused *Apoe*<sup>-/-</sup> or *Ccr4*<sup>-/-</sup>*Apoe*<sup>-/-</sup> mice were examined using ELISA. The plasma IgE levels of angiotensin II-infused *Ccr4*<sup>-/-</sup>*Apoe*<sup>-/-</sup> mice were significantly lower than those of angiotensin II-infused *Apoe*<sup>-/-</sup> mice. Nevertheless, no differences were observed in the plasma levels of IgM or IgG between the two strains (**Figure 45**).

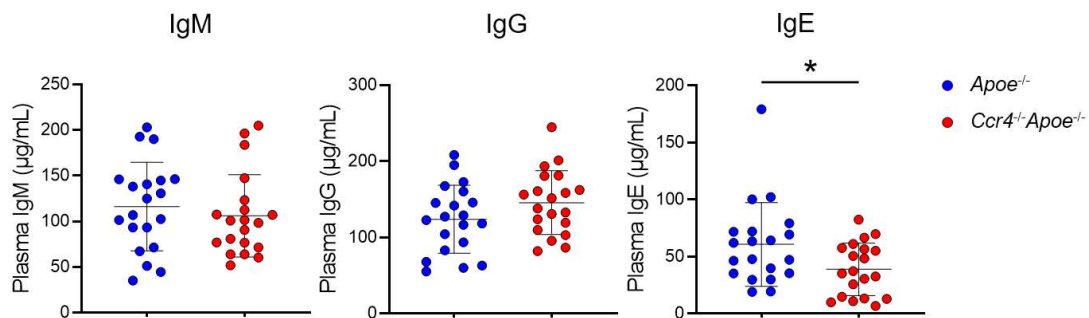


**Figure 45. CCR4 deficiency reduces serum levels of IgE in angiotensin II-infused mice.**

Four weeks after the pump implantation, angiotensin II-infused *Apoe*<sup>-/-</sup> or *Ccr4*<sup>-/-</sup>*Apoe*<sup>-/-</sup> mice were euthanized and the plasma levels of IgM, IgG, and IgE were measured. n=20 per group. Data points represent individual animals. Horizontal bars represent means. Error bars indicate s.d. \**P*<0.05; two-tailed Student's *t*-test.

The attenuation of antibody-producing B cell subsets and the subsequent reduction in plasma IgE levels were confirmed in angiotensin II-treated mice deficient in CCR4. Because Th1 cells and their signature cytokine IFN- $\gamma$  may counteract Th2 cell responses, they may

inhibit Th2 promotion of B cell activity, particularly in the production of high-affinity antibodies. This finding and the previous section data combined indicate that the increased plasma IgE levels in angiotensin II-infused *Ccr4*<sup>-/-</sup>*Apoe*<sup>-/-</sup> mice may partly be derived from the Th1 cell-skewed immune responses.

#### **1.2.6. Deficiency of CCR4 enhanced Th1 cell responses in para-aortic LNs and the thoracoabdominal aorta of angiotensin II-infused mice**

Systemic changes resulted from CCR4 deletion based on observations of immune responses in the spleen and peripheral LNs. Subsequently, evidence was collected from local immune response observations in the para-aortic LNs and the thoracoabdominal aorta to elucidate the mechanisms by which CCR4 deficiency prevents the development of angiotensin II-induced AAA.

A similar flow cytometric evaluation of the spleen and peripheral LNs was performed regarding CD4<sup>+</sup>Foxp3<sup>+</sup> Treg population. Neither angiotensin II infusion nor CCR4 deficiency affected the frequency and number of CD4<sup>+</sup>Foxp3<sup>+</sup> Tregs in the para-aortic LNs of *Apoe*<sup>-/-</sup> mice (**Figure 46**).



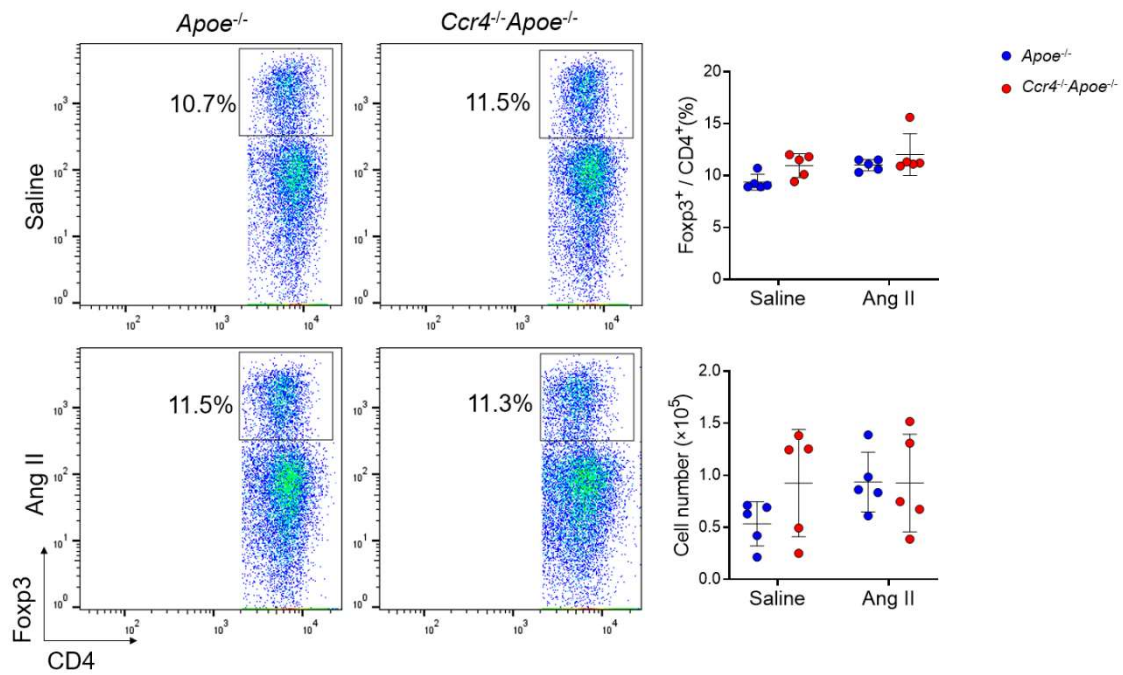


**Figure 46. CCR4 deficiency does not affect Treg frequency in the para-aortic LNs of angiotensin II-infused mice.**

Seven days after the pump implantation, the mice were euthanized and lymphoid cells from para-aortic LNs were prepared. *Apoe*<sup>-/-</sup> mice infused with angiotensin II or saline served as controls. Representative flow cytometric analysis of CD4<sup>+</sup>Fopx3<sup>+</sup> Tregs in the para-aortic LNs of *Apoe*<sup>-/-</sup> or *Ccr4*<sup>-/-</sup>*Apoe*<sup>-/-</sup> mice. The graphs represent the proportions of CD4<sup>+</sup>Fopx3<sup>+</sup> Tregs in the para-aortic LNs. n=5 per group. Data points represent individual animals. Horizontal bars represent means. Error bars indicate s.d.

Analysis of CD4<sup>+</sup>CD44<sup>high</sup>CD62L<sup>low</sup> effector memory T cells revealed that angiotensin II infusion increased the frequency of CD4<sup>+</sup>CD44<sup>high</sup>CD62L<sup>low</sup> effector memory T cells in the para-aortic LNs of *Apoe*<sup>-/-</sup> and *Ccr4*<sup>-/-</sup>*Apoe*<sup>-/-</sup> mice, whereas CCR4 deficiency did not affect this frequency whether angiotensin II infusion was applied (**Figure 47**). Nevertheless, the absolute number of CD4<sup>+</sup>CD44<sup>high</sup>CD62L<sup>low</sup> effector memory T cells remained unchanged in all groups (**Figure 47**).

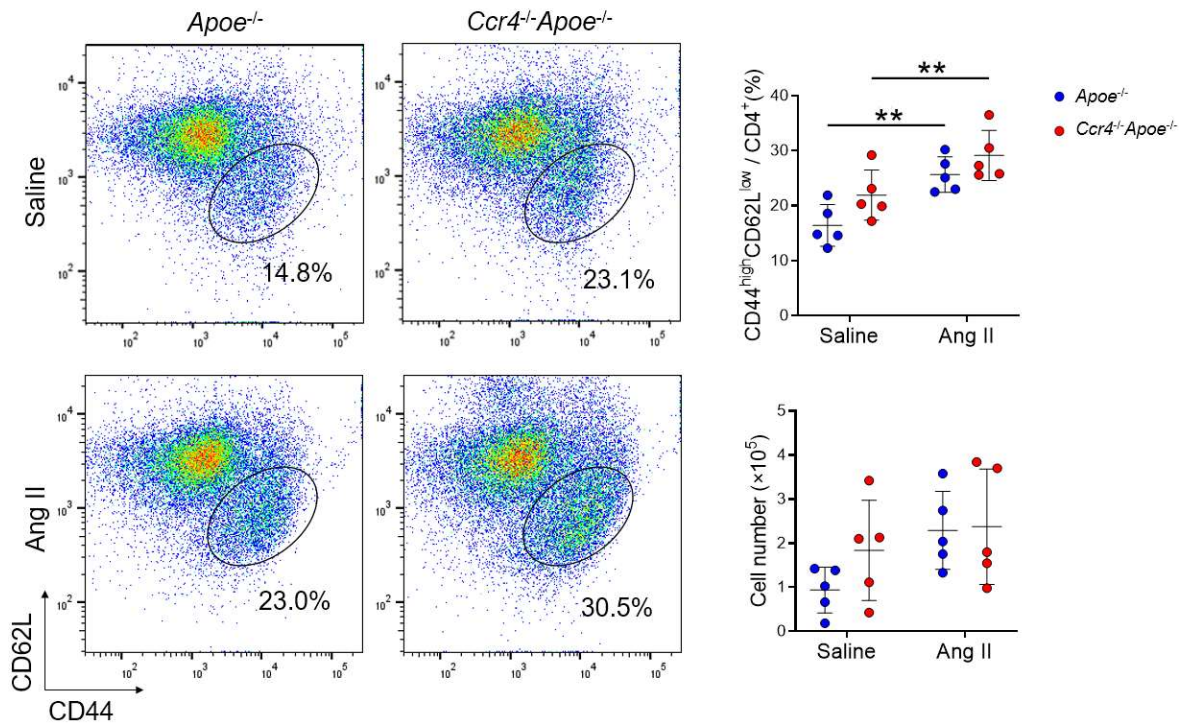


**Figure 47. CCR4 deficiency does not affect effector T cell frequency in the para-aortic LNs of angiotensin II-infused mice.** Seven days after the pump implantation, the mice were euthanized and lymphoid cells from para-aortic LNs were prepared. *Apoe*<sup>-/-</sup> mice infused with angiotensin II or saline served as controls. Representative flow cytometric analysis of CD4<sup>+</sup>CD44<sup>high</sup>CD62L<sup>low</sup> effector memory T cells in the para-aortic LNs of *Apoe*<sup>-/-</sup> or *Ccr4*<sup>-/-</sup>*Apoe*<sup>-/-</sup> mice. The graphs represent the proportions of CD4<sup>+</sup>CD44<sup>high</sup>CD62L<sup>low</sup> effector memory T cells in the para-aortic LNs. n=5 per group. Data points represent individual animals. Horizontal bars represent means. Error bars indicate s.d. \*\**P*<0.01; 2-way ANOVA followed by Tukey's multiple comparisons test.

Furthermore, ICS was performed to dissect the fractions of helper T cell subsets in para-aortic LNs. A similar enhancement of Th1 cells was identified by CCR4 deletion and augmentation of Th2 cells by angiotensin II infusion, as observed in peripheral LNs (**Figure 48**).

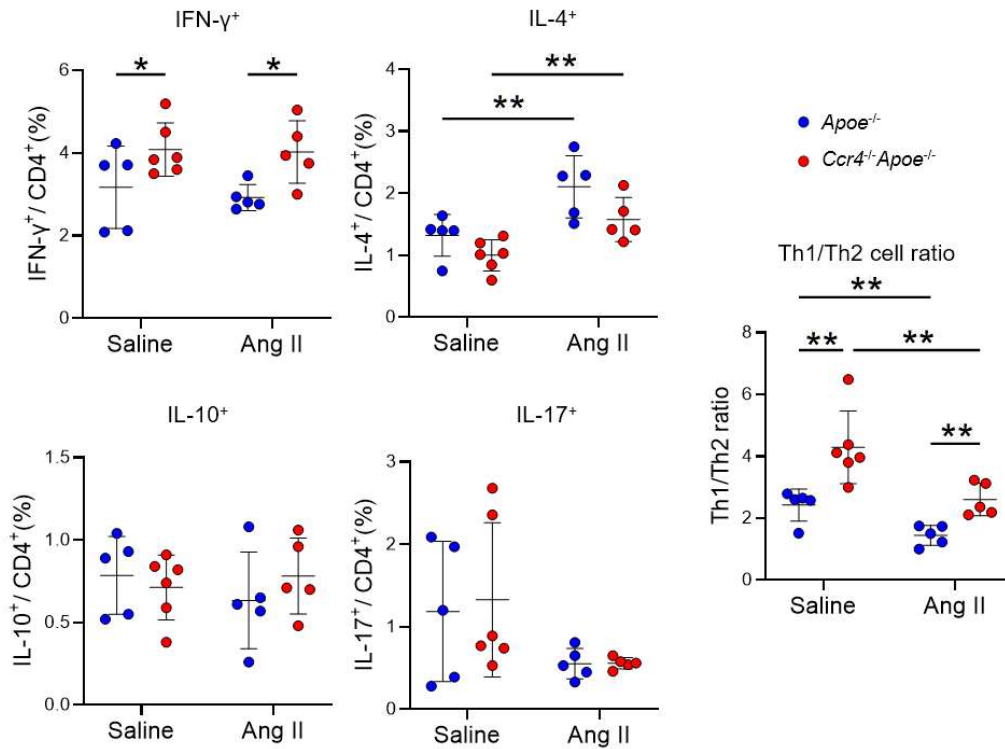


**Figure 48. CCR4 deficiency promotes Th1 cell responses in the para-aortic LNs of angiotensin II-infused mice.**

Seven days after the pump implantation, the mice were euthanized and lymphoid cells from para-aortic LNs were prepared. *Apoe*<sup>-/-</sup> mice infused with angiotensin II or saline served as controls. The graphs represent the frequencies of IFN- $\gamma$ <sup>+</sup>, IL-4<sup>+</sup>, IL-10<sup>+</sup>, and IL-17<sup>+</sup> CD4<sup>+</sup> T cells and the ratio of IFN- $\gamma$ <sup>+</sup> Th1 cells to IL-4<sup>+</sup> Th2 cells in the para-aortic LNs of *Apoe*<sup>-/-</sup> or *Ccr4*<sup>-/-</sup>*Apoe*<sup>-/-</sup> mice. *n*=5 to 6 per group. Data points represent individual animals. Horizontal bars represent means. Error bars indicate s.d. \**P* < 0.05, \*\**P* < 0.01; 2-way ANOVA followed by Tukey's multiple comparisons test.

Flow cytometric analyses of helper T cell subsets in the thoracoabdominal aortas were performed. Helper T cell subsets were distinguished using their respective signature transcription factors: T-bet, GATA3, ROR $\gamma$ t, and Foxp3 for Th1 cells, Th2 cells, Th17 cells, and Tregs, respectively. The frequency of aortic T-bet<sup>+</sup> Th1 cells in *Apoe*<sup>-/-</sup> and *Ccr4*<sup>-/-</sup>*Apoe*<sup>-/-</sup> mice was severely reduced by angiotensin II treatment. When considering cell frequency, *Ccr4*<sup>-/-</sup>*Apoe*<sup>-/-</sup> mice consistently showed a higher proportion of aortic T-bet<sup>+</sup> Th1 cells regardless of angiotensin II treatment. Meanwhile, their numbers remained similar among all groups (**Figure 49**). Even after pooling two aortas as one sample, the number of identified Th1 cells in the aorta was very low compared with other helper T cell subsets, making the gating dot plots appear unreliable. However, data reproducibility can be confirmed because the experiments for each group were conducted at least twice.

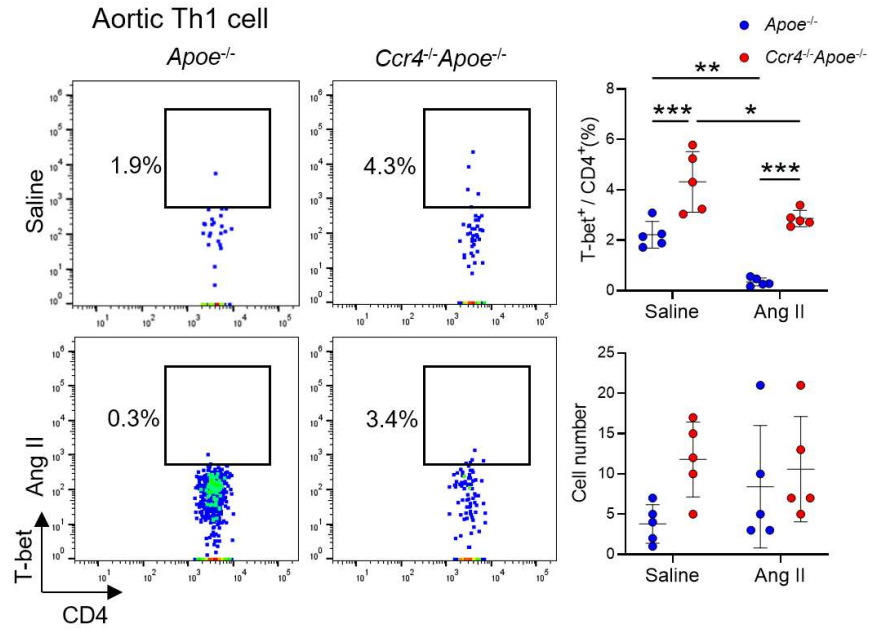


**Figure 49.** Flow cytometric analysis of T-box expressed in T cells (T-bet) expression in aortic CD3<sup>+</sup>CD4<sup>+</sup>CD45<sup>+</sup> T cells from *Apoe*<sup>-/-</sup> or *Ccr4*<sup>-/-</sup>*Apoe*<sup>-/-</sup> mice.

Seven days after the pump implantation, the mice were euthanized and lymphoid cells from thoracoabdominal aorta were prepared. *Apoe*<sup>-/-</sup> mice infused with angiotensin II or saline served as controls. The graphs represent the total numbers and frequencies of T-bet<sup>+</sup> cells among aortic CD3<sup>+</sup>CD4<sup>+</sup>CD45<sup>+</sup> T cells. n=5 per group. Pooled aortic lymphoid cells from two mice were analyzed as a sample. Data points represent individual pooled samples. Horizontal bars represent means. Error bars indicate s.d. \**P*<0.05, \*\**P*<0.01, \*\*\**P*<0.001; 2-way ANOVA followed by Tukey's multiple comparisons test. Ang II indicates angiotensin II.

No differences were detected in the frequency of aortic GATA3<sup>+</sup> Th2 cells between *Apoe*<sup>-/-</sup> and *Ccr4*<sup>-/-</sup>*Apoe*<sup>-/-</sup> mice regardless of angiotensin II infusion. Meanwhile, the number of aortic GATA3<sup>+</sup> Th2 cells was significantly lower in angiotensin II-infused *Ccr4*<sup>-/-</sup>*Apoe*<sup>-/-</sup> mice than in angiotensin II-infused *Apoe*<sup>-/-</sup> mice (**Figure 50**). Angiotensin II infusion slightly increased the number of aortic RORγt<sup>+</sup> Th17 cells in *Apoe*<sup>-/-</sup> and *Ccr4*<sup>-/-</sup>*Apoe*<sup>-/-</sup> mice. However, frequencies did not differ significantly among all groups (**Figure 51**).

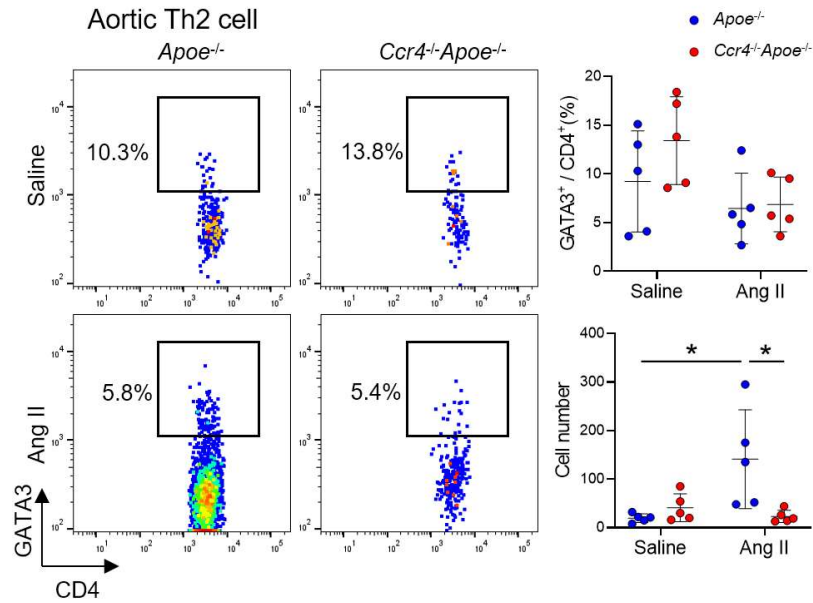


**Figure 50. Flow cytometric analysis of GATA3 expression in aortic CD3<sup>+</sup>CD4<sup>+</sup>CD45<sup>+</sup> T cells from *Apoe*<sup>-/-</sup> or *Ccr4*<sup>-/-</sup>*Apoe*<sup>-/-</sup> mice.** Seven days after the pump implantation, the mice were euthanized and lymphoid cells from thoracoabdominal aorta were prepared. *Apoe*<sup>-/-</sup> mice infused with angiotensin II or saline served as controls. The graphs represent the total numbers and frequencies of GATA3<sup>+</sup> cells among aortic CD3<sup>+</sup>CD4<sup>+</sup>CD45<sup>+</sup> T cells. n=5 per group. Pooled aortic lymphoid cells from two mice were analyzed as a sample. Data points represent individual pooled samples. Horizontal bars represent means. Error bars indicate s.d. \**P*<0.05; 2-way ANOVA followed by Tukey's multiple comparisons test. Ang II indicates angiotensin II.

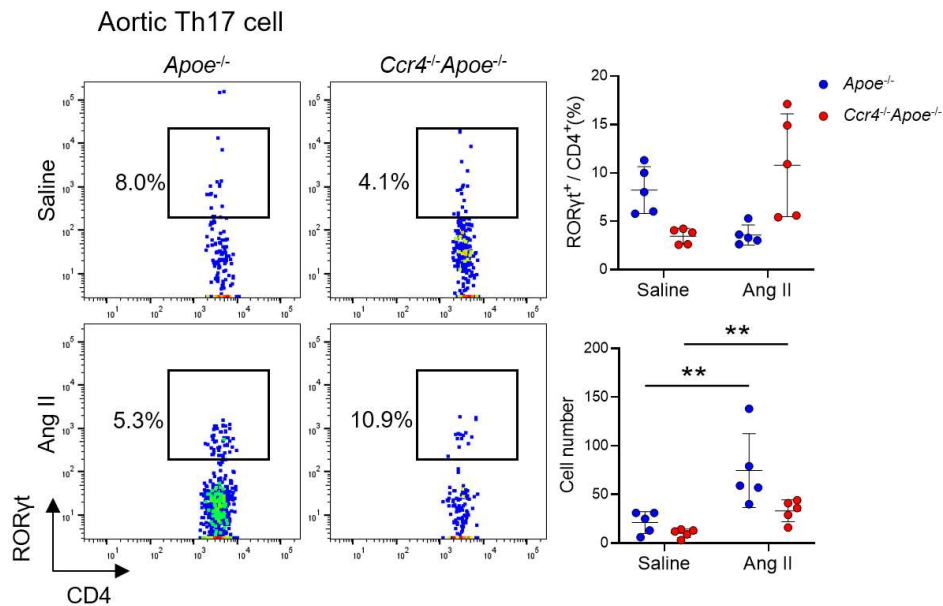


**Figure 51. Flow cytometric analysis of retinoic acid-related orphan receptor gamma t (RORγt) expression in aortic CD3<sup>+</sup>CD4<sup>+</sup>CD45<sup>+</sup> T cells from *Apoe*<sup>-/-</sup> or *Ccr4*<sup>-/-</sup>*Apoe*<sup>-/-</sup> mice.** Seven days after the pump implantation, the mice were euthanized and lymphoid cells from thoracoabdominal aorta were prepared. *Apoe*<sup>-/-</sup> mice infused with angiotensin II or saline served as controls. The graphs represent the total numbers and frequencies of RORγt<sup>+</sup> cells among aortic CD3<sup>+</sup>CD4<sup>+</sup>CD45<sup>+</sup> T cells. n=5 per group. Pooled aortic lymphoid cells from two mice were analyzed as a sample. Data points represent individual pooled samples. Horizontal bars represent means. Error bars indicate s.d. \*\**P*<0.01; 2-way ANOVA followed by Tukey's multiple comparisons test. Ang II indicates angiotensin II.

Subsequently, in agreement with lymphoid tissue data, the aortic Th1 cell/Th2 cell ratio was strikingly higher in angiotensin II-infused *Ccr4*<sup>-/-</sup>*Apoe*<sup>-/-</sup> mice than in angiotensin

II-infused *Apoe*<sup>-/-</sup> mice. Accordingly, a conclusion that Th1 cell-skewed helper T cell responses occur in aneurysmal lesions and peripheral lymphoid tissues in the absence of CCR4 was established (**Figure 52**).

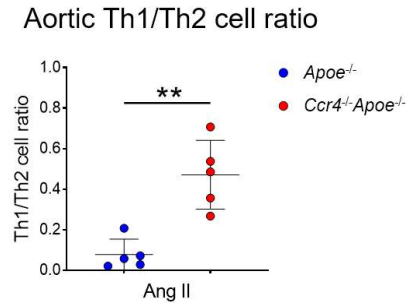


**Figure 52. Aortic ratio of T-bet<sup>+</sup> Th1 cells to GATA3<sup>+</sup> Th2 cells.**

Seven days after the pump implantation, the mice were euthanized and lymphoid cells from thoracoabdominal aorta were prepared. *Apoe*<sup>-/-</sup> mice infused with angiotensin II or saline served as controls. Pooled aortic lymphoid cells from 2 mice were analyzed as a sample. n=5 per group. Data points represent individual pooled samples. Horizontal bars represent means. Error bars indicate s.d. \*\**P*<0.01; two-tailed Student's *t*-test. Ang II indicates angiotensin II.

Angiotensin II infusion induced a likely reactive accumulation of aortic CD4<sup>+</sup>Foxp3<sup>+</sup> Tregs in *Apoe*<sup>-/-</sup> mice that was reflected in increased frequency and number. Notably, a similar phenomenon was not observed in the aorta of *Ccr4*<sup>-/-</sup>*Apoe*<sup>-/-</sup> mice (**Figure 53**). The frequency and number of aortic CD4<sup>+</sup>Foxp3<sup>+</sup> Tregs were remarkably lower in angiotensin II-infused *Ccr4*<sup>-/-</sup>*Apoe*<sup>-/-</sup> mice than in angiotensin II-infused *Apoe*<sup>-/-</sup> mice (**Figure 53**). These results revealed that the immunoinflammatory responses and reactive migration of Tregs were suppressed in the aorta of angiotensin II-infused *Ccr4*<sup>-/-</sup>*Apoe*<sup>-/-</sup> mice.

This study verified similar Th1 cell-skewed responses in the aorta and evaluated aortic B cell responses likely affected by this skewness. Flow cytometric analysis revealed that the frequency and number of aortic CD19<sup>+</sup>B220<sup>high</sup>CD45<sup>+</sup> B cells were significantly lower in angiotensin II-infused *Ccr4*<sup>-/-</sup>*Apoe*<sup>-/-</sup> mice than in angiotensin II-infused *Apoe*<sup>-/-</sup> mice (**Figure 54**).



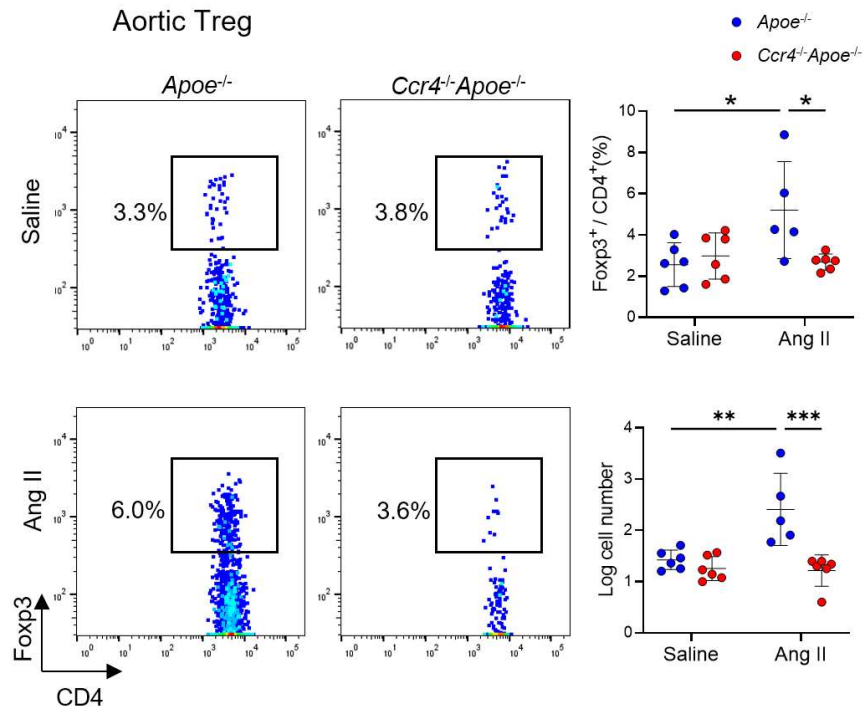


**Figure 53. Flow cytometric analysis of Foxp3 expression in aortic CD3<sup>+</sup>CD4<sup>+</sup>CD45<sup>+</sup> T cells from *Apoe*<sup>-/-</sup> or *Ccr4*<sup>-/-</sup>*Apoe*<sup>-/-</sup> mice.** Seven days after the pump implantation, the mice were euthanized and lymphoid cells from thoracoabdominal aorta were prepared. *Apoe*<sup>-/-</sup> mice infused with angiotensin II or saline served as controls. The graph represents the total numbers and frequency of Foxp3<sup>+</sup> Tregs among aortic CD3<sup>+</sup>CD4<sup>+</sup>CD45<sup>+</sup> T cells. n=5 to 6 per group. Pooled aortic lymphoid cells from two mice were analyzed as a sample. Data points represent individual pooled samples. Horizontal bars represent means. Error bars indicate s.d. \*P<0.05, \*\*P<0.01, \*\*\*P<0.001; 2-way ANOVA followed by Tukey's multiple comparisons test. Ang II indicates angiotensin II. Logarithmic transformation (log(x)) was applied to normalize distribution and stabilize variances of the cell count data.

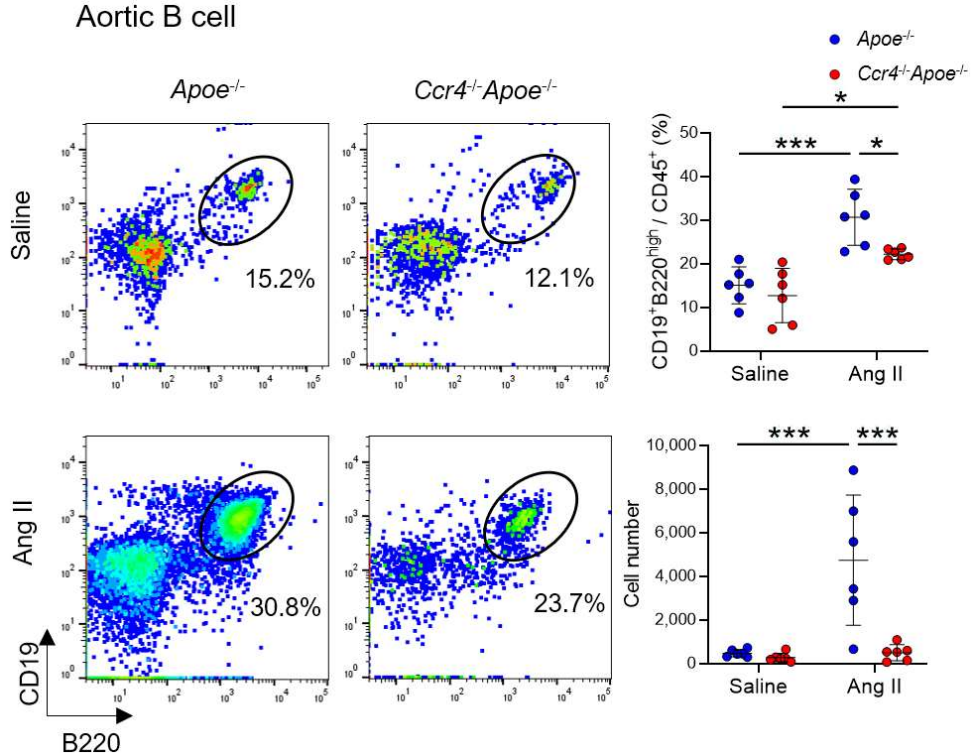


**Figure 54. Flow cytometric analysis of aortic CD19<sup>+</sup>B220<sup>high</sup>CD45<sup>+</sup> B cells from *Apoe*<sup>-/-</sup> or *Ccr4*<sup>-/-</sup>*Apoe*<sup>-/-</sup> mice.** Seven days after the pump implantation, the mice were euthanized and lymphoid cells from thoracoabdominal aorta were prepared. *Apoe*<sup>-/-</sup> mice infused with angiotensin II or saline served as controls. The graph represents the total number and proportion of CD19<sup>+</sup>B220<sup>high</sup>CD45<sup>+</sup> B cells. n=6 per group. Pooled aortic lymphoid cells from two mice were analyzed as a sample. Data points represent individual pooled samples. Horizontal bars represent means. Error bars indicate s.d. \*P<0.05, \*\*\*P<0.001; 2-way ANOVA followed by Tukey's multiple comparisons test. Ang II indicates angiotensin II.



These results collectively indicate that CCR4 deficiency skews the Th1 cell/Th2 cell ratio toward Th1 cells, which is associated with the inhibition of the angiotensin II-induced accumulation of Th2 cells and B cells in the aorta of *ApoE*<sup>-/-</sup> mice, partly contributing to the attenuation of AAA formation.

### 1.3. Discussion

This study collected evidence that genetic deficiency of CCR4 in atherosclerosis-prone mice reduced the incidence and ameliorated the severity of angiotensin II-induced AAA despite the contradictory finding of accelerated early atherosclerosis in the same mouse strain. However, this accelerated atherosclerosis appeared limited to the early stages; a previous study revealed no differences in plaque formation in older mice.<sup>53</sup> The protective effects against AAA were also evident structurally, with preserved elastin layers and reduced aortic inflammation, as indicated by decreased immune cell infiltration in the suprarenal region of the abdominal aorta.

Concurrently, a definitive shift in helper T cell responses toward Th1 predominance in peripheral lymphoid tissues and the aorta was observed in CCR4-deficient mice. This Th1-skewed T cell response is consistently associated with the aggravation of atherosclerosis,<sup>6, 7</sup> which may explain the detrimental effects of CCR4 deficiency on early atherosclerosis in these mice. Meanwhile, previous reports revealed a contradictory role of the Th1/Th2 balance between atherosclerosis and AAA, indicating that Th1 predominance resulting from CCR4 deficiency likely protects against AAA.<sup>11, 42</sup> A plausible explanation for the protective actions of Th1 cells in AAA includes the downregulation of Th2 and B cell responses and the upregulation of Th1 cell-derived IFN- $\gamma$ , which counteracts TGF- $\beta$  signaling and its profibrotic effects. Hence, this thesis elucidates the previously unidentified opposing roles of CCR4:

attenuating early atherosclerosis while mediating the development of AAA through the modulation of adaptive immune responses.

Growing evidence reveals that T cell-mediated immune responses are crucially intertwined in atherosclerosis and AAA progression.<sup>33</sup> The evidence is unequivocal in supporting the proatherogenic roles of Th1. However, the protective role of Th1 cell-mediated responses against AAA remains unclear because no direct evidence has been published. Documentation of the protective role of IFN- $\gamma$  in AAA formation supports the possibility that IFN- $\gamma$ -producing Th1 cells may similarly provide net protection against this disease.<sup>42</sup> Several studies have reported that Th2 cell-skewed immune responses promote the progression of AAA.<sup>11, 54</sup> Because Th1 cell activity antagonizes Th2 cell activity in various ways, beneficial Th1 cell-mediated responses may be partly explained by the downregulation of Th2 cell-mediated immune responses. Accordingly, Th1 cell-skewed responses in lymphoid tissues and the inflamed aorta play key roles in ameliorating angiotensin II-induced AAA. In this context, this thesis demonstrates that the augmentation of Th1 cell responses via CCR4 deletion results in unexpected protection against AAA formation while maintaining its detrimental role in early atherosclerosis. Nevertheless, the possibility that other immune mechanisms may also be involved in the improvement of AAA phenotype upon CCR4 deficiency cannot be excluded completely.

CCR4 deficiency displayed a consistent endorsement of Th1 cell responses across all lymphoid tissues and the inflamed aorta induced by hypercholesterolemia and angiotensin II infusion. Th1 cells are generally known not to express CCR4.<sup>28</sup> Hence, the possibility that CCR4 deletion directly augments Th1 cells devoid of any interaction with other immune cells can be dismissed. A previous study that performed targeted depletion of CD4<sup>+</sup>Foxp3<sup>+</sup> Tregs in hypercholesterolemic mice reported a sharp upregulation of helper T cell responses, including Th1 cell responses.<sup>41</sup> This result confirmed the indispensable regulatory roles of CD4<sup>+</sup>Foxp3<sup>+</sup>

Tregs in maintaining helper T cell immune responses during hypercholesterolemia. Subsequently, CCR4 was pivotal in helper T cell regulation by Tregs; a CCR4 deficiency severely diminished the Treg suppression capacity of conventional T cells.

The idea of the favorable attenuation of AAA despite the dysfunctional Treg phenotype is difficult to digest, as several studies have consistently provided the protective role of Tregs in AAA.<sup>39</sup> Moreover, this study reported the aggravation of early atherosclerosis in CCR4-deficient mice, which could be similarly explained by the upregulation of proatherogenic Th1 cell-responses caused by impaired Treg suppression capacity. However, the contradictory role of Th1 cells in atherosclerosis plaque buildup and AAA progression has previously been described.<sup>42</sup> In addition, upon CCR4 deletion, the favorable actions of Tregs may not necessarily be entirely negated, as CCR4-deficient Treg was significantly expanded in lymphoid tissues, and anti-inflammatory IL-10 derived from CCR4-deficient T cell culture was upregulated. Accordingly, this study deduced that augmented Th1 cell responses might significantly influence the AAA phenotype more than the impaired Treg function in angiotensin II-infused *Ccr4*<sup>-/-</sup>*Apoe*<sup>-/-</sup> mice.

The exact mechanisms by which Th1 cell-skewed responses ameliorate AAA formation remain unclear. No changes were detected in frequencies of the Th2 cell population in the peripheral lymphoid and aneurysmal tissues. However, their activities, particularly in maintaining B cell responses, were inhibited as the plasma levels of IgE related to B cell functions and immunoglobulin class switching were lower in angiotensin II-infused *Ccr4*<sup>-/-</sup>*Apoe*<sup>-/-</sup> mice than in angiotensin II-infused *Apoe*<sup>-/-</sup> mice. Furthermore, limited aortic B cell infiltration was observed under CCR4 deficiency. The above finding indicates that dampened B cell responses are likely attributed to Th2 cell antagonism by the Th1 cell-skewed responses observed in CCR4-deficient mice. Experimental evidence reveals that B cells play a detrimental role in the development of AAA through several mechanisms, including the

IgE-mediated activation of several immune cells<sup>55</sup> and the suppression of tolerogenic plasmacytoid DC and Treg responses.<sup>56</sup> Based on these reports, this study speculated that the modulation of B cell-mediated immune responses may be partially responsible for the protection against AAA in angiotensin II-infused *Apoe*<sup>-/-</sup> mice.

Genetic deficiency of the IFN- $\gamma$ -inducible T-cell chemokine CXC-motif-chemokine ligand 10 (CXCL10) in *Apoe*<sup>-/-</sup> mice promoted angiotensin II-induced AAA formation and rupture. This finding was associated with downregulated IFN- $\gamma$  expression and upregulated expression of the anti-inflammatory and profibrotic cytokine TGF- $\beta$  in the aneurysmal tissues.<sup>42</sup> In addition, the blockade of TGF- $\beta$  signaling by neutralizing antibody administration attenuated angiotensin II-induced aortic dilation, indicating that TGF- $\beta$  activation critically contributes to AAA formation under conditions of downregulated IFN- $\gamma$  expression.<sup>42</sup> IFN- $\gamma$  has an antifibrotic effect by inhibiting TGF- $\beta$  signaling.<sup>57, 58</sup> Hence, upregulated aortic TGF- $\beta$  expression in *Cxcl10*<sup>-/-</sup>*Apoe*<sup>-/-</sup> mice may result from downregulated IFN- $\gamma$  expression. The current data agree with these reports. This study noted that the angiotensin II-dependent upregulation of TGF- $\beta$ 1 and *Tgfb* mRNA expression was markedly attenuated in the aorta of angiotensin II-infused *Ccr4*<sup>-/-</sup>*Apoe*<sup>-/-</sup> mice, possibly due to Th1 cell-skewed responses. Attenuated collagen deposition in the aneurysmal lesions was also observed in these mice, possibly because of reduced fibroblast activation by downregulated TGF- $\beta$  signaling.<sup>59</sup> These reports and the data from this thesis collectively indicate that downregulated TGF- $\beta$  signaling may be central to the improvement of AAA phenotype in angiotensin II-infused *Ccr4*<sup>-/-</sup>*Apoe*<sup>-/-</sup> mice. Nevertheless, TGF- $\beta$  has complex functions; thus, its role in AAA formation remains controversial.<sup>33</sup>

The expression of chemokine receptors on a cell is linked to its migratory capabilities through binding to their respective ligands. Similarly, the CCL17/CCL22–CCR4 axes contributed to mediating CCR4-expressing Treg migration to inflamed tissues.<sup>45, 46</sup>

CD4<sup>+</sup>Foxp3<sup>+</sup> Tregs predominantly expressed CCR4 in angiotensin II-infused *Apoe*<sup>-/-</sup> mice, and Th2 cells highly expressed CCR4.<sup>28</sup> Meanwhile, CCR4 specific ligands, CCL17 and CCL22, were detected in the aneurysmal lesions of these mice. These findings indicate the pivotal role of the CCL17/CCL22–CCR4 axes in Tregs and Th2 cell migration into the aneurysmal aorta. This study reported lower numbers of aortic Tregs and Th2 cells in angiotensin II-infused *Ccr4*<sup>-/-</sup>*Apoe*<sup>-/-</sup> mice than in angiotensin II-infused *Apoe*<sup>-/-</sup> mice. The migratory inhibition of Tregs and Th2 cells may contribute to AAA development. Given their anti-inflammatory actions, Tregs are possibly protective against AAA.<sup>39</sup> However, the contribution of reduced aortic Tregs to the AAA phenotype in these angiotensin II-infused *Ccr4*<sup>-/-</sup>*Apoe*<sup>-/-</sup> mice remains unclear, as it may also be attributed to a decreased need for Treg recruitment in the less developed aneurysmal aorta. Conversely, aortic Th2 cells exacerbate AAA by producing related cytokines that upregulate the expression of various MMPs.<sup>60</sup> Therefore, decreased Th2 cell accumulation in the aorta may partly explain the mechanisms underlying attenuated AAA development in angiotensin II-infused *Ccr4*<sup>-/-</sup>*Apoe*<sup>-/-</sup> mice.

Mogamulizumab, a humanized monoclonal anti-CCR4 antibody, is clinically used to treat T cell malignancies, such as adult T cell leukemia/lymphoma and cutaneous T cell lymphomas that exhibit high expression levels of CCR4.<sup>11, 44</sup> Mogamulizumab use in patients with adult T cell leukemia/lymphoma effectively augments antitumor immunity by selectively depleting CCR4-expressing effector-type Tregs.<sup>61</sup> Based on these findings of the protective role of CCR4 deficiency in AAA, anti-CCR4 antibody treatment may hold potential for preventing the disease. Exacerbation of early atherosclerosis was observed in the current model, raising concerns about potential adverse events related to CAD. In contrast, a previous study that used similar CCR4 knockout mice reported no aggravation of atherosclerosis in older mice.<sup>53</sup> Additionally, patients with AAA are generally older and often present with advanced-stage atherosclerosis. These findings reveal that the risk of CAD-related adverse events should be

minimal when applied to the target population. However, a significant gap remains between the findings of this study and the current clinical use of mogamulizumab.

This study has notable limitations. Although Th1 cell-skewed immune responses are the central mechanism for the attenuated AAA development observed with CCR4 deficiency, no direct evidence supports this idea. This study used an animal model with global *Ccr4* gene deletion, which causes CCR4 deficiency from birth and not just during the experimental period. This could involve compensatory mechanisms that I am not aware of, potentially complicating the analysis. Additionally, this type of deficiency removes CCR4 expression from the relevant cells; however, it does not deplete the cells altogether, which may not accurately mimic mogamulizumab-induced depletion of CCR4-expressing cells.

Other experimental designs should address these limitations. For example, an immune cell-specific CCR4 deficiency model through bone marrow ablation followed by the transplantation of CCR4-deficient grafts, an inducible gene deletion in adult mice via the *Cre/lox* system, or pharmacological antagonism of CCR4 could clarify the role of CCR4 in AAA development. Once consistent experimental data are sufficiently gathered, future research should focus on human studies to provide translational findings relevant to clinical settings.

#### **1.4. Conclusion**

This thesis has detailed the protective effects of CCR4 deficiency against angiotensin II-induced AAA. In addition, this study has revealed a shift in helper T cell responses toward Th1 predominance in lymphoid tissues and the aorta despite the observed acceleration of early atherosclerosis. These Th1 cell-skewed responses are likely central in the aggravation of early atherosclerosis while limiting aneurysmal development: excessive Th2 cell-mediated responses, B cell-mediated IgE upregulation, and TGF- $\beta$  signaling, all contributing to the

prevention of AAA formation in the angiotensin II-infused *Ccr4*<sup>-/-</sup>*Apoe*<sup>-/-</sup> mice. These findings have highlighted CCR4 as a potential target of AAA immunotherapy.

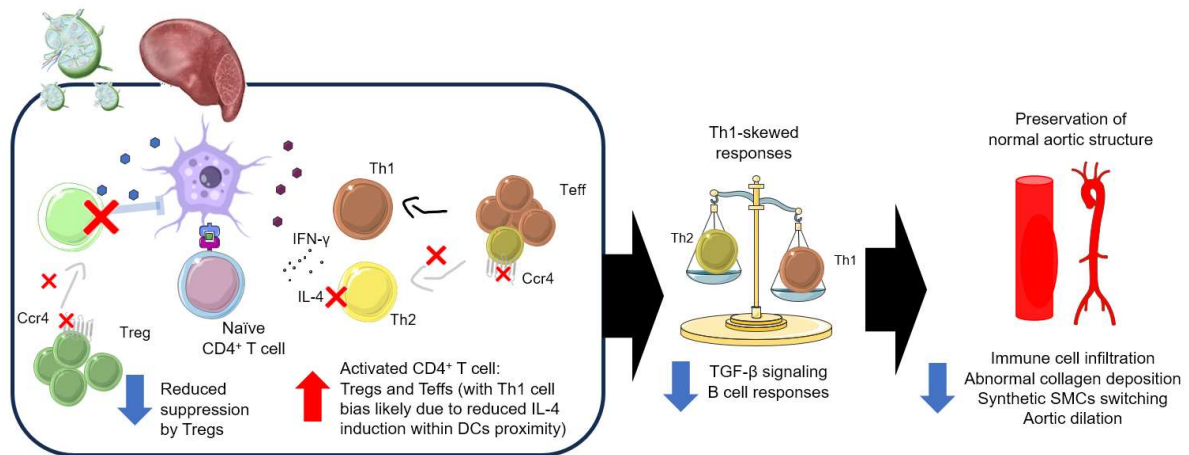


**Figure 55. Converse roles of CCR4 in atherosclerosis and AAA development.**

Genetic deletion of CCR4 causes Treg dysregulation that subsequently induces a Th1-skewed T cell responses which accelerates early atherosclerosis plaque formation while conversely attenuates aortic dilation. This figure was partly generated using Servier Medical Art, by Servier (<http://smart.servier.com>).



## **Chapter 2. Evaluating the efficacy of clinically feasible 312 nm UVB irradiation as phototherapy for atherosclerosis**

### **2.1. Introduction**

As outlined in the main introduction, substantial evidence has underscored the critical role of immunoinflammatory responses within the arterial wall, driven by dysregulated innate and adaptive immunity, in the pathogenesis of atherosclerosis. The involvement of immune mediators in regulating atherosclerosis progression is no longer a subject of controversy.<sup>34</sup> Previous clinical studies have demonstrated the potential efficacy of anti-inflammatory treatments in preventing cardiovascular and cerebrovascular ischemic events in patients with a history of myocardial infarction.<sup>30</sup> Notably, scRNA-seq analysis of carotid artery atherosclerotic plaques from patients has identified activated and differentiated T cells as the predominant immune cell types, emphasizing the significant role of effector T cell responses in the development of atherosclerotic lesions.<sup>37</sup> Consequently, experimental data further corroborate the notion that T<sub>H</sub>1 responses are integral to the pathogenesis of atherosclerosis.

Experimental studies in animal models have explored various approaches to modulate the T<sub>H</sub>1/T<sub>reg</sub> balance, utilizing interventions such as antibodies,<sup>17-19</sup> cytokines,<sup>19</sup> active vitamin D3 administration,<sup>20</sup> and vaccination strategies.<sup>21</sup> These studies have shown that shifting the T<sub>H</sub>1/T<sub>reg</sub> balance towards T<sub>reg</sub> responses may serve as a potential therapeutic strategy to mitigate the progression of atherosclerosis. However, such therapeutic strategies have not yet been implemented in clinical practice due to the inherent risk of immune dysregulation. The laboratory I am affiliated with is investigating the feasibility of utilizing UVB phototherapy—likely a safer alternative—to modulate immune responses for the prevention and treatment of atherosclerosis.

Sunlight exposure to humans consists predominantly of UVA radiation (approximately 95%), with a smaller proportion of UVB radiation. Sunlight and its interaction with skin metabolism are vital for human health, particularly in the synthesis of vitamin D and the regulation of immune functions.<sup>62</sup> Moreover, UVB-based phototherapy has proven to be an effective clinical treatment for immunoinflammatory skin diseases such as psoriasis and vitiligo.<sup>63</sup> In experimental animal models, it has been reported that BB-UVB irradiation (a broad spectrum ranging from 280 to 320 nm, with a peak at approximately 313 nm)<sup>19</sup> augments anti-inflammatory immune responses, particularly through the induction of Tregs, and reduces atherosclerotic plaque development in hypercholesterolemic *Apoe*<sup>-/-</sup> mice. Concurrently, NB-UVB (a narrow spectral output with a peak at approximately 311 nm) is widely used in clinical dermatology, particularly for psoriasis, as a preferred alternative to BB-UVB.<sup>63</sup> Based on these findings, UVB phototherapy could potentially be applied to atherosclerosis treatment, provided that the irradiation conditions, such as dose and wavelength, are carefully controlled to minimize adverse effects.

Furthermore, research into optimal irradiation conditions has sought to identify effective wavelengths for promoting atheroprotective effects. Using LED-based technology, novel irradiation devices were developed to emit specific UVB wavelengths, including 282 nm UVB (which is not found in natural sunlight) and 312 nm UVB, which corresponds to the peak wavelength used in clinical NB-UVB phototherapy. The effects of these specific UVB wavelengths on atherosclerosis and their underlying mechanisms were investigated in hypercholesterolemic *Apoe*<sup>-/-</sup> mice, focusing on immunoinflammatory responses. Notably, the investigation revealed that irradiation with 2 kJ/m<sup>2</sup> 312 nm UVB showed tendency to attenuate atherosclerotic lesion formation. However, this effect did not reach statistical significance and was not accompanied with Treg augmentation.<sup>4</sup> Given that the UVB dose used in this previous study was relatively low compared to the doses used in clinical treatment, the present study

aims to explore the effects of higher doses of 312 nm UVB irradiation on immunoinflammatory responses and atherosclerosis

## 2.2. Results

### 2.2.1. Irradiation of 312 nm UVB prevented atherosclerosis development and promoted a less inflammatory plaque phenotype

The adverse event associated with UVB irradiation that experts are most concerned about is the development of skin cancer, which can ultimately lead to mortality. Fortunately, no deaths, skin cancers, or burns were observed in mice during or after the experiment. At the time of sacrifice, after 14 irradiation cycles when mice reached 20 weeks of age, no significant differences in body weight, plasma lipid profile, and plasma levels of C-reactive protein (CRP) were identified between 5 or 10 kJ/m<sup>2</sup> 312 nm UVB-irradiated and nonirradiated mice (Table 3).

**Table 3. Body weight, plasma lipid profile, and plasma levels of CRP of 20-week-old 312 nm UVB-irradiated or nonirradiated male *Apoe*<sup>-/-</sup> mice.**

Parameters	Nonirradiated	UVB 5 kJ/m <sup>2</sup>	UVB 10 kJ/m <sup>2</sup>
Body weight (g)	29.5 ± 2.9 (n=11)	28.6 ± 2.6 (n=11)	28.8 ± 2.5 (n=11)
Total cholesterol (mg/dL)	600.2 ± 123.9 (n=10)	678.5 ± 135.2 (n=10)	701.8 ± 114.1 (n=10)
LDL-cholesterol (mg/dL)	171.0 ± 34.1 (n=10)	167.2 ± 39.1 (n=10)	165.4 ± 46.7 (n=10)
HDL-cholesterol (mg/dL)	17.7 ± 4.9 (n=10)	20.2 ± 4.8 (n=10)	19.2 ± 2.2 (n=10)
Triglycerides (mg/dL)	85.5 ± 24 (n=10)	89.7 ± 16 (n=10)	118.1 ± 43.2 (n=10)
CRP (µg/mL)	9.2 ± 1.2 (n=10)	8.6 ± 0.5 (n=10)	8.5 ± 0.9 (n=10)

All the data are expressed as the mean ± s.d. *Apoe*<sup>-/-</sup> indicates apolipoprotein E-deficient; UVB, ultraviolet B; LDL, low-density lipoprotein; HDL, high-density lipoprotein; and CRP, C-reactive protein.

A notable size reduction in aortic sinus atherosclerosis lesions was observed in the 10 kJ/m<sup>2</sup> 312 nm UVB-irradiated mice when the aortic sinus plaques at five different levels were analyzed in detail compared with the nonirradiated control mice (Figure 56). Meanwhile, lower

irradiation with the 5 kJ/m<sup>2</sup> 312 nm UVB yielded unsatisfactory results, as it did not affect atherosclerosis positively.

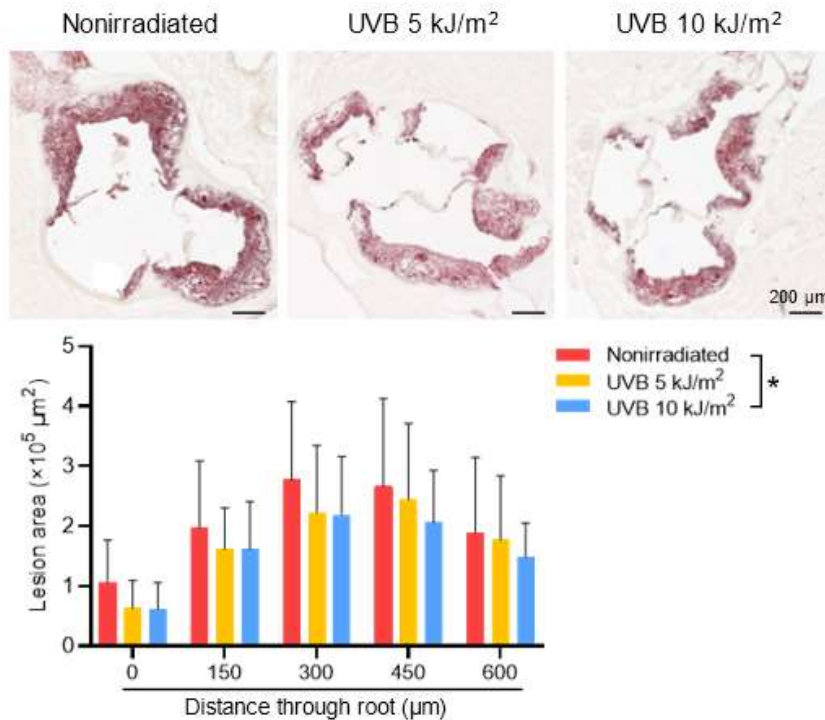


**Figure 56. 312 nm UVB irradiation inhibits the development of atherosclerosis.**

Representative photomicrographs of Oil Red O staining and quantitative analysis of atherosclerotic lesion area at 5 different levels in the aortic sinus of 312 nm UVB-irradiated or nonirradiated mice. Six-week-old male *Apoe*<sup>-/-</sup> mice were irradiated with 312 nm UVB at 5 or 10 kJ/m<sup>2</sup> once weekly for 14 weeks and euthanized at 20 weeks of age, and atherosclerotic lesions were assessed. Nonirradiated male *Apoe*<sup>-/-</sup> mice served as controls. n=11 per group. Black bars represent 200 μm. Data are expressed as the mean±s.d. \*P<0.05; 2-way ANOVA followed by Dunnett's post hoc test.

In the aortic sinus, the mean of the atherosclerotic lesion area was presented as mean ± s.d. and calculated by averaging the results of five measurement levels. The calculated values were  $2.07 \pm 0.69 \times 10^5 \mu\text{m}^2$  in control nonirradiated mice,  $1.73 \pm 0.70 \times 10^5 \mu\text{m}^2$  in 5 kJ/m<sup>2</sup> UVB-irradiated mice, and  $1.59 \pm 0.62 \times 10^5 \mu\text{m}^2$  in 10 kJ/m<sup>2</sup> UVB-irradiated mice.

Concurrent with the aortic sinus cross-section observation, this study evaluated the atherosclerosis presentation in the thoracoabdominal aortas through oil red O staining in en face analysis. No marked differences were observed between the 5 or 10 kJ/m<sup>2</sup> UVB-irradiated mice and nonirradiated control mice. The atherosclerosis lesion was presented as mean ± s.d. and measured as the percent area of the lesion compared with the total inner aortic area. The

aortic lesion measurements are  $8.02 \pm 2.15\%$  in control nonirradiated mice,  $6.98 \pm 2.17\%$  in 5 kJ/m<sup>2</sup> UVB-irradiated mice, and  $6.44 \pm 1.49\%$  in 10 kJ/m<sup>2</sup> UVB-irradiated mice (**Figure 57**).

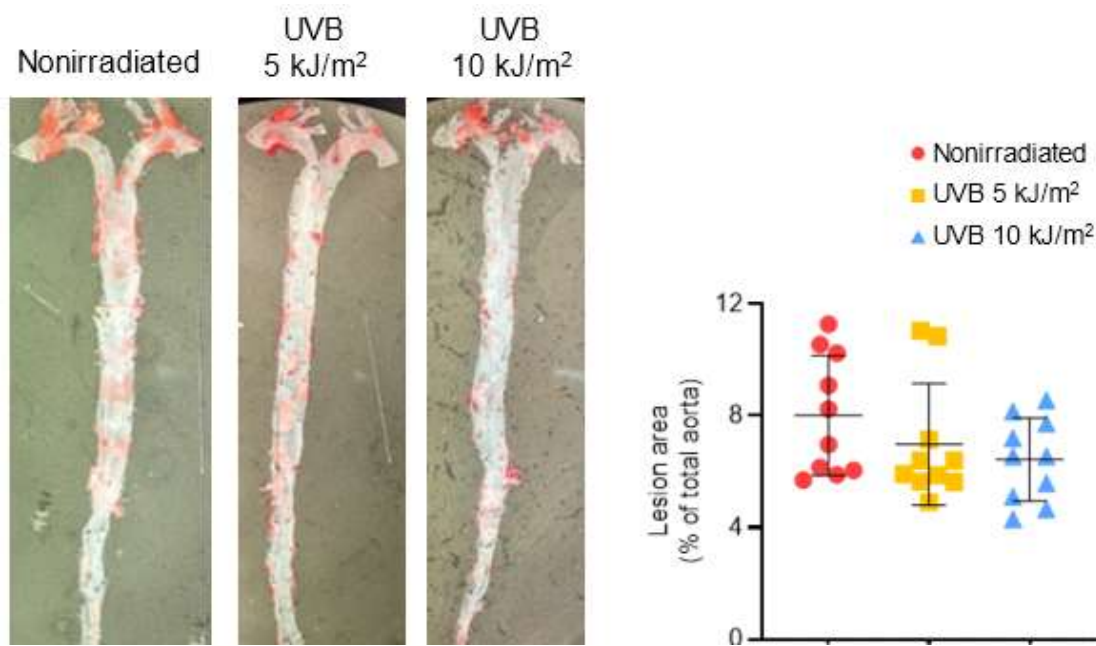


**Figure 57. 312 nm UVB irradiation does not affect atherosclerosis development in the thoracoabdominal aorta.**

Representative photomicrographs of Oil Red O staining and quantitative analysis of atherosclerotic lesion area in the thoracoabdominal aorta of 312 nm UVB-irradiated or nonirradiated mice. Six-week-old male *ApoE*<sup>-/-</sup> mice were irradiated with 312 nm UVB at 5 or 10 kJ/m<sup>2</sup> once weekly for 14 weeks and euthanized at 20 weeks of age, and atherosclerotic lesions were assessed. n=10 per group. Data points represent individual animals. Horizontal bars represent means. Error bars indicate s.d. Data are expressed as the mean±s.d.

Interventions that benefit atherosclerosis may also alter plaque characteristics (inflammation and stability). Several analyses of the aortic sinus cross section obtained from cryosection, including immunohistochemistry and Masson's trichrome collagen staining, were performed to observe such changes.

Immunohistochemistry was conducted to detect the infiltration of immune cells by staining the macrophage marker MOMA-2 and helper T cell marker CD4. MOMA-2 staining revealed a significant reduction in macrophage accumulation in 10 kJ/m<sup>2</sup> UVB irradiated mice by 20% compared with the nonirradiated control (**Figure 58**). Moreover, cells stained positive for CD4 were markedly less observed (43% less than nonirradiated control) in the plaque of 10 kJ/m<sup>2</sup> UVB-irradiated mice (**Figure 59**). Meanwhile, compared with nonirradiated mice, the

atherosclerotic lesions showed unchanged intraplaque macrophage accumulation for 5 kJ/m<sup>2</sup> UVB-irradiated mice (**Figure 58**). However, CD4<sup>+</sup> T cell infiltration was significantly lower in the 5 kJ/m<sup>2</sup> UVB-irradiated mice than in the nonirradiated mice (**Figure 59**).

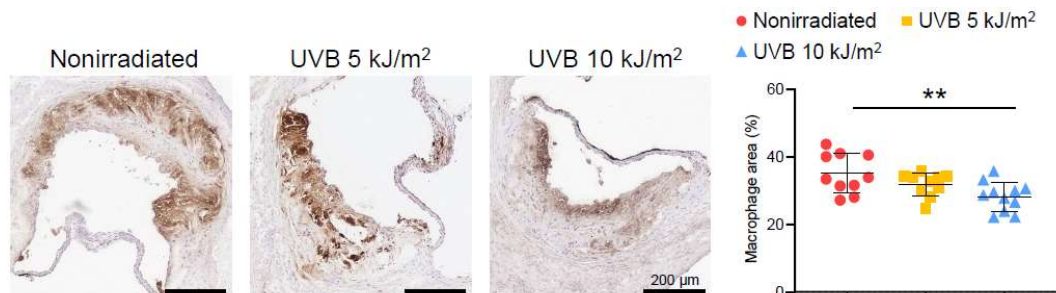


**Figure 58. 312 nm UVB irradiation reduces intraplaque macrophage accumulation.** Six-week-old male *Apoe*<sup>-/-</sup> mice were irradiated with 312 nm UVB at 5 or 10 kJ/m<sup>2</sup> once weekly for 14 weeks then euthanized at 20 weeks of age, and atherosclerotic lesions were assessed. Nonirradiated male *Apoe*<sup>-/-</sup> mice served as controls. Representative sections and quantitative analysis of MOMA-2<sup>+</sup> macrophages. n=10 mice per group. Black bars represent 200 µm as described. Data points represent individual animals. Horizontal bars represent means. Error bars indicate s.d. \*\**P*<0.01; 1-way ANOVA followed by Dunnett's post hoc test.

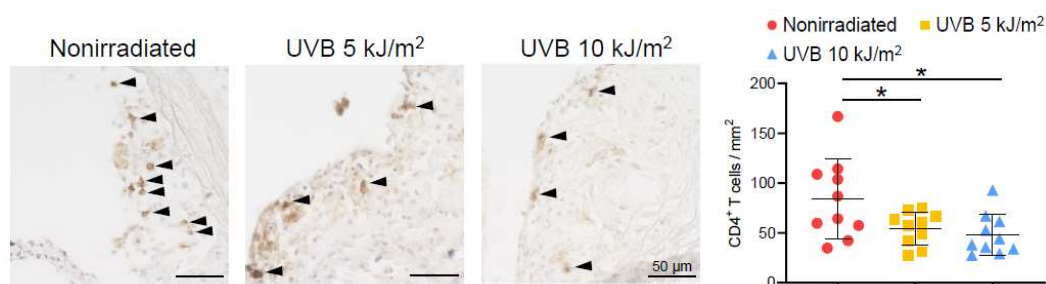


**Figure 59. 312 nm UVB irradiation reduces intraplaque infiltration of CD4<sup>+</sup> T cells.** Six-week-old male *Apoe*<sup>-/-</sup> mice were irradiated with 312 nm UVB at 5 or 10 kJ/m<sup>2</sup> once weekly for 14 weeks then euthanized at 20 weeks of age, and atherosclerotic lesions were assessed. Nonirradiated male *Apoe*<sup>-/-</sup> mice served as controls. Representative sections and quantitative analysis of CD4<sup>+</sup> T cells. Black arrowheads indicate the CD4<sup>+</sup> T cells. n=10 per group. Black bars represent 50 µm as described. Data points represent individual animals. Horizontal bars represent means. Error bars indicate s.d. \**P*<0.05; 1-way ANOVA followed by Dunnett's post

Masson's trichrome collagen staining was performed to evaluate plaque stability through collagen fiber quantification in aortic sinus plaques. Photomicrograph analyses revealed that the plaques of 312 nm UVB-irradiated mice were packed with more collagen fiber. The proportion of collagen content was significantly higher in 5 or 10 kJ/m<sup>2</sup> UVB-irradiated mice than in nonirradiated mice (**Figure 60**).

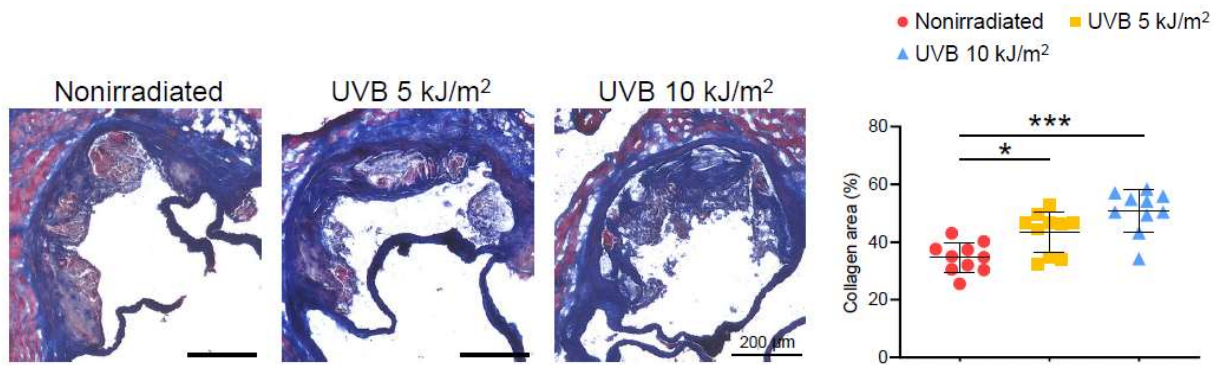


**Figure 60. 312 nm UVB induces a more stable plaque phenotype through the increase of intraplaque collagen content.**

Six-week-old male *Apoe*<sup>-/-</sup> mice were irradiated with 312 nm UVB at 5 or 10 kJ/m<sup>2</sup> once weekly for 14 weeks then euthanized at 20 weeks of age, and atherosclerotic lesions were assessed. Nonirradiated male *Apoe*<sup>-/-</sup> mice served as controls. Representative sections and quantitative analysis of collagen area. n=10 per group. Black bars represent 200 μm as described. Data points represent individual animals. Horizontal bars represent means. Error bars indicate s.d. \*P<0.05; \*\*\*P<0.001; 1-way ANOVA followed by Dunnett's post hoc test.

Total RNA from the whole aorta was extracted for quantification to investigate the effect of 312 nm UVB irradiation on aortic inflammation and immune responses. Messenger RNA expression of pro- or anti-inflammatory cytokines and transcription factors specific to helper T cell subsets or Tregs by quantitative reverse transcription PCR. No significant differences were detected in the expression of these inflammation-associated genes in the aorta between 5 or 10 kJ/m<sup>2</sup> UVB-irradiated and nonirradiated mice (**Figure 61**).

The above results indicate that higher irradiation with 10 kJ/m<sup>2</sup> 312 nm UVB inhibited the development of atherosclerosis, possibly through a reduction in proinflammatory immune responses in the aorta, although the atheroprotective effect seems confined only to aortic sinus lesions.



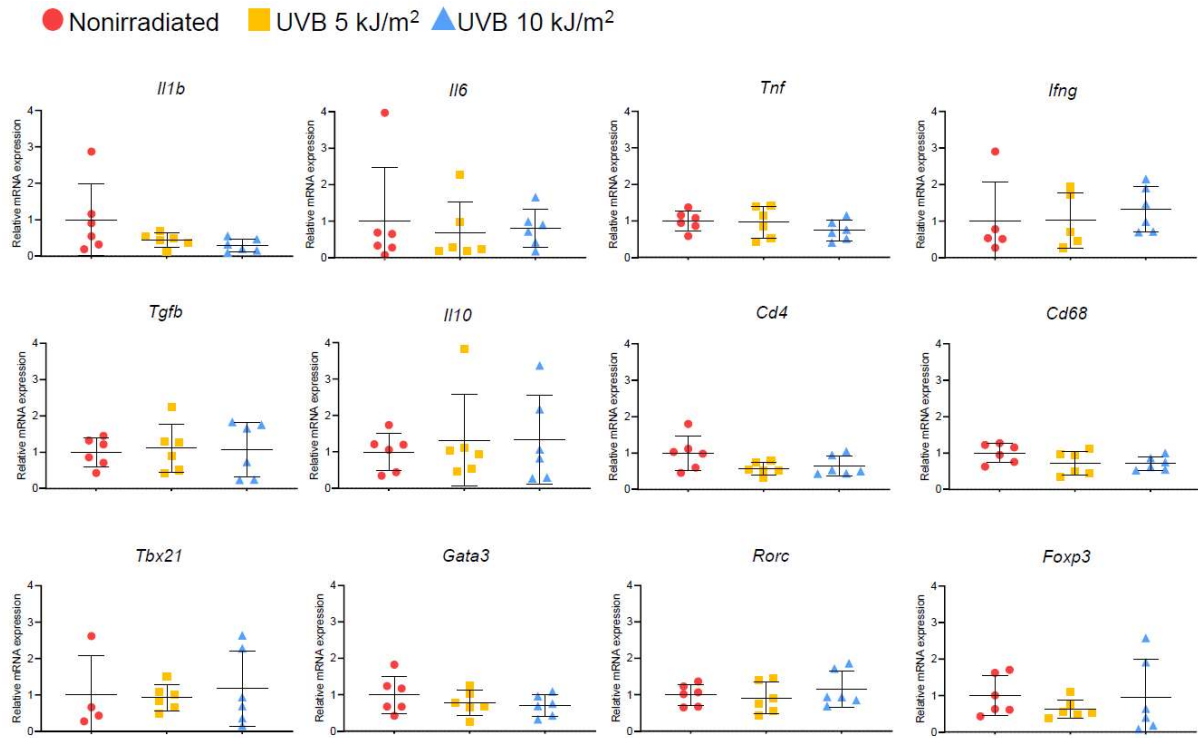


**Figure 61. The effect of 312 nm UVB on mRNA levels of immunoinflammatory markers in atherosclerotic aorta.**

Six-week-old male *Apoe*<sup>-/-</sup> mice were irradiated with 312 nm UVB at 5 or 10 kJ/m<sup>2</sup> once weekly for 14 weeks and euthanized at 20 weeks of age, and thoracoabdominal aorta was harvested. Nonirradiated male *Apoe*<sup>-/-</sup> mice served as controls. The mRNA expression of proinflammatory cytokines (*Il1b*, *Il6*, *Tnf*, and *Ifng*), anti-inflammatory cytokines (*Il10* and *Tgfb*), macrophage marker (*Cd68*), helper T cell marker (*Cd4*), helper T cell-associated transcription factors (*Tbx21*, *Gata3*, and *Rorc*), and Treg-specific transcription factor (*Foxp3*) in the aorta of 312 nm UVB-irradiated or nonirradiated *Apoe*<sup>-/-</sup> mice was quantified by quantitative reverse transcription PCR and normalized to that of  $\beta$ -actin. The expression levels of the target genes were normalized so that the mean values in nonirradiated mice were set to 1. n=4 to 6 per group. Data points represent individual animals. Horizontal bars represent means. Error bars indicate s.d.

### 2.2.2. Teff/Treg balance in peripheral lymphoid tissues shifted toward Treg responses following 312 nm UVB irradiation

The previous section reported that 10 kJ/m<sup>2</sup> 312 nm UVB irradiation protects the aortic sinus from atherosclerosis. This study first focused on observing CD4<sup>+</sup> T cell responses in peripheral lymphoid tissues to understand their atheroprotective effects. For this mechanistic investigation, a weekly irradiation course was performed on male *Apoe*<sup>-/-</sup> mice with 5 or 10 kJ/m<sup>2</sup> 312 nm UVB for 6 weeks. At the end of six irradiation courses, flow cytometry was performed on immune cells isolated from skin-draining LNs and spleens. The examination focused on CD4<sup>+</sup>Foxp3<sup>+</sup>Treg and CD4<sup>+</sup>CD44<sup>high</sup>CD62L<sup>low</sup> effector memory T cell populations.

Higher irradiation with 10 kJ/m<sup>2</sup> UVB markedly increased the frequency and number of CD4<sup>+</sup>Foxp3<sup>+</sup> Tregs in the skin-draining LNs of *Apoe*<sup>-/-</sup> mice. In comparison, lower irradiation with 5 kJ/m<sup>2</sup> UVB irradiation only managed to increase the frequency of CD4<sup>+</sup>Foxp3<sup>+</sup> Tregs without changing the total number in the skin-draining LNs. Moreover, similar observations of cells isolated from the spleen revealed that the frequency and number of CD4<sup>+</sup>Foxp3<sup>+</sup> Tregs were also increased in the 10 kJ/m<sup>2</sup> UVB-irradiated mice. The lower irradiation with 5 kJ/m<sup>2</sup> UVB did not show a similar favorable effect on Tregs (**Figure 62**).

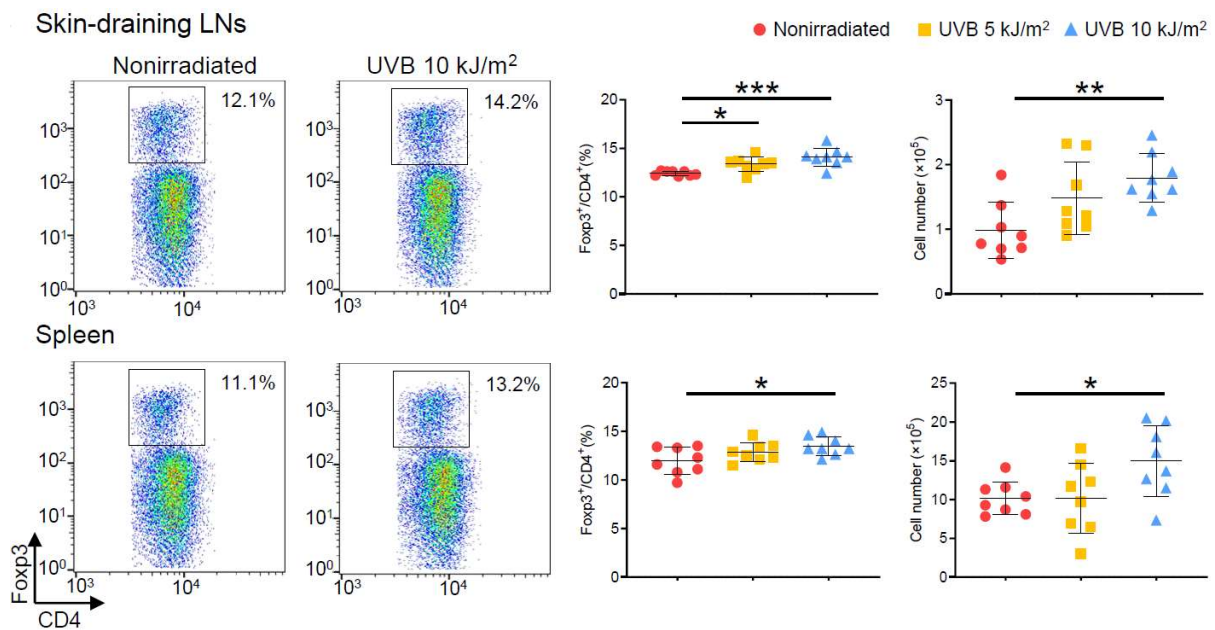


**Figure 62. 312 nm UVB irradiation increases Treg proportion and numbers in peripheral lymphoid tissues.**

Male *Apoe*<sup>-/-</sup> mice were irradiated with 312 nm UVB at 5 or 10 kJ/m<sup>2</sup> once weekly for 6 weeks. Nonirradiated male *Apoe*<sup>-/-</sup> mice served as controls. Four days after the last UVB irradiation, lymphoid cells from skin-draining LNs and spleen were prepared. Representative flow cytometric analysis of CD4<sup>+</sup>Foxp3<sup>+</sup> Tregs in the skin-draining LNs and spleen. The graphs represent the proportions and total numbers of CD4<sup>+</sup>Foxp3<sup>+</sup> Tregs in the skin-draining LNs and spleen. n=8 per group. Data points represent individual animals. Horizontal bars represent means. Error bars indicate s.d. \**P*<0.05; \*\**P*<0.01; \*\*\**P*<0.001; 1-way ANOVA followed by Dunnett's post hoc test.

In addition to the positive effect of irradiation on the Teff/Treg balance, higher irradiation with 10 kJ/m<sup>2</sup> significantly lowers the frequency and number of CD4<sup>+</sup>CD44<sup>high</sup>CD62L<sup>low</sup> effector memory T cells in the spleen compared with those in the spleens of nonirradiated mice. Similar findings were obtained for the frequency and number in the spleens of 5 kJ/m<sup>2</sup> UVB-irradiated mice (**Figure 63**). Conversely, the number of

CD4<sup>+</sup>CD44<sup>high</sup>CD62L<sup>low</sup> effector memory T cells in the skin-draining LNs was higher in the 10 kJ/m<sup>2</sup> UVB-irradiated mice than in the nonirradiated control mice (**Figure 63**).

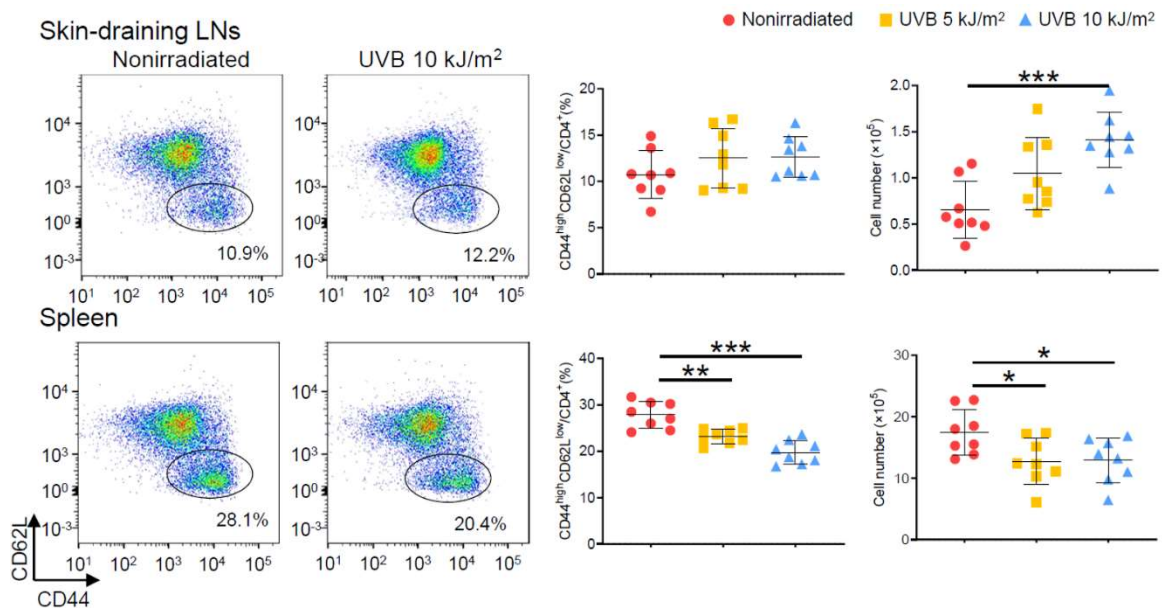


**Figure 63.** 312 nm UVB irradiation increases CD4<sup>+</sup>CD44<sup>high</sup>CD62L<sup>low</sup> effector memory T cells in the skin-draining LNs, while it reduces their proportion and numbers in spleen.

Male *Apoe*<sup>-/-</sup> mice were irradiated with 312 nm UVB at 5 or 10 kJ/m<sup>2</sup> once weekly for 6 weeks. Nonirradiated male *Apoe*<sup>-/-</sup> mice served as controls. Four days after the last UVB irradiation, lymphoid cells from skin-draining LNs and spleen were prepared. Representative flow cytometric analysis of CD4<sup>+</sup>CD44<sup>high</sup>CD62L<sup>low</sup> effector memory T cells in the skin-draining LNs and spleen. The graphs represent the proportions and total numbers of CD4<sup>+</sup>CD44<sup>high</sup>CD62L<sup>low</sup> effector memory T cells in the skin-draining LNs and spleen. n=8 per group. Data points represent individual animals. Horizontal bars represent means. Error bars indicate s.d. \*P<0.05; \*\*P<0.01; \*\*\*P<0.001; 1-way ANOVA followed by Dunnett's post hoc test.

Given the consistent findings supporting an increase in the number and proportion of Tregs, this study investigated the effect of 312 nm UVB on the activation state and functional capacity of CD4<sup>+</sup>Foxp3<sup>+</sup> Tregs. The expression of the suppressive function-associated molecule CTLA-4 and the activation-associated molecule CD103 in CD4<sup>+</sup>Foxp3<sup>+</sup> Tregs in peripheral lymphoid tissues was examined using flow cytometry. No significant changes were observed in the expression of either molecule in CD4<sup>+</sup>Foxp3<sup>+</sup> Tregs in the skin-draining LNs and spleens of 5 or 10 kJ/m<sup>2</sup> UVB-irradiated mice (**Figure 64**), indicating a minor effect of 312 nm UVB irradiation on the suppressive capacity of CD4<sup>+</sup>Foxp3<sup>+</sup> Tregs.

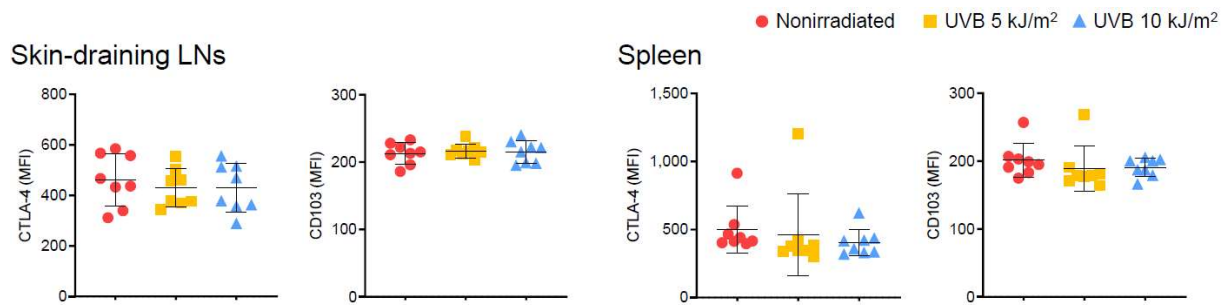


**Figure 64. No change in the expression of activation-associated molecules on Tregs after 312 nm UVB irradiation.**

Male *Apoe*<sup>-/-</sup> mice were irradiated with 312 nm UVB at 5 or 10 kJ/m<sup>2</sup> once weekly for 6 weeks. Nonirradiated male *Apoe*<sup>-/-</sup> mice served as controls. Four days after the last UVB irradiation, lymphoid cells from skin-draining LNs and spleen were prepared. The expression levels of CTLA-4 and CD103 were analyzed by gating on CD4<sup>+</sup>Foxp3<sup>+</sup> Tregs in the skin-draining LNs and spleen. n=8 per group. Data points represent individual animals. Horizontal bars represent means. Error bars indicate s.d. MFI indicates mean fluorescence intensity.

These data show that higher irradiation with 10 kJ/m<sup>2</sup> UVB systemically shifted the Teff/Treg balance toward Treg responses by synergically reducing the Teff frequency and number while increasing the Treg frequency and number in the spleen, which likely reduces the systemic inflammation that contributes to the reduction of atherosclerosis. Although similar Treg increases were observed in the skin-draining LNs of irradiated mice, an increase in the Teff number was observed, presumably due to reactive inflammatory responses to local radiation-induced injury in the skin. Lower irradiation with 5 kJ/m<sup>2</sup> UVB irradiation also resulted in a systemic decrease in Teffs; however, it had a minor effect on systemic Treg responses, indicating a modest change in the Teff/Treg balance and weak atheroprotective effects in this lower dose irradiation.

### **2.2.3. Irradiation with 312 nm UVB decreased the Th1 cell/Th2 cell ratio without affecting other immune cell responses in peripheral lymphoid tissues**

After observing that 312 nm UVB irradiation modulated Treg and Teff populations in favor of anti-inflammatory Tregs, I investigated whether it favorably affected CD4<sup>+</sup> T cell subsets. To assess changes in helper T cell subsets, I performed six cycles of irradiation on male

*Apoe*<sup>-/-</sup> mice with 5 or 10 kJ/m<sup>2</sup> 312 nm UVB once weekly and analyzed CD4<sup>+</sup> T cell subsets in immune cells isolated from the spleen using ICS.

In comparison with the nonirradiated control mice, I did not observe any remarkable change in the frequencies of IFN- $\gamma$ -producing Th1 cells, IL-4-producing Th2 cells, IL-10-producing CD4<sup>+</sup> T cells, and IL-17-producing Th17 cells in the spleens of the 5 or 10 kJ/m<sup>2</sup> UVB-irradiated mice (**Figure 65A**). Although individual frequencies did not reveal significant differences, careful calculation of the ratio of IFN- $\gamma$ -producing Th1 cells to IL-4-producing Th2 cells (Th1/Th2 ratio) exhibited a sharp reduction in 5 kJ/m<sup>2</sup> and 10 kJ/m<sup>2</sup> 312 nm UVB-irradiated mice compared with nonirradiated control mice (**Figure 65A and 65B**).

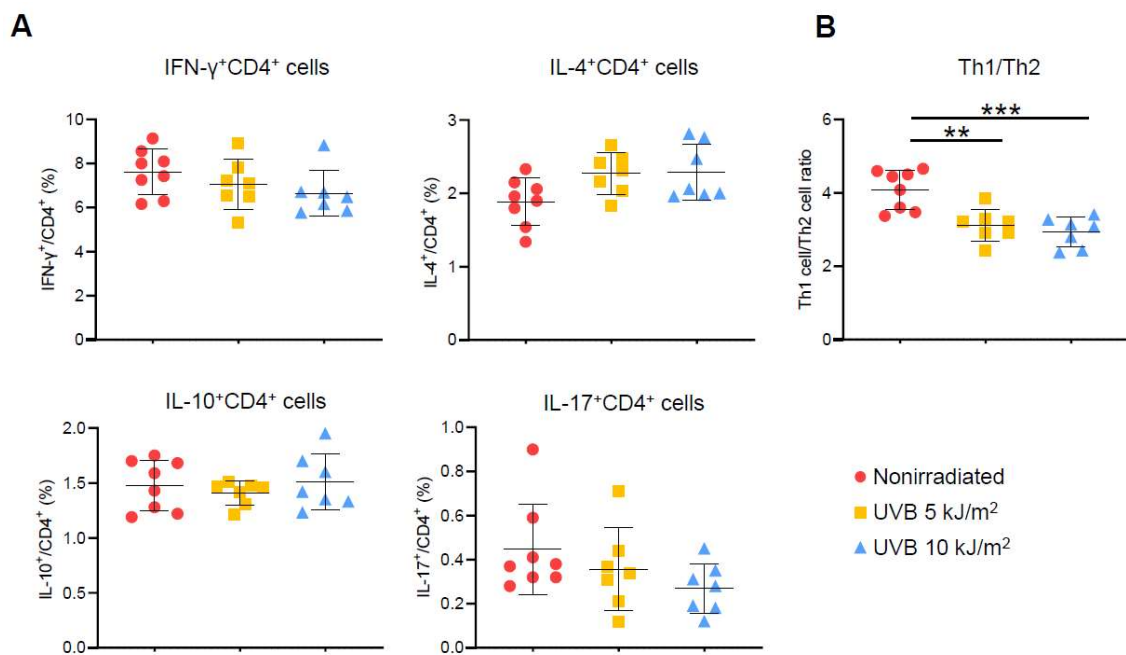


**Figure 65. 312 nm UVB irradiation decreases the ratio of Th1 to Th2 cells in peripheral lymphoid tissues.**

Male *Apoe*<sup>-/-</sup> mice were irradiated with 312 nm UVB at 5 or 10 kJ/m<sup>2</sup> once weekly for 6 weeks. Nonirradiated male *Apoe*<sup>-/-</sup> mice served as controls. Four days after the last UVB irradiation, lymphoid cells from spleen were prepared. **A** and **B**, Lymphoid cells from spleen were stimulated with phorbol 12-myristate 13-acetate and ionomycin in vitro. ICS was performed. The graphs represent the frequencies of IFN- $\gamma$ <sup>+</sup>, IL-4<sup>+</sup>, IL-10<sup>+</sup>, and IL-17<sup>+</sup> CD4<sup>+</sup> T cells (**A**) and the ratio of Th1 cells to Th2 cells (**B**) in spleen. n=7 to 8 per group. Data points represent individual animals. Horizontal bars represent means. Error bars indicate s.d. \*\**P*<0.01; \*\*\**P*<0.001; 1-way ANOVA followed by Dunnett's post hoc test.

Irradiation with 312 nm UVB positively modulated CD4<sup>+</sup> helper T cell subsets by expanding the Treg number and proportion and shifting the Th1/Th2 balance. In addition, the

effect of irradiation on other immune cells was evaluated. Therefore, male *Apoe*<sup>-/-</sup> mice were irradiated six times with 5 or 10 kJ/m<sup>2</sup> 312 nm UVB once a week using a similar setup. Flow cytometry was used to examine the proportions of other immune cells and the expression of CD80 and CD86 on DCs in the spleen. No significant effects of 5 or 10 kJ/m<sup>2</sup> UVB irradiation were observed on other immune cell responses (**Figure 66**).

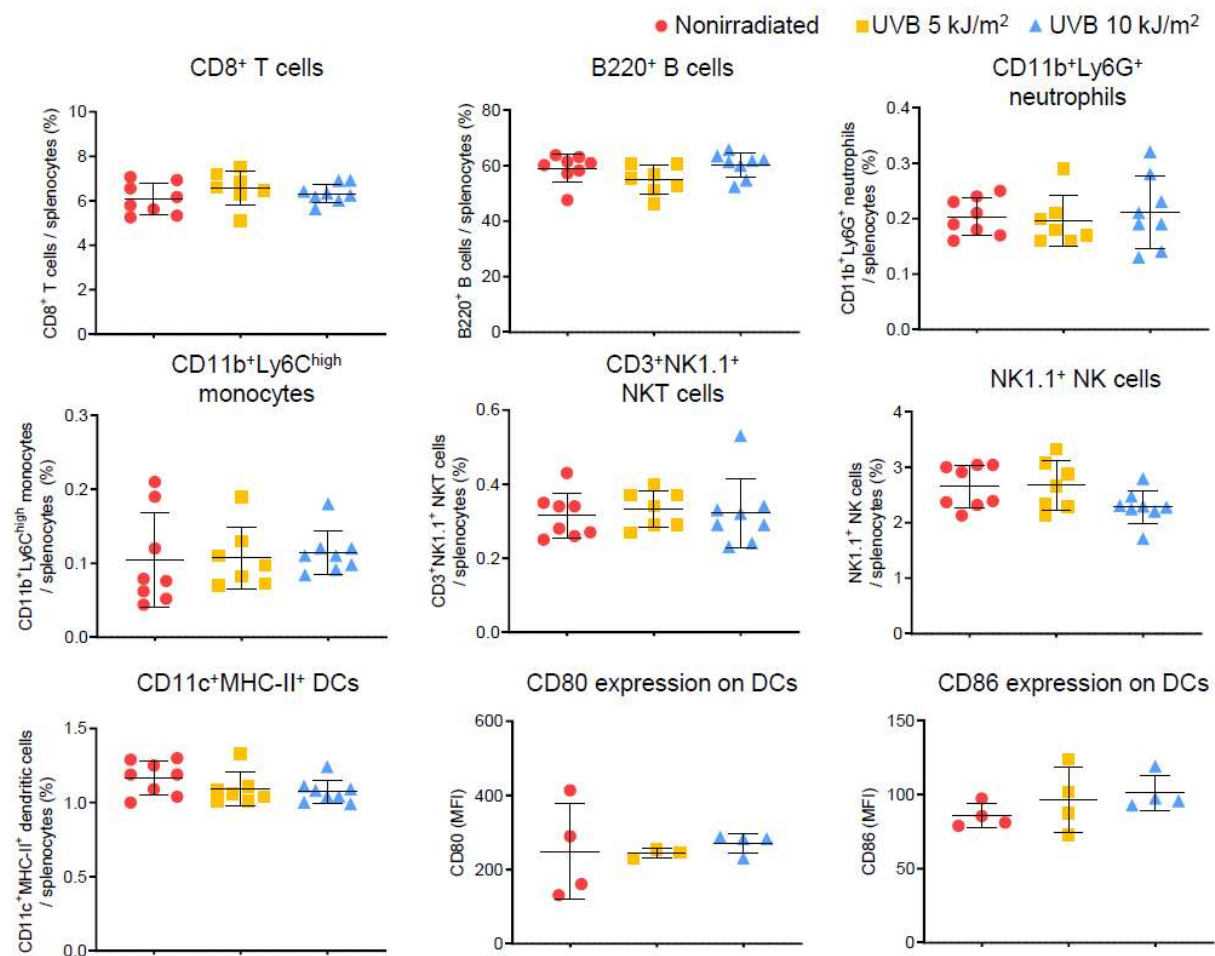


**Figure 66. 312 nm UVB does not affect other immune cell responses in peripheral lymphoid tissues.**

Male *Apoe*<sup>-/-</sup> mice were irradiated with 312 nm UVB at 5 or 10 kJ/m<sup>2</sup> once weekly for 6 weeks. Nonirradiated male *Apoe*<sup>-/-</sup> mice served as controls. Four days after the last UVB irradiation, lymphoid cells from spleen were prepared. Proportions of splenic CD8<sup>+</sup> T cells, B220<sup>+</sup> B cells, CD11b<sup>+</sup>Ly6G<sup>+</sup> neutrophils, CD11b<sup>+</sup>Ly6C<sup>high</sup> monocytes, natural killer (NK) T cells, NK cells, and CD11c<sup>+</sup> major histocompatibility complex (MHC)-II<sup>+</sup> DCs, and the expression of CD80 and CD86 on CD11c<sup>+</sup>MHC-II<sup>+</sup> DCs were determined by flow cytometry. n=7 to 8 per group for immune cell proportions and 4 per group for CD80/86 expression. Data points represent individual animals. Horizontal bars represent means. Error bars indicate s.d. MFI indicates mean fluorescence intensity.

These results confirmed the safety of using 312 nm UVB irradiation because the immunomodulatory effect of 312 nm UVB irradiation is specific to T cell responses for



favorably modulating the balance of T cells, including Tregs and helper T cells. Accordingly, 312 nm UVB irradiation is unlikely to incite undesirable immunosuppression caused by the general dysregulation of innate or adaptive immune responses.

#### **2.2.4. Elevation of proresolving lipid mediator levels in the skin after 312 nm UVB irradiation**

Accumulating evidence has linked the imbalance between proresolving and proinflammatory lipid mediators to the progression of chronic inflammatory diseases, including atherosclerosis.<sup>64</sup> Previous study reported that 282 nm UVB irradiation effectively increased various proresolving lipid mediators while reducing the proinflammatory counterpart.<sup>4</sup> In this study, similar measurements of lipid mediators were performed, noting that 312 nm UVB irradiation only had a modest effect on the amount of arachidonic acid and its derived lipid mediators in the skin (**Figure 67A**). Although the amount of docosahexaenoic acid in the skin did not change, the amounts of its derived proresolving lipid mediators, including resolvin D1, resolvin D2, resolvin D5, maresin 1, and protectin D1, increased with UVB irradiation (**Figure 67B**). UVB irradiation did not affect the amount of eicosapentaenoic acid. However, the amount of its derived proresolving resolvin E4 tended to increase in UVB-irradiated mice (**Figure 67C**). The upregulation of skin lipid mediators likely resulted from the irradiation-induced postinflammatory reaction in the epithelial layer. Given the lack of significant changes in proinflammatory lipid mediators, these results indicate that the balance of inflammatory lipid mediators shifted toward the resolution of inflammation, potentially contributing to Treg expansion in lymphoid tissues. Consequently, local Treg augmentation may have been induced, mediating anti-inflammatory and antiatherogenic responses.

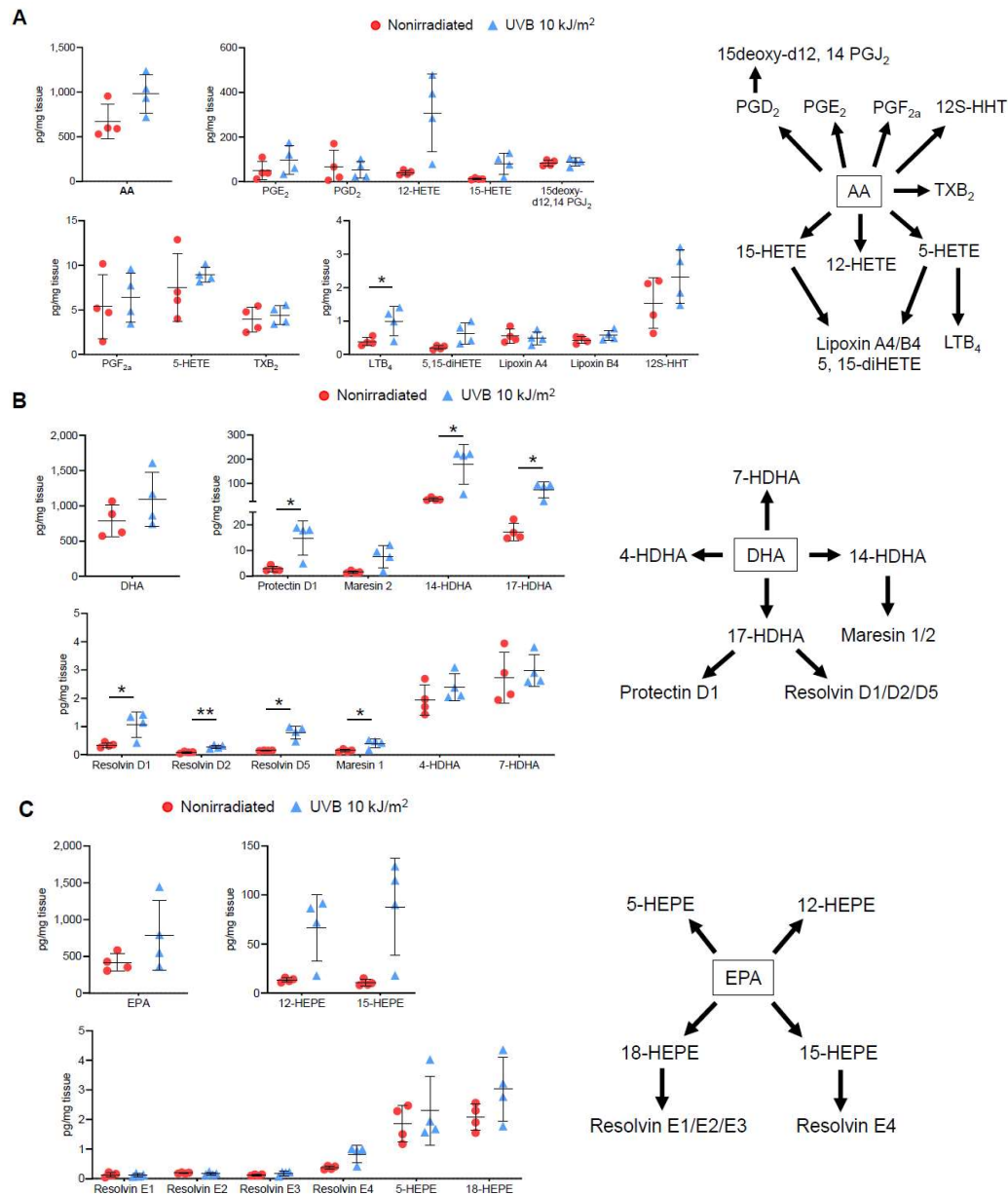


**Figure 67. 312 nm UVB irradiation increases levels of proresolving lipid mediators in the skin.**

Male *Apoe*<sup>-/-</sup> mice were irradiated with 312 nm UVB at 10 kJ/m<sup>2</sup> once weekly for 6 weeks. Nonirradiated male *Apoe*<sup>-/-</sup> mice served as controls. Four days after the last UVB irradiation, the back skin of the mice was isolated. The production of various lipid mediators in the skin was analyzed by liquid chromatography/mass spectrometry/mass spectrometry-based lipidomics. (A-C), Quantification of arachidonic acid (AA) and its derived lipid mediators (A), docosahexaenoic acid (DHA) and its derived lipid mediators (B), and eicosapentaenoic acid (EPA) and its derived lipid mediators (C) in the skin. Schematics show metabolic pathways related to AA (A), DHA (B), and EPA (C). n=4 per group. Data points represent individual animals. Horizontal bars represent means. Error bars indicate s.d. \**P*<0.05; Mann-Whitney *U*-test: protectin D1, 14-HDHA, and 17-HDHA (B); 2-tailed Student's *t*-test: LTB<sub>4</sub> (A) and resolvin D2 and maresin 1 (B); 2-tailed Welch's *t*-test: resolvin D1 and resolvin D5 (B). LTB<sub>4</sub> indicates leukotriene B<sub>4</sub>; PGD<sub>2</sub>, prostaglandin D<sub>2</sub>; PGE<sub>2</sub>, prostaglandin E<sub>2</sub>; PGF<sub>2α</sub>, prostaglandin F<sub>2α</sub>; and TXB<sub>2</sub>, thromboxane B<sub>2</sub>.



### 2.3. Discussion

Emerging evidence from experimental and clinical studies has revealed the feasibility of anti-inflammatory approaches for preventing and treating CAD.<sup>65</sup> However, therapies directly targeting immuno-inflammatory responses face significant challenges, including the risks of immunosuppression-induced infections and difficulty preventing fatal cardiac events, which limit their widespread adoption into clinical medicine. Immunomodulation through UVB phototherapy, particularly at the 311 nm peak wavelength NB-UVB, is an established and safe treatment for inflammatory skin conditions, such as vitiligo, psoriasis, and atopic dermatitis.<sup>63</sup> Building on this safety profile, similar UVB phototherapy offers a promising and feasible strategy to modulate the immunoinflammatory response for CAD prevention and treatment.

A unique LED-based 312 nm UVB device resembling the clinically established 311 nm peak NB-UVB therapy was developed. This device demonstrated the attenuation of aortic root atherosclerotic plaque development in hypercholesterolemic mice, along with beneficial changes in the plaque phenotype, such as reduced inflammation and a more stable structure. These positive effects were attributed to a favorable modulation of the T cell balance, characterized by a shift in the Teff/Treg balance toward anti-inflammatory Treg responses and a decreased Th1/Th2 ratio. In addition, the attenuation of atherosclerosis correlated with increased levels of proresolving lipid mediators in UVB-irradiated skin.

Experimental and clinical data indicate that the pathogenic immune responses mediated by Teffs, including IFN- $\gamma$ -producing Th1 cells, accelerated vascular inflammation and atherosclerosis.<sup>34</sup> In contrast, Foxp3-expressing Tregs exhibited antiatherogenic properties by regulating immunoinflammatory responses derived from innate and adaptive immunity.<sup>5</sup> Previous study on hypercholesterolemic *Apoe*<sup>-/-</sup> mice demonstrated that anti-CD3 antibodies and IL-2 complexes dramatically expanded Tregs while reducing Teff responses, resulting in

potent attenuation of atherosclerosis.<sup>19</sup> These findings confirm that the Teff/Treg balance and Th1-skewed responses greatly influence atherosclerotic plaque formation.<sup>7</sup> In this study, 10 kJ/m<sup>2</sup> 312 nm UVB irradiation increased Treg cellularity in peripheral lymphoid tissues while decreasing Teff cellularity in the spleen. Moreover, a decreased Th1/Th2 cell ratio was observed in the spleen. This shift in the Teff/Treg balance toward Treg responses, combined with a decreased Th1/Th2 cell ratio, led to reduced atherosclerotic plaque development and inflammation in the aortic root. A lower dose of 5 kJ/m<sup>2</sup> produced similar effects on Teffs and the Th1/Th2 cell ratio, although its effect was less pronounced on Tregs and the atherosclerotic plaque phenotype. The finding of reduced Teff cellularity aligns with an earlier study using an even lower dose of 2 kJ/m<sup>2</sup>, which was exclusively demonstrated by 312 nm UVB rather than other wavelengths.<sup>4</sup> Given Tregs' failure to control Teff responses under inflammatory condition,<sup>66</sup> these results underscore the critical contribution of synergistic Treg augmentation and Teff suppression to the antiatherogenic effects of 10 kJ/m<sup>2</sup> 312 nm UVB phototherapy. Furthermore, UVB doses used in this study fell within the clinical range for treating skin diseases, supporting the potential safety and efficacy of 312 nm UVB phototherapy for atherosclerosis treatment.

Proresolving lipid mediators play a crucial role in stabilizing atherosclerotic plaques and may contribute to the immune-modulating effects of UVB irradiation observed in this study. Although 10 kJ/m<sup>2</sup> 312 nm UVB significantly increased the levels of some proresolving lipid mediators in the skin of irradiated mice, only a modest change was observed in the levels of proinflammatory lipid mediators. This finding partially aligns with a previous study that used 2 kJ/m<sup>2</sup> 282 nm UVB, demonstrating a similar increase in proresolving mediators and a decrease in proinflammatory mediators.<sup>4</sup> These changes likely result from the UVB-induced postinflammatory reactions in the epithelial layer, which favor proresolving activity. Mediators such as resolvin D1, resolvin D2, and maresin 1, which markedly increased following 312 nm

UVB irradiation, regulate Treg function and differentiation<sup>64, 67, 68</sup> via the G protein-coupled receptor 32 and formyl-peptide receptor 2.<sup>67, 69</sup> The augmented production of these mediators likely contributes to UVB-induced Treg expansion, reinforcing the observed anti-inflammatory effects on atherosclerotic plaques.

UVB-based phototherapy, known for its diverse immune-modulating effects,<sup>62</sup> is a clinically established treatment for various skin diseases; it has few severe side effects when carefully controlled. Therefore, understanding the distinct effects of wavelengths is essential. Previous study reported that 282 nm UVB irradiation at 2 kJ/m<sup>2</sup> reduced atherosclerotic plaque in hypercholesterolemic mice. However, similar doses of 301 nm and 312 nm UVB did not produce a significant reduction, indicating a stronger atheroprotective effect of 282 nm UVB.<sup>4</sup> The plaque reduction observed in 282 nm UVB-irradiated mice resulted from the enhanced activation state, migratory capability, and cellularity of Tregs in peripheral lymphoid tissues without significant changes in Teffs. Although the antiatherogenic activity of 282 nm UVB is intriguing, considering that this shorter wavelength does not naturally reach the ground level, its biological effects and safety profile require further investigation. In contrast, the current study using 10 kJ/m<sup>2</sup> 312 nm UVB irradiation demonstrated increased Treg cellularity (without enhancement of Treg function), decreased Teff cellularity, and reduced the Th1 cell/Th2 cell ratio. These findings verify that the effects of UVB on T cell immunity and atherosclerosis are wavelength- and dose-dependent, as discussed earlier.

Clinical studies of patients with psoriasis<sup>63, 70</sup> have reported improved disease outcomes associated with the expansion of peripheral Tregs after NB-UVB irradiation,<sup>70</sup> highlighting the broader potential of UVB therapy to modulate immune responses. The findings of the current study align with these clinical observations and provide mechanistic insights into the therapeutic effects of NB-UVB irradiation. Although the current results were obtained using an atherosclerotic mouse model, they highlight the potential for translational application to

human conditions other than atherosclerosis, particularly in inflammatory diseases linked to systemic immune modulation.

Patients with psoriasis have an increased risk of CAD, likely driven by chronic inflammation involving pathogenic Th1 or Th17 cell responses because both conditions share common inflammatory pathways and immune dysregulation. The current data indicate that 312 nm UVB phototherapy may mitigate inflammation not only in the skin but also systemically. In this study, the entire back of mice was irradiated with 312 nm UVB. Meanwhile, in patients with psoriasis, the irradiation area is typically limited to skin lesions. Broader irradiation in mice may have enhanced systemic immune modulation, an effect potentially less pronounced in localized human treatments. However, whether the irradiation area size is critical for achieving antiatherogenic effects remains unclear. Exploring the implications of whole-body *versus* localized UVB irradiation, including their effects on systemic inflammation and immune balance, could provide valuable insights for optimizing therapeutic strategies against CAD.

Conventional anti-inflammatory therapies, such as statins, reduce CRP levels and cardiovascular events by inhibiting proinflammatory cytokine production. However, no significant differences in plasma CRP levels were observed between the UVB-irradiated and nonirradiated mice, indicating that 312 nm UVB achieved its antiatherogenic effects through distinct mechanisms. The finding of T cell balance modulation after UVB irradiation—favoring anti-inflammatory Tregs over proinflammatory T effs and reducing the Th1/Th2 cell ratio—is the key factor underlying the antiatherogenic effects of 312 nm UVB therapy.

Nevertheless, this study has some limitations. Although 312 nm UVB irradiation significantly attenuated plaque formation and inflammation in the aortic root, it had no significant effects on the thoracoabdominal aorta. These discrepancies may arise from differences in lesion characteristics or limited efficacy of UVB treatment in certain regions.

Furthermore, the current model only demonstrated the ability to attenuate atherosclerotic plaque formation. Additional studies on the potential to induce regression of established plaques would enhance the translational relevance for clinical applications. Future studies should optimize key variables, such as irradiation dose, frequency, duration, treatment area, and delivery method, to ensure consistent and effective outcomes. Furthermore, incorporating plaque regression models into experimental settings is crucial before translating these findings into human studies.

## 2.4. Conclusion

Clinically feasible 312 nm UVB irradiation effectively limits atherosclerotic plaque formation in the aortic root. It also improves plaque stability by favorably modulating the T cell balance in lymphoid tissues and increasing the levels of proresolving lipid mediators in the skin. These findings provide an attractive immunomodulatory approach for the treatment of CAD using similar dose and wavelength already employed in clinical settings.

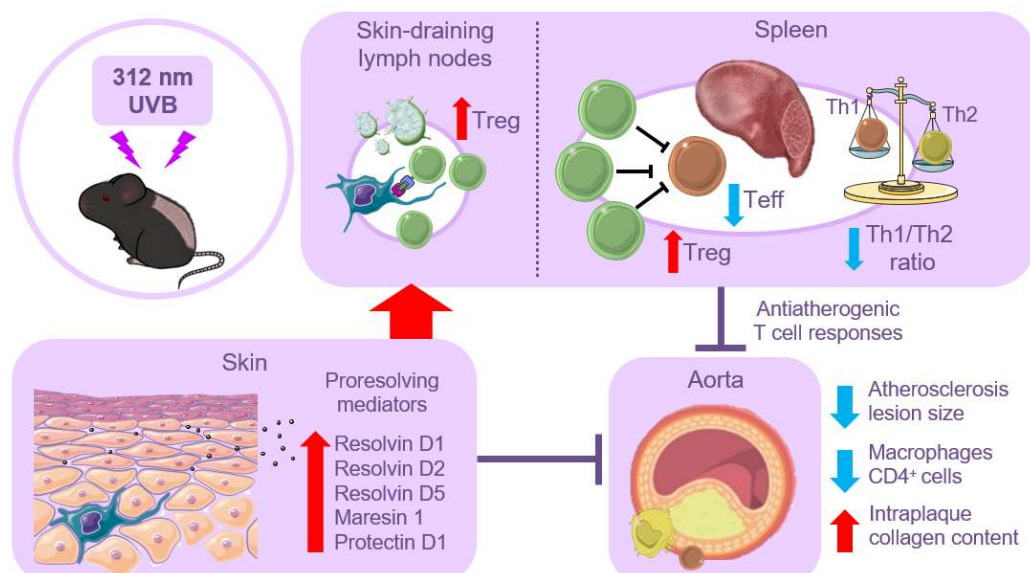


**Figure 68. UVB irradiation at 312 nm provides protection against atherosclerosis development.**

Irradiation enhances Treg cellularity in local skin-draining LNs and the spleen, likely associated with the upregulation of proresolving lipid mediators in the skin. Meanwhile, a synergistic attenuation of Teff cellularity and a reduction in the Th1/Th2 ratio are observed systemically in the spleen. These combined mechanisms provide a beneficial atheroprotective effect. This figure was partly generated using Servier Medical Art, by Servier (<http://smart.servier.com>).

## Summary

This thesis investigates the modulation of helper T cell-mediated immune responses as a therapeutic strategy for atherosclerotic diseases. Emphasizing the immunoinflammatory basis of these diseases, as outlined in the introduction, the work explores two complementary approaches: targeting CCR4 to manipulate T cell migration and responses, and utilizing UVB irradiation to directly influence immune cell balance. Despite the differences in their mechanisms, both interventions share a common goal of favorably modulating adaptive immunity to mitigate disease progression (**Figure 69**).

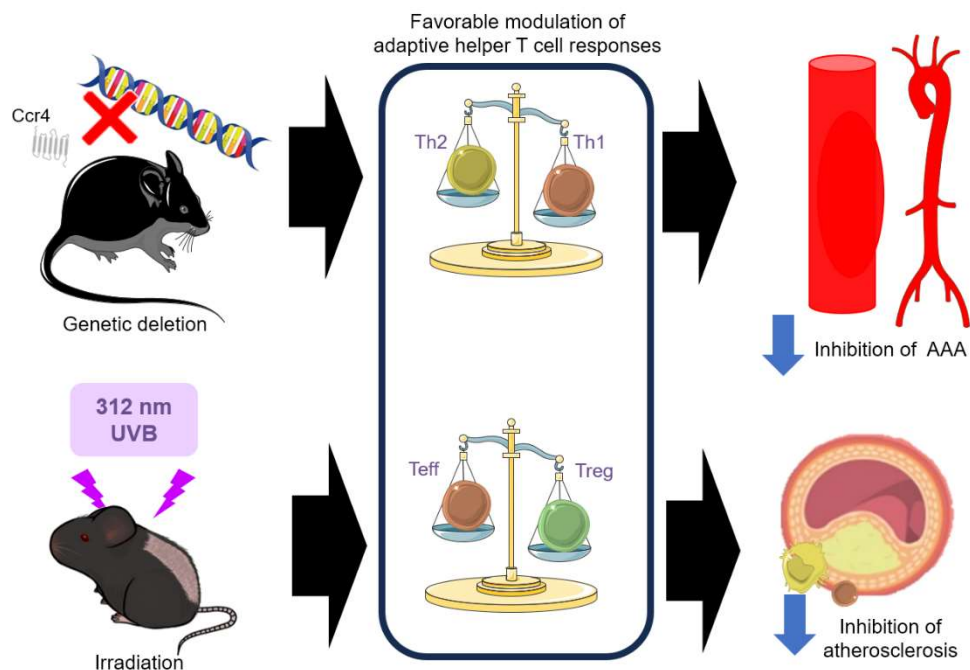


**Figure 69. Favorable modulation of adaptive helper T cell responses effectively attenuates atherosclerotic disease progression.** Genetic deletion of CCR4 induces Th1 cell predominance, which protects against AAA development. Meanwhile, 312 nm UVB irradiation skews the Treg/Teff balance toward antiatherogenic Tregs, preventing plaque formation. Both interventions provide evidence that favorable modulation of helper T cell balance can be targeted for treating atherosclerotic diseases. This figure was partly generated using Servier Medical Art, by Servier (<http://smart.servier.com>).

The first approach focuses on CCR4, a chemokine receptor highly expressed by Tregs and Th2 cells. By analyzing CCR4-deficient mice, this study demonstrated that the absence of CCR4 induced a Th1 cell-skewed immune response, which protected against AAA while exacerbating atherosclerosis albeit limited to early stages. This duality underscores the disease-

and stage-specific role of Th1 cells in these diseases, with proatherogenic effects in atherosclerosis contrasting with their protective role in AAA. These findings suggest that anti-CCR4 monoclonal antibodies, such as mogamulizumab, might serve as a novel therapeutic strategy for AAA, while highlighting adequate caution in their application to atherosclerosis.

The second approach evaluates 312 nm UVB irradiation, a clinically-feasible phototherapy known to modulate immune responses. In hypercholesterolemic mice, 312 nm UVB reduced plaque formation and inflammation by shifting the Treg/Teff balance toward antiatherogenic Tregs, while also reducing the Th1/Th2 cell ratio. These findings align with the observed role of CCR4 in Treg migration, suggesting a potential synergy between UVB-induced immune modulation and CCR4-targeted interventions.

Despite their differences, both strategies converge on the central theme of the thesis: the critical importance of adaptive immune regulation in the progression of atherosclerotic diseases. CCR4 deficiency and UVB irradiation independently demonstrate that favorably altering the balance of helper T cell subsets can attenuate chronic vascular inflammation. Together, these findings pave the way for multimodal immunotherapeutic approaches, combining molecular and physical interventions to address the diverse immune mechanisms underlying atherosclerosis and AAA. However, both strategies are currently documented in experimental animal models, and future translational data are necessary to confirm these findings. Therefore, future studies on the incidence of AAA in patients treated with anti-CCR4 mogamulizumab and cardiovascular events in patients treated with 311 nm peak NB-UVB phototherapy are highly anticipated.

## Acknowledgments

As I finish writing this doctoral thesis, I would like to express my deep gratitude to Professor Yoshiyuki Rikitake from the Laboratory of Medical Pharmaceutics who has given me the opportunity to do my doctorate at his laboratory. His scientific guidance, laboratory equipment, and frequent afternoon treats gave me an eventful experience during my study.

I would especially like to thank Associate Professor Naoto Sasaki for supervising my doctoral thesis and the constructive scientific exchange also for the opportunity to realize my own ideas. I would sincerely thank Specially-Appointed Assistant Professor Toru Tanaka who has continuously provided me with kind encouragement and assistance with various experiments throughout my study.

I would like to thank Professor Noriaki Emoto of the Laboratory of Clinical Pharmaceutical Science, the chief thesis examiner, and Associate Professor Yoshiaki Nakayama of the Laboratory of Microbial Chemistry, the vice examiner of my thesis, for their helpful advice and guidance in reviewing this research thesis.

I would like to thank Lecturer Sayo Horibe, Dr. Hilman Zulkifli Amin, Ken Ito, and other members of the Laboratory of Medical Pharmaceutics who have generously supported me in this study by participating in discussions, carrying out experiments, providing a wonderful research environment.

I would like to express my sincere gratitude to co-authors from Kobe University Graduate School of Medicine. Professor Masakazu Shinohara for the fruitful analysis of liquid chromatography-mass spectrometry of skin samples from my UVB project. Professor Ken-ichi Hirata, Professor Tomoya Yamashita, and Dr. Takuo Emoto for the helpful suggestion and discussion about methodology.



I would like to thank to co-authors from the Division of Chemotherapy, Faculty of Pharmacy, Kindai University. Professor Takashi Nakayama, for the generous gift of *Ccr4* knockout mouse and fruitful methodological suggestion, and Associate Professor Kazuhiko Matsuo, for the suggestion.

I would like to thank Professor Motoaki Iwaya from the Department of Materials Science and Engineering, Meijo University and Associate Professor Atsushi Fukunaga from the Department of Dermatology, Osaka Medical and Pharmaceutical University for their discussion about the UVB experimental method.

I would like to express my deepest gratitude to the Japanese Ministry of Education, Culture, Sports, Science and Technology for the MEXT scholarship I received over the four years from 2021.

Finally, I would like to express my sincere gratitude to my family for their continued support and encouragement in my research career so far.

## Experimental section

### Chapter 1. Materials

#### 1.1. General equipment

**Table 4. List of equipment**

Equipment	Source
Autoclave	HVE-25 HICLAVE (Hirayama, Kasukabe, Japan)
Centrifuge (high-speed)	High-Speed Refrigerated Centrifuge AX-511 (TOMY, Tokyo, Japan)
Centrifuge (low-speed)	Low-Speed Refrigerated Centrifuge AX-511 (TOMY, Tokyo, Japan)
Cryostat (for frozen section)	CM1860 Cryostat (Leica, Wetzlar, Germany)
Flow cytometer	FACSAria™ III Cell Sorter (BD Bioscience (Franklin Lakes, USA))
Fluorescence plate reader	Infinite 200 PRO plate reader (Tecan, Männedorf, Switzerland)
Incubator block (for 1.5 mL tubes)	Block Incubator BI-516S (Astec, Fukuoka, Japan)
Incubator chamber (CO <sub>2</sub> infused)	Direct heat type CO <sub>2</sub> /multi-gas incubator SCA-165D (Astec, Fukuoka, Japan)
Laminar flow hood (clean bench)	Bio Clean Bench MCV- B131S (Sanyo, Osaka, Japan)
MACS separator	MACS® MultiStand, QuadroMACS™ Separator, MiniMACS™ Separator all from Miltenyi Biotec, Westphalia, Germany
Micropipette 10 µL	Reference® 2 - Single-Button Pipette (Eppendorf, Hamburg, Germany)
Micropipette 20 µL, 100 µL, 200 µL, 1000 µL	PIPETMAN™ Classic Pipet (Gilson, Madison, USA)
Microscope	BX50/System Biological Microscope (Olympus, Tokyo, Japan)
Microscope (digital)	BZ-X810 All-in-one Fluorescence Microscope (Keyence, Osaka, Japan)
Microscope (stereo)	Stemi 2000 + CL1500 ECO (Zeiss, Oberkochen, Germany)
Mini centrifuge machine	MCF-2360 (LMS, Frankfurt, Germany); FastGene™ Mini Centrifuge NE-NG002B (Nippon Genetics, Tokyo, Japan)
PCR cycler (for reverse transcription)	PCR Thermal Cycler Dice Touch TP350 (Takara Bio, Shiga, Japan)
Plate (96-well) centrifuge machine	BSR-M001 Plate Centrifuge (Bio Medical Science Inc., Tokyo, Japan)

Real-time PCR cycler	StepOnePlus Real-Time PCR Systems (ThermoFischer (Applied Biosystems), Waltham, USA)
Serological pipette gun	Serial no. 43119s (Drummond Scientific, Broomall, USA)
Sonicator (ultrasonic bath)	1510 Ultrasonic Cleaner (Branson Ultrasonics, Danbury, USA)
Spectrometer	NanoDrop ND-1000 Spectrophotometer (Thermo Scientific, Waltham, USA)
Tap water direct-connected ultrapure water production equipment (Milli Q)	Direct-Q® UV 3 (Merck Millipore, Burington, USA)
Vortex mixer device	VORTEX-GENIE 2 Mixer (M&S Instrument Inc. Osaka, Japan)

## 1.2. Consumables

**Table 5. List of consumables**

Consumables	Source
Cell strainer 70 $\mu$ m	Corning, New York, USA
FACS tube	Micronic, Lelystad, The Netherland
Grounding glass slide	FF-001 Matsuyama, Tokyo, Japan
Hypodermic needle 21 G, 26 G	Terumo, Tokyo, Japan
MACS column	LD, LS, MS column (Miltenyi Biotec, Westphalia, Germany)
Micropipette tip 10 $\mu$ L, 20 $\mu$ L, 100 $\mu$ L, 200 $\mu$ L, 1000 $\mu$ L	Watson, Tokyo, Japan
Microscope glass slide	MAS-01 Matsuyama, Tokyo, Japan
OCT plastic mold	Cryomeld No. 2 and No. 3 (Sakura FineTek, Tokyo, Japan)
PCR plate (96-well)	INA-OPTIKA, Osaka, Japan
PCR tube	Watson, Tokyo, Japan
Petri dish 60 mm	Iwaki, Tokyo, Japan
Plate (96-well) round, flat, and V-bottomed	Corning, New York, USA
Reaction tube 1.5 mL, 5 mL, 15 mL, 50 mL	Watson, Tokyo, Japan
Serological pipette glass 5 mL, 10 mL, 25 mL, 50 mL	Costar Stripette (Corning, New York, USA)
Syringe 0.5 mL, 1 mL, 5 mL, 20 mL	Terumo, Tokyo, Japan

### 1.3. Buffers, chemicals, media, and solutions

**Table 6. List of buffers, chemicals, media, and solutions**

<b>Buffers chemicals, media and solutions</b>	<b>Source</b>
FACS buffer	9.6g Acudia D-PBS(-) powder (Shimadzu, Tokyo, Japan) + 1L Milli-Q water + 2% FBS
Formaldehyde	Nacalai Tesque, Kyoto, Japan
ICS buffer/culture medium	RPMI + 10% FBS + P/S + 2-ME
MACS buffer	9.6g Acudia D-PBS(-) powder (Shimadzu, Tokyo, Japan) + 1L Milli-Q water + 2% FBS + 2mM EDTA
Normal saline	Otsuka, Tokyo, Japan
OCT compound	Sakura FineTek, Tokyo, Japan
Paraformaldehyde	Nacalai Tesque, Kyoto, Japan
PBS (10x concentration, stock solution)	80g NaCl + 2g KCl + 2g KH <sub>2</sub> PO <sub>4</sub> (MW 136.09) + 29.01g Na <sub>2</sub> HPO <sub>4</sub> ·12H <sub>2</sub> O (MW 358.14) all from Nacalai Tesque, Kyoto, Japan diluted in 1L Milli-Q water
RPMI	RPMI 1640 with L-Gln, liquid (Nacalai Tesque, Kyoto, Japan)
Trizol	TRIzol™ Reagent (ThermoFischer (Invitrogen), Waltham, USA)
Tween 20	Nacalai Tesque, Kyoto, Japan

### 1.4. Reagents and kits

**Table 7. List of reagents and kits**

<b>Reagent kit etc.</b>	<b>Source</b>
CD4 <sup>+</sup> T Cell Isolation Kit, mouse	130-104-454 (Miltenyi Biotec, Westphalia, Germany)
CD4 <sup>+</sup> CD25 <sup>+</sup> Regulatory T Cell Isolation Kit, mouse	130-091-041 (Miltenyi Biotec, Westphalia, Germany)
ICS cell fixation and staining buffer kit	BD Cytfix/Cytoperm™ 554714 (BD Bioscience, Franklin Lakes, USA)
Intracellular transcription factor staining kit	eBioscience™ Foxp3 / Transcription Factor Staining Buffer Set (ThermoFischer (Invitrogen), Waltham, USA)
Mouse C-Reactive Protein/CRP ELISA Kit	Quantikine MCRP00 (R&D Systems, Minneapolis, USA)
Mouse Immunoglobulin ELISA kit	Mouse IgE Uncoated ELISA Kit with Plates 88-50460-22; Mouse IgM Uncoated ELISA Kit with Plates 88-50470-22; Mouse IgG (Total) Uncoated ELISA Kit with Plates 88-50400-22; All from ThermoFischer (Invitrogen), Waltham, USA

## 1.5. Primers for real-time PCR

**Table 8. List of primers used in real-time PCR**

Gene	Forward Primer (5'-3')	Reverse Primer (5'-3')
<i>Actb</i>	CATCCGTAAAGACCTCTATGCCAAC	ATGGAGCCACCGATCCACA
<i>Ccr4</i>	TCTACAGCGGCATCTTCTTCAT	CAGTACGTGTGGTTGTGCTCTG
<i>Cd4</i>	TCACACATGAAGCATGTCAGG	GCACTGGTTAGAATGTGAGTCTGG
<i>Cd68</i>	CATCAGAGCCCGAGTACAGTCTACC	AATTCTGCGCCATGAATGTCC
<i>Foxp3</i>	CTCATGATAGTGCCTGTGTCCTCAA	AGGGCCAGCATAGGTGCAAG
<i>Gapdh</i>	TGTGTCCGTCGTGGATCTGA	TTGCTGTTGAAGTCGCAGGAG
<i>Gata3</i>	GGATGTAAGTCGAGGCCCAAG	ATTGCAAAGGTAGTGCCCGGTA
<i>Ifng</i>	CGGCACAGTCATTGAAAGCCTA	GTTGCTGATGGCCTGATTGTC
<i>Il10</i>	GACCAGCTGGACAACATACTGCTAA	GATAAGGCTTGGAACCCAAGTAA
<i>Il1b</i>	TCCAGGATGAGGACATGAGCAC	GAACGTCACACACCAGCAGGTTA
<i>Il6</i>	CCACTTCACAAGTCGGAGGCTTA	GCAAGTGCATCATCGTTGTTTCATAC
<i>Rorc</i>	CACAGAGACACCACCGGACAT	CGTGCAGGAGTAGGCCACATT
<i>Tbx21</i>	CTGCCTACCAGAACGCAGA	AAACGGCTGGGAACAGGA
<i>Tgfb</i>	GTGTGGAGCAACATGTGGAACCTCTA	TTGGTTCAGCCACTGCCGTA
<i>Tnf</i>	CCACCACGCTCTTCTGTCTAC	AGGGTCTGGGCCATAGAACT

## 1.6. Antibodies for immunostaining

If not stated otherwise, all antibodies used (**Table 9**) were reactive to mouse.

**Table 9. List of antibodies used in immunostaining**

Antibodies	Clone	Conjugate	Source
anti-CCL17 Ab	-	-	Abcam ab182793
anti-CCL22 Ab	-	-	R&D Systems AF439
anti-CD4 Ab	RM4-5	-	BD Biosciences 550280
anti-Goat IgG	-	Alexa Fluor 568	Thermo Fisher Scientific A11057
anti-Goat IgG	-	HRP	Abcam ab97110
anti-MMP-2 Ab	-	-	R&D Systems AF1488

anti-MMP-9 Ab	-	-	R&D Systems AF909
anti-MOMA-2 Ab	-	-	BMA Biomedical T-2007
anti-Rabbit IgG	-	Alexa Fluor 568	Thermo Fisher Scientific A11011
anti-Rabbit IgG	-	Biotin	Abcam ab97049
anti-Rat IgG	-	Alexa Fluor 488	Thermo Fisher Scientific A21208
anti-Rat IgG	-	Biotin	Abcam ab102250
anti-TGF beta 1 Ab	EPR21143	-	Abcam ab215715

### 1.7. Antibodies for flow cytometry

If not stated otherwise, all antibodies used (**Table 10**) were reactive to mouse.

**Table 10. List of antibodies used in flow cytometry**

<b>Antibodies</b>	<b>Clone</b>	<b>Fluorescent dye</b>	<b>Source/Catalog Number</b>
anti-B220 Ab	RA3-6B2	PE	BD Pharmingen 553090
anti-CCR4 Ab	2G12	PE	BioLegend 131204
anti-CD103 Ab	M290	FITC	BD Pharmingen 557494
anti-CD11b Ab	M1/70	V450	BD Horizon 560455
anti-CD11c Ab	HL3	V450	BD Horizon 560521
anti-CD138 Ab	281-2	APC	BD Pharmingen 561705
anti-CD152 Ab	UC10-4B9	APC	eBioscience 17-1522-82
anti-CD16/CD32 Ab	2.4G2	-	BD Pharmingen 553142
anti-CD19 Ab	1D3	FITC	BD Pharmingen 557398
anti-CD25 Ab	PC61	PE	BD Pharmingen 553866
anti-CD3 Ab	145-2C11	APC	BD Pharmingen 553066
anti-CD3 Ab	145-2C11	FITC	BD Pharmingen 553062
anti-CD3 Ab	145-2C11	PECy7	BD Pharmingen 552774
anti-CD3 Ab	500A2	V450	BD Pharmingen 560801
anti-CD4 Ab	RM4-5	PECy7	BD Pharmingen 552775
anti-CD44 Ab	IM7	PE	BD Pharmingen 553134
anti-CD45 Ab	30-F11	PerCPCy5.5	BD Pharmingen 550994
anti-CD62L Ab	MEL-14	FITC	BD Pharmingen 553150

anti-CD8 Ab	53-6.7	PerCPCy5.5	BD Pharmingen 553033
anti-CD80 Ab	16-10A1	PE	BD Pharmingen 553769
anti-CD86 Ab	GL1	APC	BD Pharmingen 558703
anti-CD95 Ab	Jo2	PECy7	BD Pharmingen 557653
anti-Foxp3 Ab	FJK-16s	V450	eBioscience 48-5773-82
anti-GATA3 Ab	L50-823	Alexa Fluor 488	BD Pharmingen 560163
anti-GL7 Ab	GL7	BV421	BD Pharmingen 568852
anti-I-Ab Ab	AF6-120.1	FITC	BD Pharmingen 553551
anti-IFN- $\gamma$ Ab	XMG1.2	PE	BD Pharmingen 554412
anti-IL-10 Ab	JES5-16E3	APC	BD Pharmingen 554468
anti-IL-17 Ab	TC11-18H10	APC	BD Pharmingen 560184
anti-IL-4 Ab	11B11	PE	BD Pharmingen 554435
anti-Ly6C Ab	AL-21	APC	BD Pharmingen 560595
anti-Ly6G Ab	1A8	FITC	BD Pharmingen 551460
anti-NK1.1 Ab	PK136	APC	BD Pharmingen 550627
anti-ROR $\gamma$ t Ab	Q31-378	PE	BD Pharmingen 562607
anti-T-bet Ab	4B10	APC	BioLegend 644814

### 1.8. Angiotensin II and mini-osmotic pump

Angiotensin II preparation was procured as synthetic angiotensin II acetate salt. Molecular weight:1046.19; Formula: C<sub>50</sub>H<sub>71</sub>N<sub>13</sub>O<sub>12</sub>; Purity: 99.4%; Product Number: 4006473; Source from Bachem, Bubendorf, Switzerland. Mini-osmotic pumps were alzet model 2004 procured from DURECT Corporation, Cupertino, USA.

## Chapter 2. Methods

### 2.1. Mouse acquisition and housing condition

For AAA experiment, *Apoe*<sup>-/-17</sup> and *Ccr4*<sup>-/-</sup> mice<sup>71</sup> on a C57BL/6 background are previously described. *Ccr4*<sup>-/-</sup> mice were crossed with *Apoe*<sup>-/-</sup> mice to generate *Ccr4*<sup>-/-</sup>*Apoe*<sup>-/-</sup> mice.<sup>72</sup> As for the experiment for the effect of 312 nm UVB irradiation on atherosclerosis, all mice were *Apoe*<sup>-/-</sup> on a C57BL/6 background. Mice were fed a standard chow diet (CLEA, Tokyo, Japan) unless indicated otherwise. Water was given ad libitum for all experiments.

I housed mice in cages for each strain or treatment group in a specific pathogen-free animal facility at Kobe Pharmaceutical University. Randomization and allocation concealment were performed. Littermate mice of each genotype were randomly allocated to each experimental group. During the experiments, animal/cage location was not controlled. The investigators were not blinded to the mouse genotype or treatment allocation. The experimental procedures were performed in laboratory rooms or animal facility.

All animal experiments were approved by the Animal Care Committee of Kobe Pharmaceutical University (the role of CCR4 in atherosclerosis and AAA: permit numbers 2018-008, 2019-011, 2020-050, 2021-038, 2022-005, 2023-038, and 2024-014; 312 nm-UVB: permit numbers 2021-034, 2022-006, 2023-036, and 2024-012) and conformed to the National Institutes of Health Guide for the Care and Use of Laboratory Animals and the ARRIVE guidelines (Animal Research: Reporting of In Vivo Experiments).

### 2.2. Angiotensin II-induced AAA model

Six-week-old *Apoe*<sup>-/-</sup> and *Ccr4*<sup>-/-</sup>*Apoe*<sup>-/-</sup> male mice were fed a high-fat and high-cholesterol diet containing 0.2% cholesterol and 21% fat (CLEA Japan, Tokyo, Japan).



Twelve-week-old mice were implanted with mini osmotic pumps (Alzet, Model 2004; DURECT Corp) filled with either angiotensin II (1000 ng/kg/min, Sigma) for AAA induction or saline for sham-operated group, which were guaranteed to deliver a constant pumping rate for the duration of experiment (up to 28 days). During the procedure, anesthesia was administrated by intraperitoneal injection of medetomidine hydrochloride (0.3 mg/kg), midazolam (4 mg/kg), and butorphanol tartrate (5 mg/kg) (all from WAKO, Osaka, Japan). Osmotic pump infusion duration was either 1 or 4 weeks after which mice were sacrificed. Only pumps with same lot number were used within the same batch of experiment.

### **2.3. UVB irradiation**

An LED lamp (Nikkiso Co., Ltd., Japan) that can emit 312 nm a wavelength of UVB was previously developed and used in this study. The irradiance of the 312 nm UVB device was 2.52 J/m<sup>2</sup>/second at a distance of 14 cm. The mice were placed 14 cm below the bank of lamps and were irradiated for 14 weeks or six weeks as indicated after shaving their fur in the animal facility, while nonirradiated mice were not subjected to these procedures. The UVB irradiation dose used in this study was 5 or 10 kJ/m<sup>2</sup> as indicated which translates to 33 minutes 5 seconds and 66 minutes 10 seconds of irradiation duration using this irradiation setup.

### **2.4. Blood pressure measurement**

Using a noninvasive tail-cuff device (BP-98 Softron, Tokyo, Japan), I conditioned mice inside a body warmer set at 37°C and waited until they calmed down and measured their SBP. I measured SBP at least five times for each time point: at baseline (pre) and 4 weeks after angiotensin II pump implantation (post). The mean SBP for each group was calculated by averaging the SBP of each mouse included in that group.

## **2.5. Assessment of biochemical parameters**

Any diet was removed the day before sacrifice to apply overnight fasting prior to blood collection. The mice were anesthetized as described above and then a cardiac puncture was performed to rapidly collect blood. Plasma was extracted from the blood sample through centrifugation within two hours of blood collection and then plasma lipid profile was analyzed. Concentrations of plasma total cholesterol, high-density lipoprotein-cholesterol, and triglycerides were determined enzymatically using an automated chemistry analyzer (Oriental Yeast Co., Ltd., Tokyo, Japan). In the 312 nm UVB-atherosclerosis experiment, plasma C-reactive protein levels were measured using a Mouse C-Reactive Protein/CRP Quantikine ELISA Kit according to the manufacturer's instructions (R&D Systems). In the experiment for the role of CCR4 in AAA, immunoglobulin levels were measured using a mouse immunoglobulin ELISA KIT (Invitrogen) according to the manufacturer's instructions.

## **2.6. Morphological analysis of AAA**

Aortic diameters and AAA incidence were determined as described previously.<sup>73</sup> Mice were anesthetized as described above and then the aorta was perfused with cold saline and dissected from the ascending artery to the bifurcation of the iliac artery. The isolated aorta was cleaned from periaortic adipose tissue and fixed in 10% buffered formalin. The largest portion of the suprarenal aorta was determined and the maximum external diameter was measured using the ImageJ (National Institutes of Health). Aortic aneurysm was defined by the increase of external suprarenal aorta diameter of 1.5 times or more than the baseline saline-infused mice aorta. Based on that definition, I calculated the incidence of aneurysm.

I used a previously described classification system<sup>39</sup> to categorize the morphological severity of the aneurysms: no aneurysm (less than 1.5 times larger than normal baseline diameter), type I (a distinguishable dilation that is 1.5 to 2 times the diameter of a normal baseline diameter), type II (a single large dilation that is more than 2 times the diameter of a normal baseline diameter), type III (multiple dilations with possibility of an extension toward the proximal of the suprarenal region), type IV (fatal outcome due to rupture of the aorta).

## **2.7. Assessment of atherosclerotic lesions**

Mice were anesthetized as described above and perfused with cold saline. Thoracoabdominal aorta sample was collected by dissecting from the ascending aorta to the bifurcation of the iliac artery. The isolated aorta was cleaned from periaortic adipose tissue and fixed in 10% buffered formalin. After at least 24 hours of fixation, the thoracoabdominal aorta was cut open longitudinally, stained with Oil Red O (Sigma), and positioned for an en face observation of atherosclerotic lesion.

An aortic sinus sample was collected by cutting loose the ascending aorta from the heart and putting the upper half of the heart that contains the aortic sinus in the OCT compound, and was frozen to prepare cryosections using Cryostat (Leica, Wetzlar, Germany). Cryosections with 10  $\mu\text{m}$  thickness were acquired from the proximal aortic sinus at five different distances from the root with 150  $\mu\text{m}$  intervals. Tissue sections were fixed in 10% buffered formalin for at least 24 hours and stained with hematoxylin eosin (HE). Lesion size was quantified using ImageJ from the HE-stained sections. Some of the sections were stained with Oil Red O for representative figures.

## **2.8. Histological and immunohistochemical analysis of atherosclerosis and aneurysmal lesions**

Aneurysmal tissue cryosections were prepared as follows: mice were anesthetized as described above, the aorta was perfused with cold saline, the suprarenal abdominal aorta including AAA lesions if any was carefully dissected and embedded in OCT compounds (Tissue-Tek; Sakura Finetek, Tokyo, Japan), and a serial of at least four sections of the most dilated portion of the suprarenal aorta (10  $\mu$ m thickness each) with approximately 100  $\mu$ m interval was collected to each tissue slide. Aortic sinus tissue cryosections were prepared as described above.

For immunohistochemistry preparation, cryosections were fixated using 4% paraformaldehyde, blocked using bovine serum albumin (BSA), and peroxidase-inhibited. To quantify immune cells such as macrophages or CD4<sup>+</sup> T cells, immunohistochemistry was performed using anti-MOMA-2 (BMA Biomedicals) or anti-CD4 (BD Biosciences) antibodies, followed by detection with biotinylated secondary antibodies and streptavidin-horseradish peroxidase (streptavidin-HRP), as described previously.<sup>39</sup> Quantitative analysis of macrophage area was presented as a percentage of the AAA cross-section total area or percentage of plaque area in the aortic sinus. Quantitative analysis of CD4<sup>+</sup> T cells of the AAA lesions was performed by counting the number of positively stained cells, which was divided by the total area of each AAA cross-section, while in aortic sinus it was divided by atherosclerotic plaque area.

Immunohistochemical analysis of MMP-2 or MMP-9 in AAA lesions was performed on the above-prepared cryosections using goat anti-MMP-2 or goat anti-MMP-9 antibodies (R&D Systems), followed by detection with streptavidin-HRP-conjugated secondary antibody. Immunohistochemical analysis of TGF- $\beta$ 1 in AAA lesions was performed on the prepared cryosections using a rabbit anti-TGF- $\beta$ 1 antibody (Abcam), followed by detection with a biotinylated secondary antibody and subsequent streptavidin-HRP

For the determination of elastin degradation, I performed Elastica van Gieson staining and counted intact elastin layers in the aneurysmal lesions. Meanwhile, Masson's trichrome staining (Muto Pure Chemicals, Tokyo, Japan) was performed to delineate the fibrous area. Stained sections were digitally captured using a microscope (BZ-X810; KEYENCE, Osaka, Japan), and the stained area was quantified using the ImageJ (National Institutes of Health). At least four sections of the aortic sinus or AAA lesions were analyzed in each mouse and the average values were used for statistical analysis.

Immunofluorescence staining of CCL17 and CCL22 in lymphoid tissues and atherosclerotic lesions was performed on 4% paraformaldehyde-fixed BSA-blocked cryosections of mouse LNs, aortic roots, and aneurysmal tissues using rabbit anti-CCL17 (1:200; Abcam) or goat anti-CCL22 (1:200; R&D Systems) antibodies, followed by detection with fluorescent secondary antibodies. To detect the colocalization of macrophages in the above cryosections, anti-MOMA-2 (1:400; BMA Biomedicals) and fluorescent secondary antibodies were also used (except for lymphoid tissues). The primary and secondary antibodies used are listed in **Table 9**.

## **2.9. In situ zymography of aneurysmal lesions**

In situ zymography of aneurysmal lesions was performed according to the previous report.<sup>74</sup> Unfixed suprarenal aorta cryosections (10  $\mu$ m thickness) were exposed to 10  $\mu$ g/ml DQ-gelatin (D12054, Molecular Probes) and incubated in a CO<sub>2</sub> chamber for 3 hours at 37°C. Fluorescence signal was detected using a fluorescence microscope (BZ-X810; KEYENCE). 1,10-phenanthroline was used as an inhibitor of MMPs for negative control. Mean gray value of the positive signal was quantified using the ImageJ (National Institutes of Health)

## **2.10. Preparation of primary cell suspension**

After tissue collection, peripheral LNs (axillary and inguinal), para-aortic LNs, or spleen organs were homogenized in a 60 mm dish using grounding glass slides with FACS buffer as a suspending medium. The resultant homogenate was passed through a 70  $\mu$ m cell mesh. Filtered homogenate from spleens was lysed with red blood cell lysis buffer for 10 min. After several washing steps, the homogenate passed through a 70  $\mu$ m cell mesh prior to final centrifugation. The collected cell pellets were then resuspended for subsequent analysis.

The aorta sample was isolated carefully to include minimal to none periaortic adipose tissue. Two aortas were combined into a single container filled with RPMI solution. Mechanical homogenization using small scissors was conducted to break aortas into small pieces. The homogenate was incubated with liberase TM (Roche Diagnostics) for enzymatic digestion of aortic fibers at 37°C for 45 minutes with frequent vortexing and being passed through a 21G needle. The incubated homogenate was pressed through a 70  $\mu$ m cell strainer with a 1 mL syringe plunger and flushed with FACS buffer prior to centrifugation. The collected cell pellets were then resuspended for subsequent analysis.

## **2.11. Flow cytometry**

After primary cell suspension was prepared, it was used for flow cytometry analysis. Fc receptor was blocked with anti-CD16/CD32 (BD Biosciences) prior to all fluorochrome staining procedures. Surface antigens can be stained directly after Fc-blocking. Intercellular antigens and transcription factors were stained after permeabilization utilizing a Foxp3 staining buffer set (Thermo Fisher Scientific) according to the manufacturer's instructions. FACS Aria III (BD Biosciences) and FlowJo software version 10.8.1 (Tree Star) were used for flow cytometric analysis. The antibodies used are listed in **Table 10**.

## 2.12. Antibody staining of intracellular cytokine

Primary immune cell suspension from lymphoid tissues was stimulated with 20 ng/ml phorbol 12-myristate 13-acetate (Sigma) and 1 mmol/L ionomycin (Sigma) for 5 hours in the presence of Brefeldin A (Thermo Fisher Scientific) at 37°C in CO<sub>2</sub> chamber. ICS for IFN- $\gamma$ , IL-4, IL-10, and IL-17 was performed as described previously<sup>4</sup> after Fc blocking and surface staining of CD4 molecules. BD Cytofix/Cytoperm™ was used according to the manufacturer's instructions. Antibodies used are listed in **Table 10**.

## 2.13. Cytokine assay

RPMI 1640 medium (Sigma) supplemented with 10% fetal calf serum, 50  $\mu$ mol/L 2 $\beta$ -mercaptoethanol, and antibiotics were used in cell culture experiments. Cytokine secretion from CD4<sup>+</sup> T cells was examined as described previously.<sup>23</sup> Splenic CD4<sup>+</sup> T cells ( $1 \times 10^5$  cells) isolated using MACS (Miltenyi Biotec) were cultured under stimulation with plate-bound anti-CD3 (10  $\mu$ g/mL, clone 145-2C11; BD Biosciences) and soluble anti-CD28 antibodies (2  $\mu$ g/mL, clone 37.51; BD Biosciences) in 96-well round-bottomed plates for 48 hours. Cytokine levels for IL-4, IL-10, IL-17, and IFN- $\gamma$  in culture supernatants were determined by ELISA using paired antibodies specific for corresponding cytokines (R&D Systems).

## 2.14. Treg suppression assay

For analysis of the *in vitro* suppressive function of Tregs, CD4<sup>+</sup>CD25<sup>+</sup> Tregs and CD4<sup>+</sup>CD25<sup>-</sup> T cells were purified from peripheral LNs and spleen of *Apoe*<sup>-/-</sup> or *Ccr4*<sup>-/-</sup>*Apoe*<sup>-/-</sup> mice using a CD4<sup>+</sup>CD25<sup>+</sup> Regulatory T Cell Isolation Kit (Miltenyi Biotec) and anti-CD4 beads (Miltenyi Biotec) according to the manufacturer's instructions. The purity of

each population was >95%, as determined by flow cytometric analysis. Purified CD4<sup>+</sup>CD25<sup>+</sup> Tregs from *Apoe*<sup>-/-</sup> or *Ccr4*<sup>-/-</sup>*Apoe*<sup>-/-</sup> mice were cocultured with carboxyfluorescein diacetate succinimidyl ester (Thermo Fisher Scientific)-labeled CD4<sup>+</sup>CD25<sup>-</sup> conventional T cells (2.5×10<sup>4</sup> cells) from *Apoe*<sup>-/-</sup> mice at the indicated ratios in the presence of mitomycin C (WAKO)-treated antigen-presenting cells (5×10<sup>4</sup> cells) and soluble anti-CD3 antibody (0.5 µg/mL) in 96-well round-bottomed plates. The cocultured cells were maintained at 37°C with 5% CO<sub>2</sub> for 3 days. The proliferation of carboxyfluorescein diacetate succinimidyl ester-labeled CD4<sup>+</sup>CD25<sup>-</sup> conventional T cells was analyzed by flow cytometry. Similar experiments were also conducted with mice fed with a high-cholesterol diet and infused with angiotensin II.

## 2.15. Quantitative reverse transcription PCR analysis

Using TRIzol reagent (Thermo Fisher Scientific), I extracted total RNA from the aorta which was perfused with cold saline and subsequently soaked in RNA later (Thermo Fisher Scientific). For reverse transcription, a PrimeScript RT reagent Kit (Takara, Shiga, Japan) was used. Quantitative PCR was performed using a TB Green Ex Taq (Takara) and a StepOnePlus Real-Time PCR System (Thermo Fisher Scientific) according to the manufacturer's protocol. The primers used are listed in **Table 8**. Amplification reactions were performed in duplicate and fluorescence curves were analyzed with the included software. GAPDH or β-actin was used as an endogenous control reference.

## 2.16. Statistical analysis

Data distribution was assessed using the Shapiro-Wilk normality test. Two-tailed Student's *t*-test or Mann-Whitney *U*-test was used to detect significant differences between 2



groups when appropriate. One-way or 2-way ANOVA followed by Dunnet's multiple comparisons test or 2-way ANOVA followed by Tukey's multiple comparisons test was performed for multiple groups where appropriate. A value of  $P < 0.05$  was considered statistically significant. No data were excluded from the analysis. The investigators were not blinded to the data analysis. For statistical analysis, GraphPad Prism version 9.0 (GraphPad Software Inc.) was used.

## References

1. Global burden of 288 causes of death and life expectancy decomposition in 204 countries and territories and 811 subnational locations, 1990-2021: a systematic analysis for the Global Burden of Disease Study 2021. *The Lancet*. 2024;403(10440):2100-32.
2. Moriya J. Critical roles of inflammation in atherosclerosis. *J Cardiol*. 2019;73(1):22-7.
3. Emoto T, Yamamoto H, Yamashita T, et al. Single-cell RNA sequencing reveals a distinct immune landscape of myeloid cells in coronary culprit plaques causing acute coronary syndrome. *Circulation*. 2022;145(18):1434-6.
4. Tanaka T, Sasaki N, Krisnanda A, et al. Novel UV - B phototherapy with a light - emitting diode device prevents atherosclerosis by augmenting regulatory T - cell responses in mice. *J Am Heart Assoc*. 2024;13(2):e031639.
5. Tanaka T, Sasaki N, Rikitake Y. Recent advances on the role and therapeutic potential of regulatory T cells in atherosclerosis. *J Clin Med*. 2021;10(24):5907.
6. Gupta S, Pablo AM, Jiang X, et al. IFN-gamma potentiates atherosclerosis in ApoE knock-out mice. *J Clin Invest*. 1997;99(11):2752-61.
7. Buono C, Binder CJ, Stavrakis G, et al. T-bet deficiency reduces atherosclerosis and alters plaque antigen-specific immune responses. *Proc Natl Acad Sci U S A*. 2005;102(5):1596-601.
8. Niccoli G, Calvieri C, Flego D, et al. Allergic inflammation is associated with coronary instability and a worse clinical outcome after acute myocardial infarction. *Circ Cardiovasc Interv*. 2015;8(8):e002554.
9. Liu J, Sawada H, Howatt DA, et al. Hypercholesterolemia accelerates both the initiation and progression of angiotensin II-induced abdominal aortic aneurysms. *Ann Vasc Med Res*. 2020;6(2):1099.

10. Schönbeck U, Sukhova GK, Gerdes N, et al. T(H)2 predominant immune responses prevail in human abdominal aortic aneurysm. *Am J Pathol.* 2002;161(2):499-506.
11. Shimizu K, Shichiri M, Libby P, et al. Th2-predominant inflammation and blockade of IFN- $\gamma$  signaling induce aneurysms in allografted aortas. *J Clin Invest.* 2004;114(2):300-8.
12. Ju X, Ijaz T, Sun H, et al. Interleukin-6-signal transducer and activator of transcription-3 signaling mediates aortic dissections induced by angiotensin II via the T-helper lymphocyte 17-interleukin 17 axis in C57BL/6 mice. *Arterioscler Thromb Vasc Biol.* 2013;33(7):1612-21.
13. Sharma AK, Lu G, Jester A, et al. Experimental abdominal aortic aneurysm formation is mediated by IL-17 and attenuated by mesenchymal stem cell treatment. *Circulation.* 2012;126(11\_suppl\_1):S38-S45.
14. Wei Z, Wang Y, Zhang K, et al. Inhibiting the Th17/IL-17A-related inflammatory responses with digoxin confers protection against experimental abdominal aortic aneurysm. *Arterioscler Thromb Vasc Biol.* 2014;34(11):2429-38.
15. Tamassia N, Arruda-Silva F, Wright HL, et al. Human neutrophils activated via TLR8 promote Th17 polarization through IL-23. *J Leukoc Biol.* 2019;105(6):1155-65.
16. Sumarac-Dumanovic M, Stevanovic D, Ljubic A, et al. Increased activity of interleukin-23/interleukin-17 proinflammatory axis in obese women. *Int J Obes.* 2009;33(1):151-6.
17. Sasaki N, Yamashita T, Takeda M, et al. Oral anti-CD3 antibody treatment induces regulatory T cells and inhibits the development of atherosclerosis in mice. *Circulation.* 2009;120(20):1996-2005.
18. Kita T, Yamashita T, Sasaki N, et al. Regression of atherosclerosis with anti-CD3 antibody via augmenting a regulatory T-cell response in mice. *Cardiovasc Res.* 2014;102(1):107-17.

19. Kasahara K, Sasaki N, Yamashita T, et al. CD3 antibody and IL-2 complex combination therapy inhibits atherosclerosis by augmenting a regulatory immune response. *J Am Heart Assoc.* 2014;3(2):e000719.
20. Takeda M, Yamashita T, Sasaki N, et al. Oral administration of an active form of vitamin D3 (calcitriol) decreases atherosclerosis in mice by inducing regulatory T cells and immature dendritic cells with tolerogenic functions. *Arterioscler Thromb Vasc Biol.* 2010;30(12):2495-503.
21. Nilsson J, Hansson GK. Vaccination strategies and immune modulation of atherosclerosis. *Circ Res.* 2020;126(9):1281-96.
22. Amin HZ, Sasaki N, Yamashita T, et al. CTLA-4 protects against angiotensin II-induced abdominal aortic aneurysm formation in mice. *Sci Rep.* 2019;9(1):1-11.
23. Matsumoto T, Sasaki N, Yamashita T, et al. Overexpression of cytotoxic T-lymphocyte-associated antigen-4 prevents atherosclerosis in mice. *Arterioscler Thromb Vasc Biol.* 2016;36(6):1141-51.
24. Sasaki N, Yamashita T, Kasahara K, et al. UVB exposure prevents atherosclerosis by regulating immunoinflammatory responses. *Arterioscler Thromb Vasc Biol.* 2017;37(1):66-74.
25. Hayashi T, Sasaki N, Yamashita T, et al. Ultraviolet B exposure inhibits angiotensin II-induced abdominal aortic aneurysm formation in mice by expanding CD4<sup>+</sup>Foxp3<sup>+</sup> regulatory T cells. *J Am Heart Assoc.* 2017;6(9):e007024.
26. Sasaki N. Ultraviolet B irradiation as a novel strategy to prevent atherosclerotic cardiovascular disease. *Photomed Photobiol.* 2018;39:7-15.
27. Yamamoto J, Adachi Y, Onoue Y, et al. Differential expression of the chemokine receptors by the Th1- and Th2-type effect or populations within circulating CD4<sup>+</sup> T cells. *J Leukoc Biol.* 2002;68(4):568-74.

28. Griffith JW, Sokol CL, Luster AD. Chemokines and chemokine receptors: positioning cells for host defense and immunity. *Annu Rev Immunol.* 2014;32:659-702.
29. Weber C, Habenicht AJR, von Hundelshausen P. Novel mechanisms and therapeutic targets in atherosclerosis: inflammation and beyond. *Eur Heart J.* 2023;44(29):2672-81.
30. Ridker PM, Everett BM, Thuren T, et al. Anti-inflammatory therapy with Canakinumab for atherosclerotic disease. *N Engl J Med.* 2017;377(12):1119-31.
31. Tardif JC, Kouz S, Waters DD, et al. Efficacy and safety of low-dose Colchicine after myocardial infarction. *N Engl J Med.* 2019;381(26):2497-505.
32. Golledge J. Abdominal aortic aneurysm: update on pathogenesis and medical treatments. *Nat Rev Cardiol.* 2019;16(4):225-42.
33. Marquez-Sanchez AC, Koltsova EK. Immune and inflammatory mechanisms of abdominal aortic aneurysm. *Front Immunol.* 2022;13:989933.
34. Roy P, Orecchioni M, Ley K. How the immune system shapes atherosclerosis: roles of innate and adaptive immunity. *Nat Rev Immunol.* 2022;22(4):251-65.
35. Li B, Song X, Guo W, et al. Single-cell transcriptome profiles reveal fibrocytes as potential targets of cell therapies for abdominal aortic aneurysm. *Front Cardiovasc Med.* 2021;8:753711.
36. Zhao G, Lu H, Chang Z, et al. Single-cell RNA sequencing reveals the cellular heterogeneity of aneurysmal infrarenal abdominal aorta. *Cardiovasc Res.* 2021;117(5):1402-16.
37. Fernandez DM, Rahman AH, Fernandez NF, et al. Single-cell immune landscape of human atherosclerotic plaques. *Nat Med.* 2019;25(10):1576-88.
38. Sakaguchi S, Mikami N, Wing JB, et al. Regulatory T cells and human disease. *Annu Rev Immunol.* 2020;38:541-66.

39. Yodoi K, Yamashita T, Sasaki N, et al. Foxp3<sup>+</sup> regulatory T cells play a protective role in angiotensin II-induced aortic aneurysm formation in mice. *Hypertension*. 2015;65(4):889-95.
40. Ait-Oufella H, Salomon BL, Potteaux S, et al. Natural regulatory T cells control the development of atherosclerosis in mice. *Nat Med*. 2006;12(2):178-80.
41. Kasahara K, Sasaki N, Amin HZ, et al. Depletion of Foxp3(+) regulatory T cells augments CD4(+) T cell immune responses in atherosclerosis-prone hypercholesterolemic mice. *Heliyon*. 2022;8(7):e09981.
42. King VL, Lin AY, Kristo F, et al. Interferon-gamma and the interferon-inducible chemokine CXCL10 protect against aneurysm formation and rupture. *Circulation*. 2009;119(3):426-35.
43. Noels H, Weber C, Koenen RR. Chemokines as therapeutic targets in cardiovascular disease. *Arterioscler Thromb Vasc Biol*. 2019;39(4):583-92.
44. Yoshie O. CCR4 as a therapeutic target for cancer immunotherapy. *Cancers (Basel)*. 2021;13(21):5542.
45. Yuan Q, Bromley SK, Means TK, et al. CCR4-dependent regulatory T cell function in inflammatory bowel disease. *J Exp Med*. 2007;204(6):1327-34.
46. Faustino L, da Fonseca DM, Takenaka MC, et al. Regulatory T cells migrate to airways via CCR4 and attenuate the severity of airway allergic inflammation. *J Immunol*. 2013;190(6):2614-21.
47. Alferink J, Lieberam I, Reindl W, et al. Compartmentalized production of CCL17 in vivo: strong inducibility in peripheral dendritic cells contrasts selective absence from the spleen. *J Exp Med*. 2003;197(5):585-99.
48. Tang HL, Cyster JG. Chemokine upregulation and activated T cell attraction by maturing dendritic cells. *Science*. 1999;284(5415):819-22.

49. Rapp M, Wintergerst MWM, Kunz WG, et al. CCL22 controls immunity by promoting regulatory T cell communication with dendritic cells in lymph nodes. *J Exp Med*. 2019;216(5):1170-81.
50. Kikuchi T, Nakae J, Kawano Y, et al. Foxo in T cells regulates thermogenic program through Ccr4/Ccl22 axis. *iScience*. 2019;22:81-96.
51. Hu Z, Lancaster JN, Sasiponganan C, et al. CCR4 promotes medullary entry and thymocyte–dendritic cell interactions required for central tolerance. *J Exp Med*. 2015;212(11):1947-65.
52. Cowan JE, McCarthy NI, Parnell SM, et al. Differential requirement for CCR4 and CCR7 during the development of innate and adaptive  $\alpha\beta$ T cells in the adult thymus. *J Immunol*. 2014;193(3):1204-12.
53. Döring Y, van der Vorst EPC, Yan Y, et al. Identification of a non-canonical chemokine-receptor pathway suppressing regulatory T cells to drive atherosclerosis. *Nat Cardiovasc Res*. 2024;3(2):221-42.
54. Shimizu K, Mitchell RN, Libby P. Inflammation and cellular immune responses in abdominal aortic aneurysms. *Arterioscler Thromb Vasc Biol*. 2006;26(5):987-94.
55. Wang J, Lindholt JS, Sukhova GK, et al. IgE actions on CD4<sup>+</sup> T cells, mast cells, and macrophages participate in the pathogenesis of experimental abdominal aortic aneurysms. *EMBO Mol Med*. 2014;6(7):952-69.
56. Schaheen B, Downs EA, Serbulea V, et al. B-cell depletion promotes aortic infiltration of immunosuppressive cells and is protective of experimental aortic aneurysm. *Arterioscler Thromb Vasc Biol*. 2016;36(11):2191-202.
57. Ulloa L, Doody J, Massague J. Inhibition of transforming growth factor-beta/SMAD signalling by the interferon-gamma/STAT pathway. *Nature*. 1999;397(6721):710-3.

58. Weng H, Mertens PR, Gressner AM, et al. IFN-gamma abrogates profibrogenic TGF-beta signaling in liver by targeting expression of inhibitory and receptor Smads. *J Hepatol.* 2007;46(2):295-303.
59. Wynn TA. Common and unique mechanisms regulate fibrosis in various fibroproliferative diseases. *J Clin Invest.* 2007;117(3):524-9.
60. Xu J, Ehrman B, Graham LM, et al. Interleukin-5 is a potential mediator of angiotensin II-induced aneurysm formation in apolipoprotein E knockout mice. *J Surg Res.* 2012;178(1):512-8.
61. Sugiyama D, Nishikawa H, Maeda Y, et al. Anti-CCR4 mAb selectively depletes effector-type FoxP3+CD4+ regulatory T cells, evoking antitumor immune responses in humans. *Proc Natl Acad Sci U S A.* 2013;110(44):17945-50.
62. Hart PH, Norval M, Byrne SN, et al. Exposure to ultraviolet radiation in the modulation of human diseases. *Annual Review of Pathology.* 2019;14(Volume 14, 2019):55-81.
63. Morita A. Current developments in phototherapy for psoriasis. *J Dermatol.* 2018;45(3):287-92.
64. Fredman G, Hellmann J, Proto JD, et al. An imbalance between specialized pro-resolving lipid mediators and pro-inflammatory leukotrienes promotes instability of atherosclerotic plaques. *Nat Commun.* 2016;7:12859.
65. Soehnlein O, Libby P. Targeting inflammation in atherosclerosis - from experimental insights to the clinic. *Nat Rev Drug Discov.* 2021;20(8):589-610.
66. Korn T, Reddy J, Gao W, et al. Myelin-specific regulatory T cells accumulate in the CNS but fail to control autoimmune inflammation. *Nat Med.* 2007;13(4):423-31.
67. Chiurchiu V, Leuti A, Dalli J, et al. Proresolving lipid mediators resolvin D1, resolvin D2, and maresin 1 are critical in modulating T cell responses. *Sci Transl Med.* 2016;8(353):353ra111.



68. Viola JR, Lemnitzer P, Jansen Y, et al. Resolving lipid mediators maresin 1 and resolvin D2 prevent atheroprogession in mice. *Circ Res.* 2016;119(9):1030-8.
69. Luan H, Wang C, Sun J, et al. Resolvin D1 protects against ischemia/reperfusion-induced acute kidney injury by increasing Treg percentages via the ALX/FPR2 pathway. *Front Physiol.* 2020;11:285.
70. Furuhashi T, Saito C, Torii K, et al. Photo(chemo)therapy reduces circulating Th17 cells and restores circulating regulatory T cells in psoriasis. *PLoS One.* 2013;8(1):e54895.
71. Matsuo K, Itoh T, Koyama A, et al. CCR4 is critically involved in effective antitumor immunity in mice bearing intradermal B16 melanoma. *Cancer Lett.* 2016;378(1):16-22.
72. Sasaki N, Yamashita T, Takaya T, et al. Augmentation of vascular remodeling by uncoupled endothelial nitric oxide synthase in a mouse model of diabetes mellitus. *Arterioscler Thromb Vasc Biol.* 2008;28(6):1068-76.
73. Daugherty A, Manning MW, Cassis LA. Angiotensin II promotes atherosclerotic lesions and aneurysms in apolipoprotein E-deficient mice. *J Clin Invest.* 2000;105(11):1605-12.
74. Nakao T, Horie T, Baba O, et al. Genetic ablation of microRNA-33 attenuates inflammation and abdominal aortic aneurysm formation via several anti-inflammatory pathways. *Arterioscler Thromb Vasc Biol.* 2017;37(11):2161-70.